

1. Report No. FHWA/TX-87/324-1		2. Government Accession No.		3. Recipient's Catalog No.	
4. Title and Subtitle Positive Moment Tests for Precast Concrete Panel-Decked Composite Bridges				5. Report Date September 1987	
				6. Performing Organization Code	
7. Author(s) R. A. Osegueda, and J. S. Noel				8. Performing Organization Report No. Research Report 324-1	
9. Performing Organization Name and Address Texas Transportation Institute The Texas A&M University System College Station, Texas				10. Work Unit No.	
				11. Contract or Grant No. Study no. 2-5-82-324	
				13. Type of Report and Period Covered Interim - September 1981 September 1987	
12. Sponsoring Agency Name and Address Texas State Department of Highways and Public Transportation, Transportation Planning Division P. O. Box 5051 Austin, Texas 78763				14. Sponsoring Agency Code	
15. Supplementary Notes Research performed in cooperation with DOT, FHWA. Research Study Title: Rapid Bridge Deck Replacement					
16. Abstract <p>Bridge deck replacement using precast concrete panels minimizes replacement time as well as traffic interference. An experimental study consisting of static load test on a 1/3 scale model of a 60-ft long steel I-girder bridge with precast concrete panels connected with epoxy mortar and shear connectors to accomplish composite action is described.</p> <p>Three major static load tests were conducted. The first test was conducted on the bare steel stringers. The second was conducted with the precast concrete panels connected to the steel stringers only by pocket connections consisting of epoxy mortar and shear connectors. The third test was conducted with the precast panels connected to each other by built-in shear key joints grouted with epoxy mortar in addition to being connected by the pocket connection to the steel stringers.</p> <p>The results of the static load tests were evaluated as the 1/3 model went through a transition from noncomposite to composite. Composite action was accomplished when the epoxy mortar of the pocket connections and shear key joints cured. No significant composite action was developed by the pocket connections alone.</p>					
17. Key Words Bridge Decks, Precast Concrete, Composite Bridges, Epoxy Mortar, Shear Connectors, Structural Models, Static Load Test			18. Distribution Statement No restrictions. This document is available to the public through the National Technical Information Service 5285 Port Royal Road Springfield, Virginia 22161		
19. Security Classif. (of this report) Unclassified		20. Security Classif. (of this page) Unclassified		21. No. of Pages 190	22. Price

POSITIVE MOMENT TESTS FOR PRECAST CONCRETE PANEL-DECKED
COMPOSITE BRIDGES

by

Roberto A. Osegueda
Research Assistant

and

James S. Noel
Research Engineer

Research Report Number 324-1

Research Study Number 2-5-82-324
Rapid Bridge Deck Replacement

Sponsored by
Texas State Department of Highways and Public Transportation
in cooperation with
The United States Department of Transportation
Federal Highway Administration

September 1987
Texas Transportation Institute
Texas A&M University
College Station, Texas

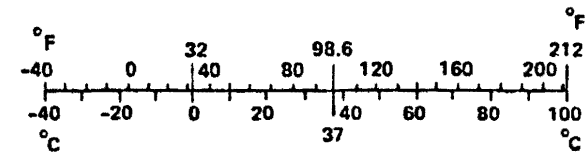
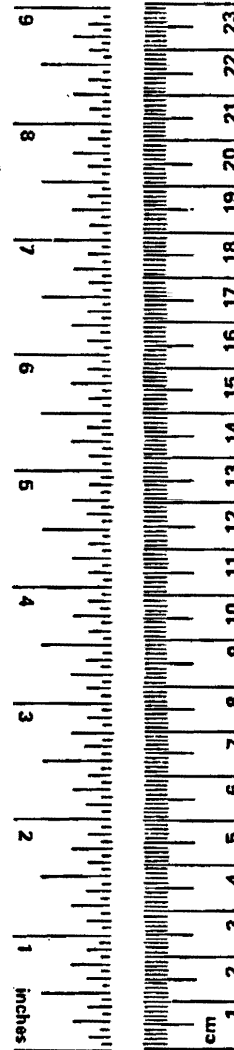
METRIC CONVERSION FACTORS

Approximate Conversions to Metric Measures

Symbol	When You Know	Multiply by	To Find	Symbol
LENGTH				
in	inches	*2.5	centimeters	cm
ft	feet	30	centimeters	cm
yd	yards	0.9	meters	m
mi	miles	1.6	kilometers	km
AREA				
in ²	square inches	6.5	square centimeters	cm ²
ft ²	square feet	0.09	square meters	m ²
yd ²	square yards	0.8	square meters	m ²
mi ²	square miles	2.6	square kilometers	km ²
	acres	0.4	hectares	ha
MASS (weight)				
oz	ounces	28	grams	g
lb	pounds	0.45	kilograms	kg
	short tons (2000 lb)	0.9	tonnes	t
VOLUME				
tsp	teaspoons	5	milliliters	ml
Tbsp	tablespoons	15	milliliters	ml
fl oz	fluid ounces	30	milliliters	ml
c	cups	0.24	liters	l
pt	pints	0.47	liters	l
qt	quarts	0.95	liters	l
gal	gallons	3.8	liters	l
ft ³	cubic feet	0.03	cubic meters	m ³
yd ³	cubic yards	0.76	cubic meters	m ³
TEMPERATURE (exact)				
°F	Fahrenheit temperature	5/9 (after subtracting 32)	Celsius temperature	°C

Approximate Conversions from Metric Measures

Symbol	When You Know	Multiply by	To Find	Symbol
LENGTH				
mm	millimeters	0.04	inches	in
cm	centimeters	0.4	inches	in
m	meters	3.3	feet	ft
m	meters	1.1	yards	yd
km	kilometers	0.6	miles	mi
AREA				
cm ²	square centimeters	0.16	square inches	in ²
m ²	square meters	1.2	square yards	yd ²
km ²	square kilometers	0.4	square miles	mi ²
ha	hectares (10,000 m ²)	2.5	acres	
MASS (weight)				
g	grams	0.035	ounces	oz
kg	kilograms	2.2	pounds	lb
t	tonnes (1000 kg)	1.1	short tons	
VOLUME				
ml	milliliters	0.03	fluid ounces	fl oz
l	liters	2.1	pints	pt
l	liters	1.06	quarts	qt
l	liters	0.26	gallons	gal
m ³	cubic meters	35	cubic feet	ft ³
m ³	cubic meters	1.3	cubic yards	yd ³
TEMPERATURE (exact)				
°C	Celsius temperature	9/5 (then add 32)	Fahrenheit temperature	°F



* 1 in = 2.54 (exactly). For other exact conversions and more detailed tables, see NBS Misc. Publ. 286, Units of Weights and Measures, Price \$2.25, SD Catalog No. C13.10:286.

DISCLAIMER

The contents of this report reflect the views of the authors, who are responsible for the opinions, findings, and conclusions presented herein. The contents do not necessarily reflect the official views or policies of the Federal Highway Administration. This report does not constitute a standard, specification, or regulation.

KEY WORDS

Bridge Decks, Precast Concrete, Composite Bridges, Epoxy Mortar, Shear Connectors, Structural Models, Static Load Test.

ACKNOWLEDGEMENTS

The authors are grateful to The Texas State Department of Highways and Public Transportation and The Federal Highway Administration for sponsoring this study, to Mr. John Panak, whose professional advice was most helpful and to Dr. Mrinmay Biswas who was instrumental in the preliminary phases of the project.

The gracious contributions and the cooperation received from Mr. William Wayman of Ivey Steel Co., Mr. Greg Fredericks of Erico Jones Inc., and Mr. John Stampley of Mosher Steel of San Antonio are greatly appreciated.

TABLE OF CONTENTS

Chapter		Page
I	INTRODUCTION	1
	Nature of the Problem	1
	Background and Significant Work	1
	Purdue University-Indiana State Highway Commission	2
	New York State Thruway Authority	4
	New York State Department of Transportation	8
	Pennsylvania Turnpike Commission	14
	Interstate 80 Overpass, Oakland, California	14
	Maryland State Highway Administration-Federal Highway Administration	16
	Summary	19
	Objectives of Study	19
	Scope of Study	20
II	EXPERIMENTAL WORK	21
	General	21
	Selection of Prototype Bridge	21
	Model Design	25
	Design of Model Stringers	25
	Design of Shear Connectors	31
	Design of Precast Panels	32
	Design of Reinforcing Steel	34
	Design of Model Concrete	36
	Model Construction	39
	Forms	39
	Reinforcing Steel	42
	Panel Casting	42
	Steel Stringers	43

Chapter	Page
Compression Tests on Model Concrete	45
Design of Epoxy Mortar	45
Aggregates	48
Trial Mixes	48
Split Tensile Tests	52
Compression Tests	52
Loading System	54
Loading Frame	54
Hydraulic System	54
Instrumentation	54
Load Cells	55
Strain Gages	55
Dial Indicators	56
Displacement Transducers	59
Assembly of Model	59
Grouting of Pocket Connections	61
Grouting of Shear Key Joints	61
Cylinder Tests on Epoxy Mortar of Connections	63
Compression Tests	63
Split Tensile Tests	63
Determination of Tangent Moduli	66
III STATIC LOAD TEST RESULTS	67
General	67
Test No. 1. Noncomposite Test	67
Description of Test No. 1	67
Flexural Strain Distribution	68
Shear Strain Distribution	69
Deflections	80

Chapter	Page
Test No. 2. Static Load Test with Pocket Connections	
Grouted	80
Description of Test No. 2	88
Flexural Strain Distribution	88
Deflections	98
Test No. 3. Full Composite Test	98
Description of Test No. 3	101
Flexural Strain Distribution	101
Shear Strain Distribution	102
Deflections	102
Relative Slip Displacement	110
 IV DISCUSSION OF TEST RESULTS	 114
General	114
Noncomposite Test	115
Normalized Flexural Stress Distribution	115
Normalized Shear Stress Distribution	115
Partial Composite Test	118
Normalized Flexural Stress Distribution	118
Full Composite Test	118
Normalized Flexural Stress Distribution	118
Normalized Shear Stress Distribution	120
Comparison of Flexural Stress Distribution	120
Comparison of Shear Stress Distribution	124
Comparison of Midspan Deflections	127
Comparison of Full Composite Test Results to	
Prototype	131
Flexural Strains	131
Deflections	133
Discussion of Slip Displacements	136

Chapter	Page
Comparison to Design Stresses	138
Flexural Strains and Stresses	140
Horizontal Shear Forces at Panel-Stringers	
Interface	140
Relationship of Applied Loads to Yield and Ultimate Load	142
 V CONCLUSIONS AND RECOMMENDATIONS	 143
General	143
Conclusions	143
Recommendations	146
 REFERENCES	 148
 APPENDIX A - NOTATION	 150
 APPENDIX B - DIMENSIONAL ANALYSIS	 152
 APPENDIX C - DESIGN COMPOSITE INERTIA CALCULATION OF PROTOTYPE AND MODEL	 159
 APPENDIX D - INERTIA CALCULATIONS OF ACTUAL MODEL AND PROTOTYPE	 167
 APPENDIX E - DERIVATION OF MIDSPAN DEFLECTION EQUATION	 175

LIST OF TABLES

Table		Page
1	Prototype Stringer Sectional Properties At Midspan, 36 WF 150 with Cover Plates	23
2	Prototype Stringer Sectional Properties at Supports 36 WF 150	24
3	Summary of the Reinforcement Meeting AASHTO Code Requirements	26
4	Scale Factors for 1/3 Model Bridge	27
5	Composite Sectional Properties of Prototype, 1/3 Ideal Model, and 1/3 Design Model at the Middle and End Sections	30
6	Reinforcement Provided in the 1/3 Model, Compared to AASHTO and Ontario Bridge Codes Requirements	35
7	AASHTO Grading Requirements for 3/4 in. Coarse Aggregate and Fine Concrete Sand	37
8	Gradation Data for the 3/8 in. Bryco Pea Gravel	37
9	Fine Masonry Sand Gradation Data	40
10	Design Volume Mix Proportions of Model Concrete	40
11	Flange Width Measurements of Model Stringers	46
12	Average Moment of Inertia of the Model Steel Stringers and Design Moment of Inertia	46
13	Compression Test Results of Model Concrete of Precast Panels	47
14	Grading Limits for the Texas Highway Department Grade No. 1 Aggregate	49
15	Gradation Data of the Texblast Sandblasting Sands No. 2, No. 3, No. 4, and a 50-50% Blend of No. 2 and No. 4	50
16	Laboratory Split Tensile Test Results of Epoxy Mortar at 24 Hours	53
17	Laboratory Compression Test Results of Epoxy Mortar at 24 Hours	53

Table		Page
18	Compressive Strength of Epoxy Mortar of Connections at 24 Hours	65
19	Tensile Strength of Epoxy Mortar of Connections at 24 Hours ..	65
20	Tangent Moduli of Epoxy Mortar of Connections	66
21	Theoretical Correlation Factor of Flexural Strain Gages	70
22	Average Percent Error of Shear Strain Rosettes	81
23	Deflections of Model Stringer 1, Test No. 1	85
24	Deflections of Model Stringer 2, Test No. 1	86
25	Deflections of Model Stringer 1, Test No. 2	99
26	Deflections of Model Stringer 2, Test No. 2	99
27	Deflections of Model Stringer 1, Test No. 3	111
28	Deflections of Model Stringer 2, Test No. 3	111
29	Apparent Sectional Properties of Model	125
30	Ratio of Statical Moment and Moment of Inertia About the Neutral Axis, Q/I , Tests No. 1 and No. 3	128
31	Rate of Midspan Deflection and Percent Reduction	132
32	Comparison of Maximum Flexural Strains and Stresses of Model with Design Strains and Stresses of Prototype	141
33	Comparison of Maximum Applied Shear Forces of Model with Design Shear Forces of Prototype	142
B-1	Parameters Involved in Dimensional Analysis	153
B-2	Dimensionless Terms and Summary of Computations	155
C-1	Prototype Middle Section Inertia Calculations	160
C-2	Prototype End Section Inertia Calculations	161
C-3	Design 1/3 Model Middle Section Inertia Calculations	163
C-4	Design 1/3 Model End Section Inertia Calculations	165
D-1	Actual Model Middle Section Inertia Calculations	168
D-2	Actual Model End Section Inertia Calculations	169
D-3	Actual Prototype Middle Section Inertia Calculations	171
D-4	Actual Prototype End Section Inertia Calculations	173

LIST OF FIGURES

Figure		Page
1	Tongue-and-Groove Joint Details, Purdue Tests, and Indiana State Highway Commission	3
2	Schematic of Purdue Tests, Bloomington and Knightstown Bridges. Indiana State Highway Commission	3
3	Bolted Connection Details, Amsterdam, New York. New York Thruway Authority	5
4	Welded Channel Connection Details, Amsterdam, New York. New York Thruway Authority	5
5	Shear Key Joint Details. New York Thruway Authority	6
6	Welded Stud Connection Details, Albany, New York. New York Thruway Authority	7
7	Roundout Creek Bridge Deck, Kingston, New York. New York State Department of Transportation	9
8	Delaware River Bridge, New York-Pennsylvania. New York State Department of Transportation	10
9	Erie County Bridge Deck Connection Details, New York. New York State Department of Transportation	11
10	Batchelerville Bridge, Saratoga County, New York. New York State Department of Transportation	12
11	Batchelerville Bridge Details, Saratoga County, New York. New York State Department of Transportation	13
12	Precast Panel Connection Details, Clark's Summit Bridge, Pennsylvania. Pennsylvania Turnpike Commission	15
13	Schematic of Woodrow Wilson Memorial Bridge Deck Replacement. Maryland State Highway Administration- Federal Highway Administration	17
14	Typical Panel, Woodrow Wilson Memorial Bridge	18
15	Panel-to-Panel Joint Details, Woodrow Wilson Memorial Bridge	18

Figure		Page
16	Details of Prototype Bridge. Texas Highway Department	22
17	Details of Model Stringers	29
18	Model Precast Concrete Panel Details	32
19	Model Shear Key Joint Details	33
20	Gradation Chart of 3/8 in. Bryco Pea Gravel	38
21	Gradation Chart of Bryco Fine Masonry Sand	41
22	Plexiglass Form Before Casting and Concrete Panel After Casting	44
23	Gradation Chart of Sandblasting Sand for Epoxy Mortar	51
24	Location of Instrumented Cross Sections	57
25	Typical Cross Section Instrumented for Flexure	58
26	Typical Cross Section Instrumented for Shear	58
27	Electrical Displacement Transducer to Measure Slip Displacements	60
28	Bearing Devices for Panels	60
29	Sealing Devices Supported from Floor	62
30	Grouting of Pocket Connections	62
31	One-Third Model After All Grouting was Completed	64
32	Flexural Strain Distribution, Cross Section 1-1, Test No. 1 ..	71
33	Flexural Strain Distribution, Cross Section 2-2, Test No. 1 ..	72
34	Flexural Strain Distribution, Cross Section 3-3, Test No. 1 ..	73
35	Flexural Strain Distribution, Cross Section 4-4, Test No. 1 ..	74
36	Flexural Strain Distribution, Cross Section 5-5, Test No. 1 ..	75
37	Flexural Strain Distribution, Cross Section 6-6, Test No. 1 ..	76
38	Flexural Strain Distribution, Cross Section 7-7, Test No. 1 ..	77
39	Flexural Strain Distribution, Cross Section 8-8, Test No. 1 ..	78
40	Shear Strain Distribution, Cross Section A-A, Test No. 1	82
41	Shear Strain Distribution, Cross Section B-B, Test No. 1	83
42	Shear Strain Distribution, Cross Section C-C, Test No. 1	84
43	Mid-Span Deflections, Test No. 1	87

Figure		Page
44	Typical Location of Cross Section Instrumented for Flexure Relative to Shear Key Joints	89
45	Flexural Strain Distribution, Cross Section 1-1, Test No. 2 ..	90
46	Flexural Strain Distribution, Cross Section 2-2, Test No. 2 ..	91
47	Flexural Strain Distribution, Cross Section 3-3, Test No. 2 ..	92
48	Flexural Strain Distribution, Cross Section 4-4, Test No. 2 ..	93
49	Flexural Strain Distribution, Cross Section 5-5, Test No. 2 ..	94
50	Flexural Strain Distribution, Cross Section 6-6, Test No. 2 ..	95
51	Flexural Strain Distribution, Cross Section 7-7, Test No. 2 ..	96
52	Flexural Strain Distribution, Cross Section 8-8, Test No. 2 ..	97
53	Mid-Span Deflections, Test No. 2	100
54	Flexural Strain Distribution, Cross Section 1-1, Test No. 3 ..	103
55	Flexural Strain Distribution, Cross Section 2-2, Test No. 3 ..	104
56	Flexural Strain Distribution, Cross Section 3-3, Test No. 3 ..	105
57	Flexural Strain Distribution, Cross Section 4-4, Test No. 3 ..	106
58	Shear Strain Distribution, Cross Section A-A, Test No. 3	107
59	Shear Strain Distribution, Cross Section B-B, Test No. 3	108
60	Shear Strain Distribution, Cross Section C-C, Test No. 3	109
61	Mid-Span Deflections, Test No. 3	112
62	Slip Displacements, Test No. 3	113
63	Normalized Flexural Stress Distribution, Test No. 1	116
64	Normalized Shear Stress Distribution, Test No. 1	117
65	Normalized Flexural Stress Distribution, Test No. 2	119
66	Normalized Flexural Stress Distribution, Test No. 3	121
67	Normalized Shear Stress Distribution, Test No. 3	122
68	Comparison of Flexural Stress Distributions of Tests No. 1, No. 2, and No. 3	126
69	Comparison of Shear Stress Distributions of Tests No. 1 and No. 3	129
70	Comparison of Mid-Span Deflections, Tests No. 1, No. 2 and No. 3	130

Figure	Page
71	Comparison of Model Composite Flexural Strains at Bottom Fibers of Stringers with Prototype 134
72	Comparison of Model Composite Flexural Strains at Top Fibers of Panels with Prototype 135
73	Comparison of Mid-Span Deflections with Theoretical Model and Prototype Mid-Span Deflections 137
74	Slip Displacements of Pocket Connections Compared to Empirical Slip Displacements of Two 1/4 in. Studs in Concrete 139
C-1	Prototype Composite Middle Section 159
C-2	Prototype Composite End Section 161
C-3	Design 1/3 Model Middle Section 163
C-4	Design 1/3 Model End Section 165
D-1	Actual Model Middle Section 167
D-2	Actual Model End Section 169
D-3	Actual Prototype Middle Section 171
D-4	Actual Prototype End Section 173
E-1	Stringer System 175
E-2	Moment Diagram 175
E-3	Area Moment Diagram 176

C H A P T E R I

INTRODUCTION

Nature of the Problem

There are many bridges in the United States that have the deck so deteriorated that it is beyond repair by the usual methods of patching or overlay. The only solution is to replace the deck. However, if the deck is replaced by using cast-in-place concrete, the procedure takes too long and interferes extensively with the flow of traffic.

By using precast concrete panels, the deck replacement time of short span bridges is reduced considerably, and traffic interference is minimized. Still, the following problems and questions are faced: 1) Can a structural system be built and be at least as strong as the original structure? 2) Can the new structure be built rapidly to minimize traffic interference? 3) Can fit-up problems with existing steel systems and with adjacent slabs be overcome? 4) Will the behavior of the new structure be similar to that of the original structure?

Several preliminary designs, details and construction procedures have been developed and used by at least four major highway agencies to rehabilitate many bridge structures. These methods essentially involve use of epoxy mortar and standard welded shear connectors. The overall method appears to be viable and economical. However, several serious questions, especially regarding structural behavior, strength and durability, remain unanswered.

Background and Significant Work

The advantages of replacing deteriorated bridge decks with precast concrete panels were recognized in the late 1960's by many major public highway agencies. However, only a few have tried the method in practice. The work done by some agencies is described in the following paragraphs.

Purdue University-Indiana State Highway Commission

In 1969, a research project at Purdue University (6) was conducted to determine the feasibility of using precast, prestressed concrete deck panels for steel bridges. The research consisted of comprehensive prototype testing in the laboratory and testing of two bridge decks constructed by the Indiana State Highway Commission.

The laboratory test bridge deck at Purdue University consisted of precast, pretensioned panels placed transversely to the traffic flow. The panels were connected together with a tongue-and-groove joint, as illustrated in Fig. 1, and post-tensioned longitudinally, as illustrated in Fig. 2. The panels were subjected to more than 10 million cycles of a simulated 18-kip, single axle load applied on adjacent sides of a joint without apparent deterioration.

One of the significant conclusions obtained from the laboratory testing was that nearly full composite action between the deck and supporting steel stringers was achieved under static and dynamic loading. However, the method by which this conclusion was reached is somewhat questionable, since it depends entirely on an assumption of distribution of loads between steel stringers.

The conclusions and results obtained from the laboratory tests led to the construction of two bridge decks on the Indiana highway system (13). The first one was a replacement deck for an existing bridge on IN-37 near Bloomington, Indiana; the other was a deck for a new bridge on IN-140 near Knightstown, Indiana.

The deck placed on the Bloomington bridge consisted of precast, prestressed panels 4 ft wide, with the tongue-and-groove joints similar to the Purdue test. A 1/16 in. thick neoprene strip was placed between the panels to reduce local stress concentration. Even though the tongue-and-groove joints were successful in the Purdue tests, they were not on the Bloomington bridge. Irregularities in such joints caused high stress concentrations, producing water leakage and severe concrete spalling.

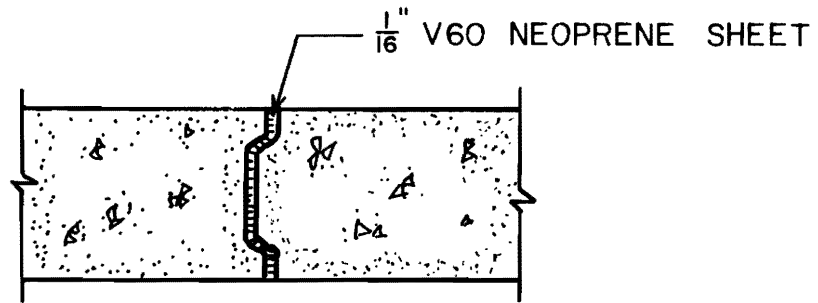


FIG. 1. Tongue-and-Groove Joint Details, Purdue Tests, and Indiana State Highway Commission (6).

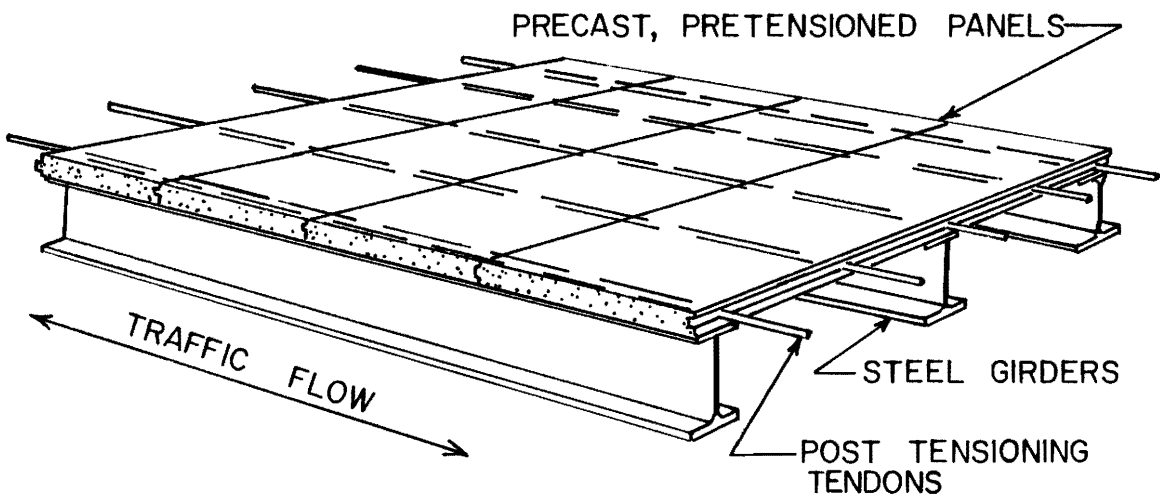


FIG. 2. Schematic of Purdue Tests, Bloomington and Knightstown Bridges. Indiana State Highway Commission (6).

Despite these problems, the panels were placed in two days, which indicates the time that can be saved using precast concrete deck.

The bridge near Knightstown experienced exactly the same problems of water leakage and severe spalling at the tongue-and-groove joints.

New York State Thruway Authority

The New York State Thruway Authority (2,3) has installed precast concrete decks to replace deteriorated concrete slabs on three different bridges. The first one was in Amsterdam, New York, and was set up as an experimental project.

The objective of this project was to evaluate the effectiveness of welded and bolted connections designed to achieve composite action with the steel stringers. Only one-half of one span was replaced using precast panels. A total of seven precast panels was placed, three of which were connected with bolted connections, as shown in Fig. 3. The other four were connected with welded channel connectors, as shown in Fig. 4. Epoxy mortar was used on these panels as bedding and grouting material to transfer forces between precast panels and steel systems. A shear key with epoxy mortar was used in the transfer connections between adjacent panels, as illustrated in Fig. 5. The purpose of the epoxy mortar at this connection was to transfer normal forces to assure complete composite action of the structure. The adhesive strength of the epoxy mortar was not considered in the design of the connections. The interaction forces for composite action in the structure were designed to be taken only by mechanical shear connectors.

The second bridge constructed using this type of precast panels was at the thruway at Krum Kill Road near Albany, New York. This is a single-span highway overpass. Connections similar to those used in the welded portion of the Amsterdam bridge were used. The only difference was that standard welded steel stud connectors were used instead of channel connectors, as shown in Fig. 6.

The third bridge was the entrance ramp to the thruway in Harriman, New York. This is a curved, superelevated bridge. The flat precast panels did

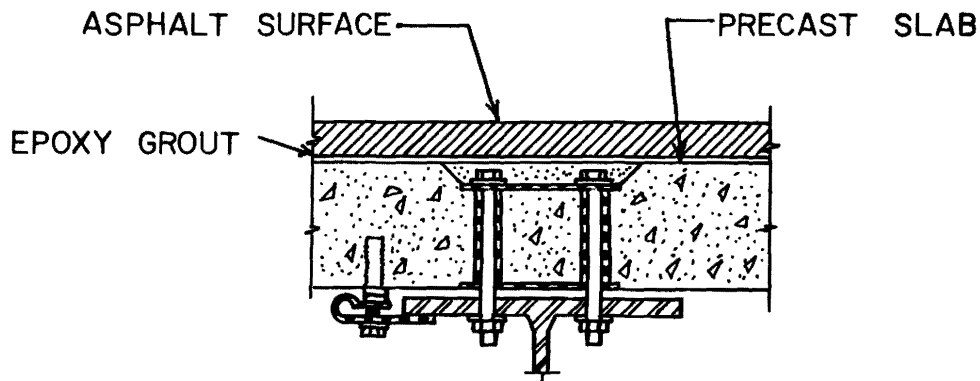


FIG. 3. Bolted Connection Details, Amsterdam, New York. New York Thruway Authority (2).

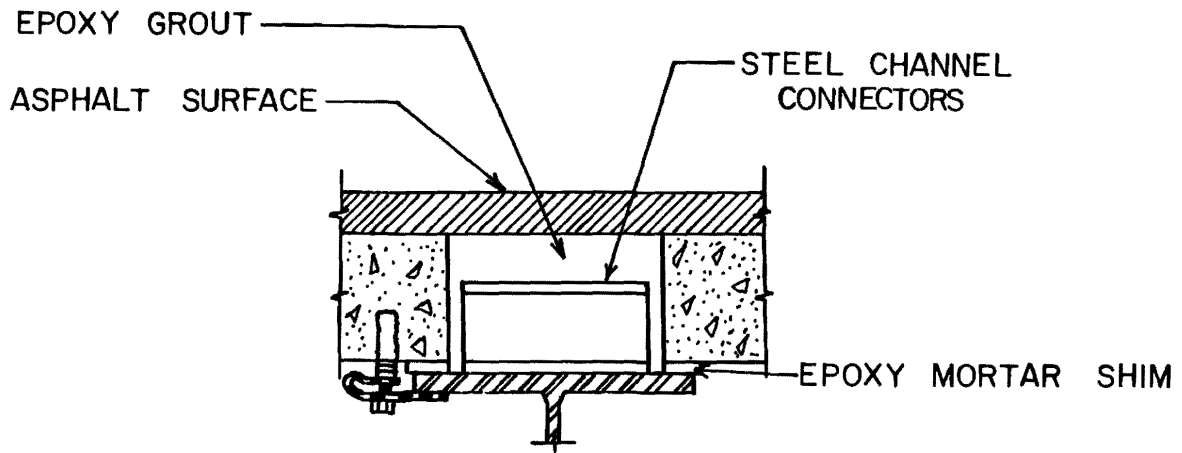


FIG. 4. Welded Channel Connection Details, Amsterdam, New York. New York Thruway Authority (2).

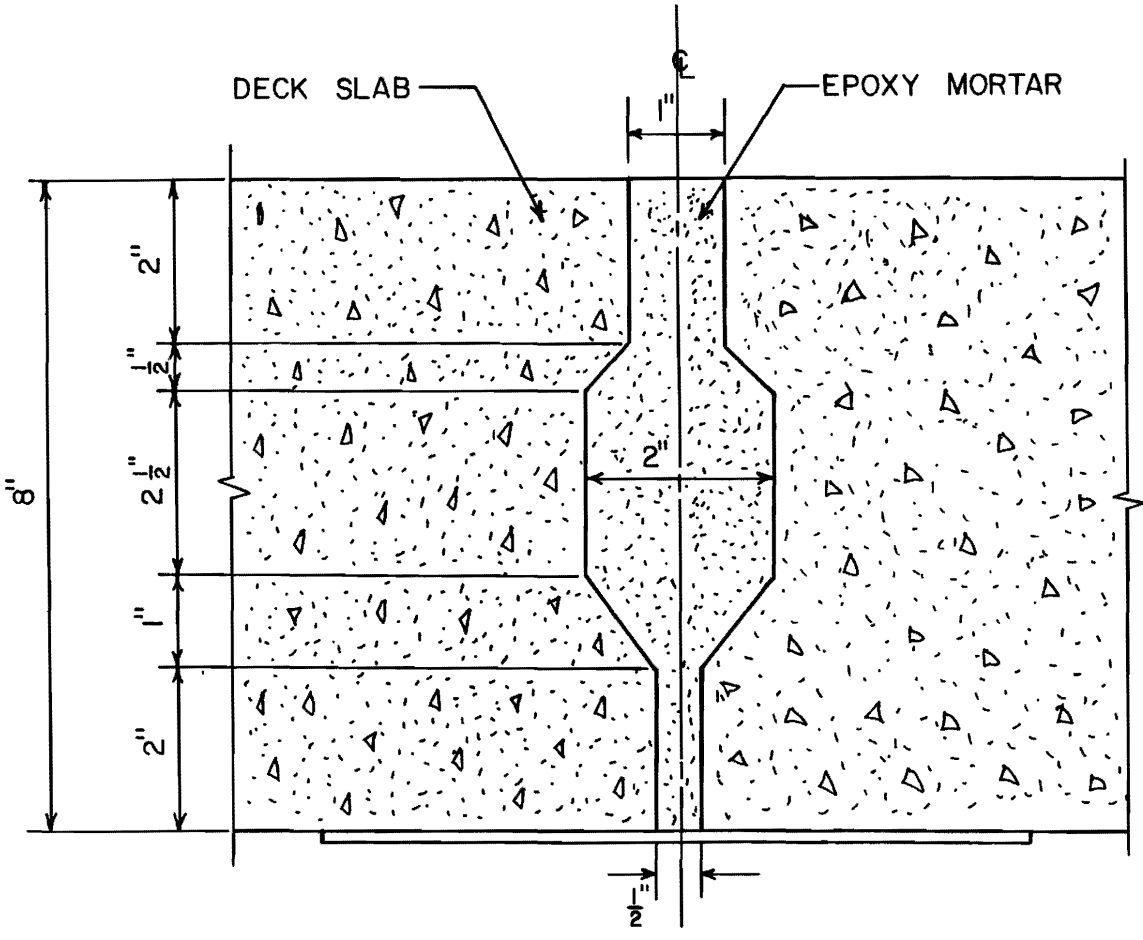
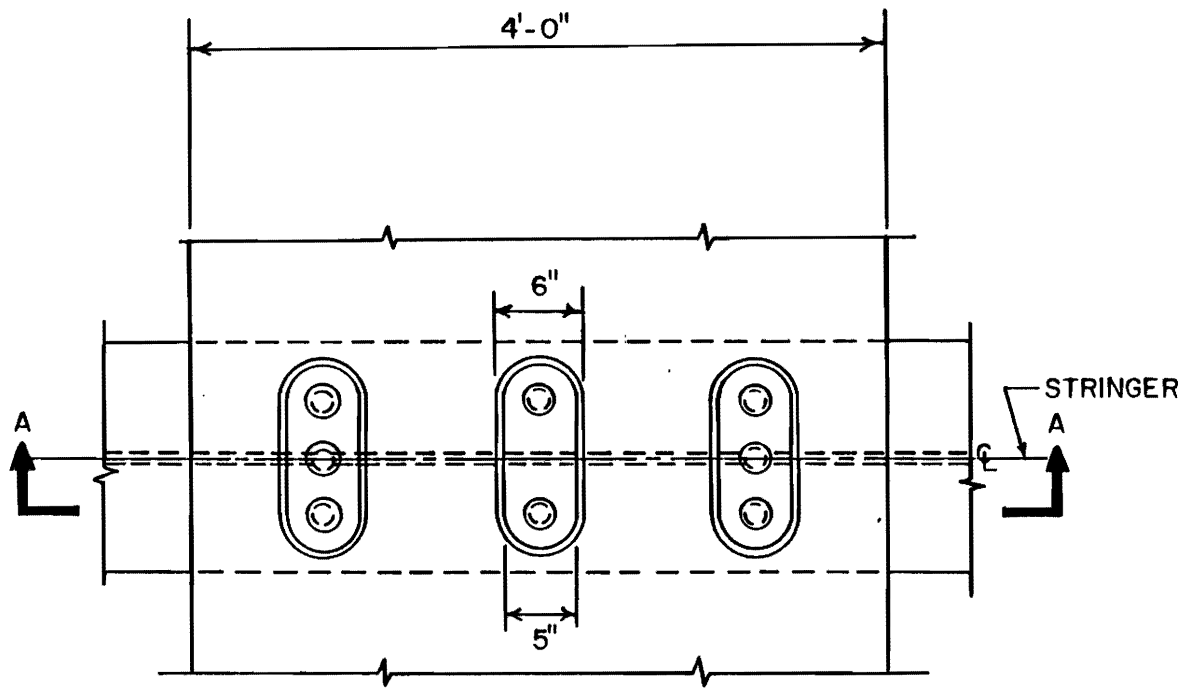
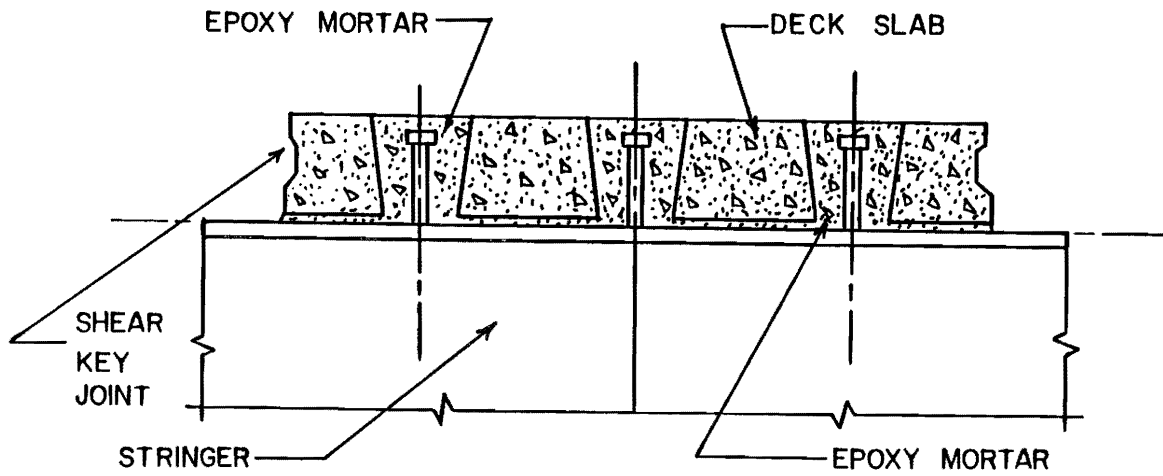


FIG. 5. Shear Key Joint Details. New York Thruway Authority (2).



(a) PLAN



(b) SECTION A-A

FIG. 6. Welded Stud Connection Details, Albany, New York. New York Thruway Authority (2,3).

not fit level on the beam flanges, therefore epoxy mortar was used to level the panels on the beam flanges.

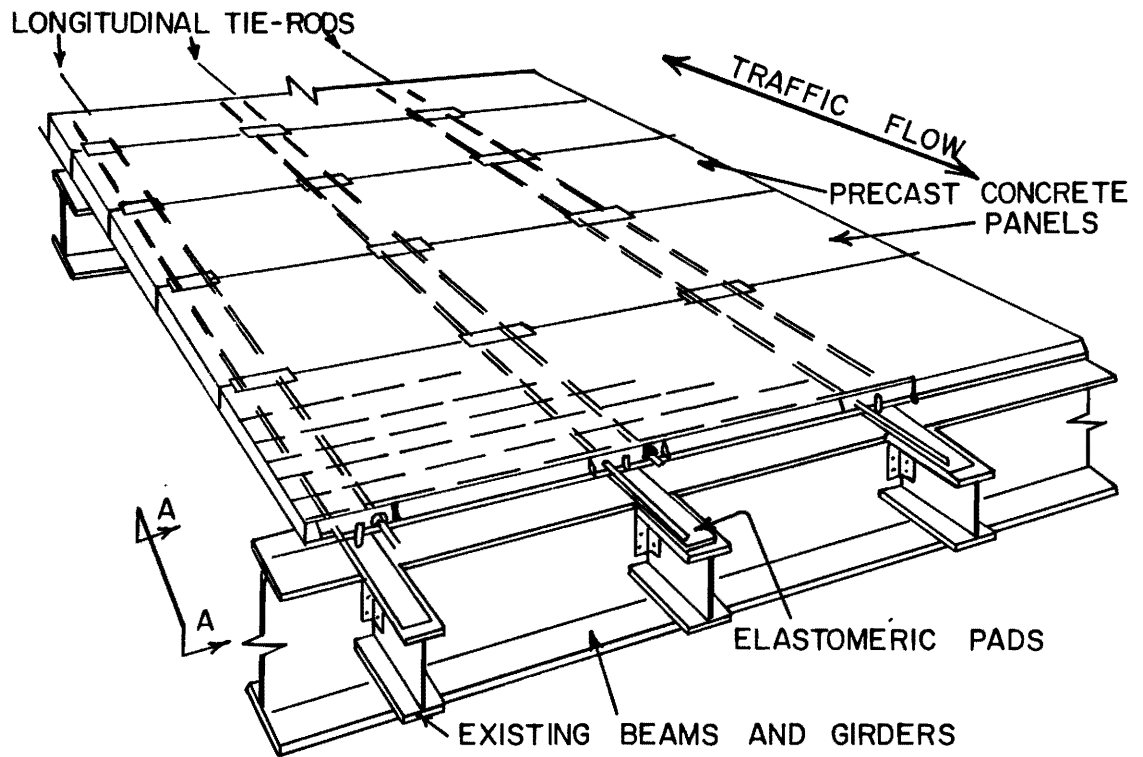
New York State Department of Transportation

The New York State Department of Transportation has replaced deteriorated concrete decks on several steel bridges with precast concrete panels (17). The first one was a 1040 ft long suspension bridge over Rondout Creek near Kingston, New York. The precast deck was chosen because of the need to load and unload the suspension bridge in a certain sequence, as well as the need for fast replacement. The precast panels were 9 ft long by 24 ft wide. The connection with adjacent panels was a V-shaped male-female joint with no grouting. The panels were bolted together longitudinally with tie rods. Details are shown in Fig. 7.

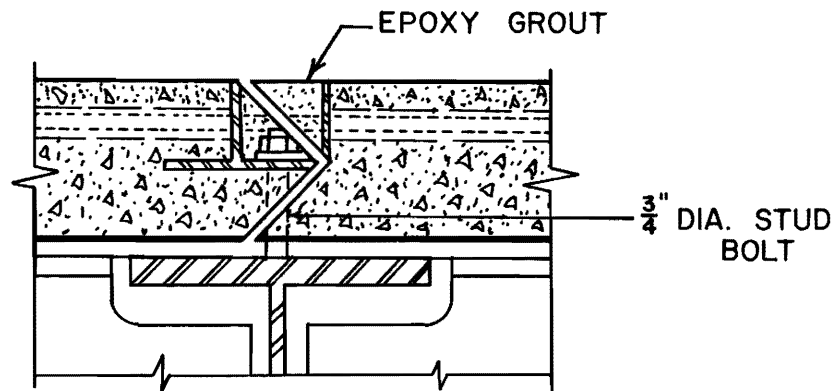
Another application of this method of construction was a three-span bridge over the Delaware River between Sullivan County, New York and Wayne County, Pennsylvania. This 675-ft structure has precast concrete panels 7 ft 6 in. long by 13 ft 10-1/2 in. wide, joined together transversely and longitudinally at the centerline by epoxy shear keys. A single welded steel stud at two points on each panel was used as the connection to the steel stringers to keep the panels together and was not designed as a shear transfer mechanism with adjacent steel stringers. Details are shown in Fig. 8.

Another bridge is in southern Erie County, New York, and it is also a three-span bridge 540 ft long. It was built in 1979. The panels were 8 ft by 22 ft, with transverse and longitudinal centerline joints identical to those used in the Delaware River bridge. The attachment of the panels to the stringers is somewhat different as shown in Fig. 9.

The biggest bridge deck replacement reported by the New York State Department of Transportation is on the Batchelerville bridge at County Road 98 across Great Sacandaga Lake, Saratoga County, New York. This bridge consists of 21 spans and is 3075 ft long, as illustrated in Fig. 10. The connection between adjacent panels was a flat joint grouted with epoxy mortar, as shown in Fig. 11. On this project the contractor was allowed to

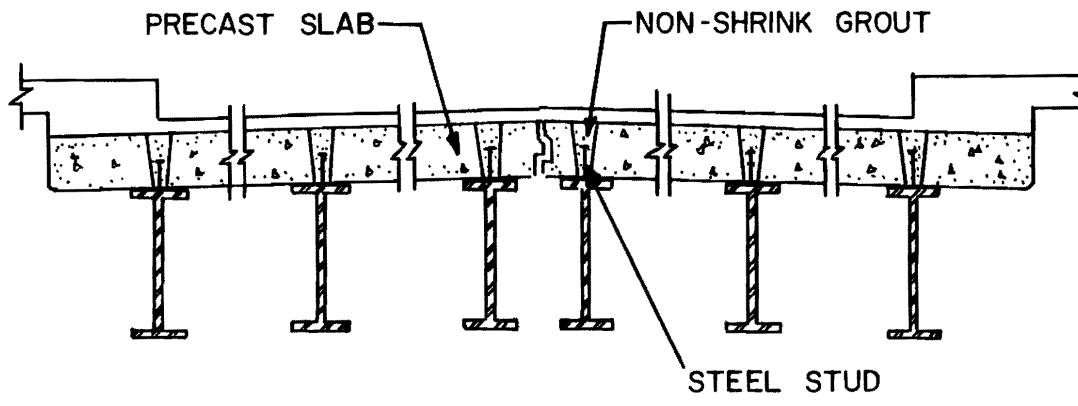


(a) SCHEMATIC SHOWING CONSTRUCTION

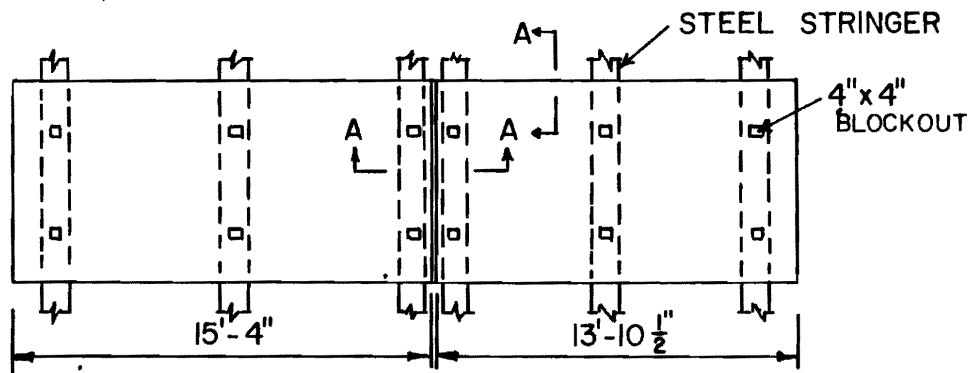


(b) SECTION A-A

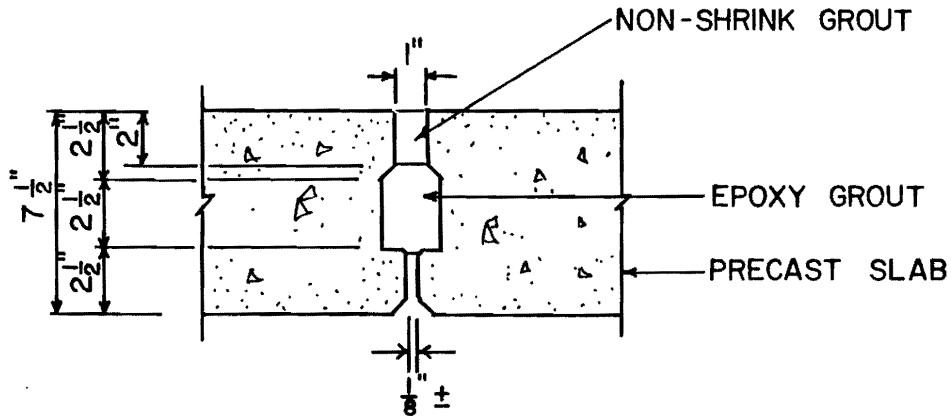
FIG. 7. Roundout Creek Bridge Deck, Kingston, New York. New York State Department of Transportation (17).



(a) TRANSVERSE SECTION



(b) PLAN



(c) SECTION A-A

FIG. 8. Delaware River Bridge, New York-Pennsylvania. New York State Department of Transportation (17).

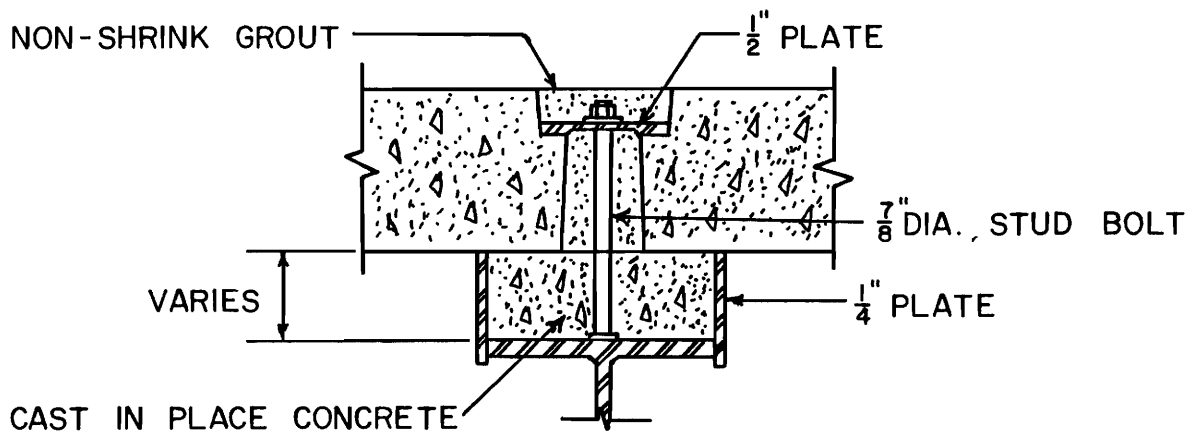


FIG. 9. Erie County Bridge Deck Connection Details, New York.
 New York State Department of Transportation (17).

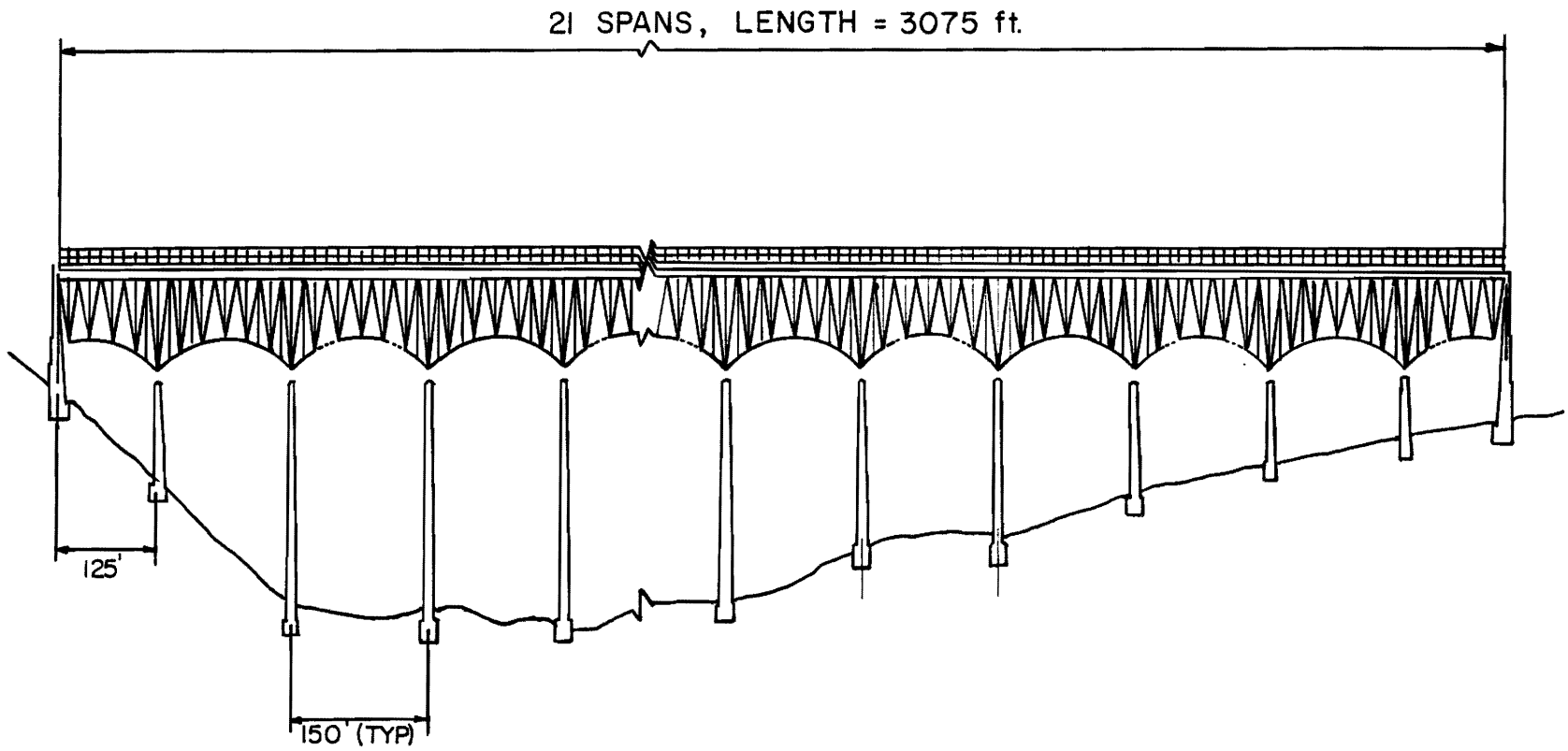
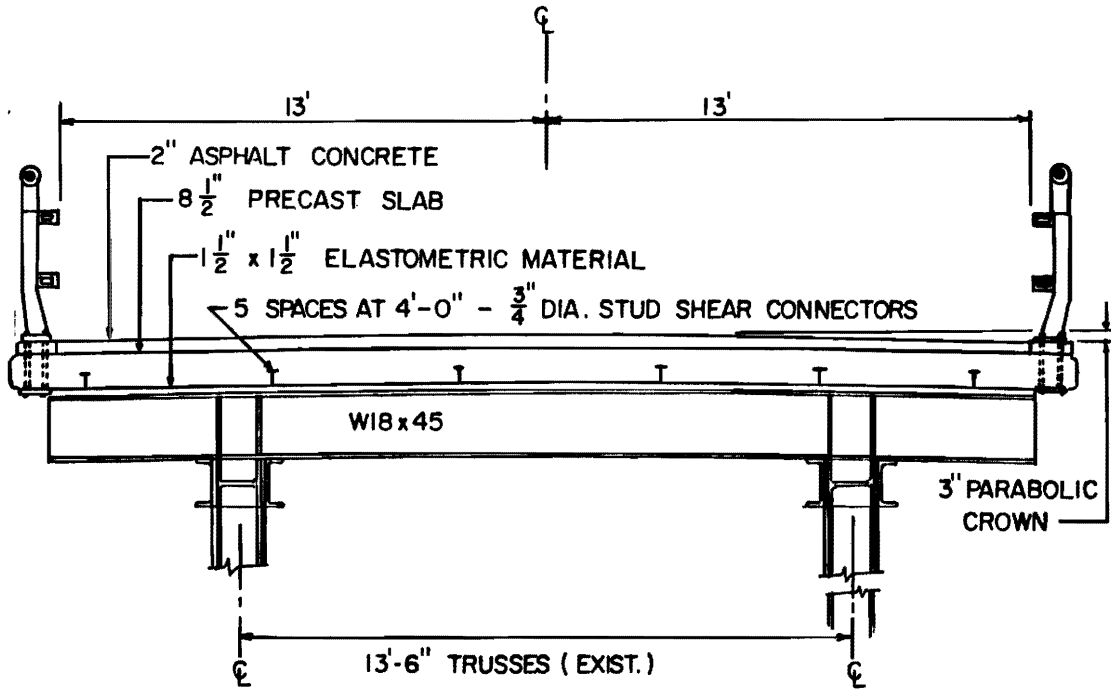
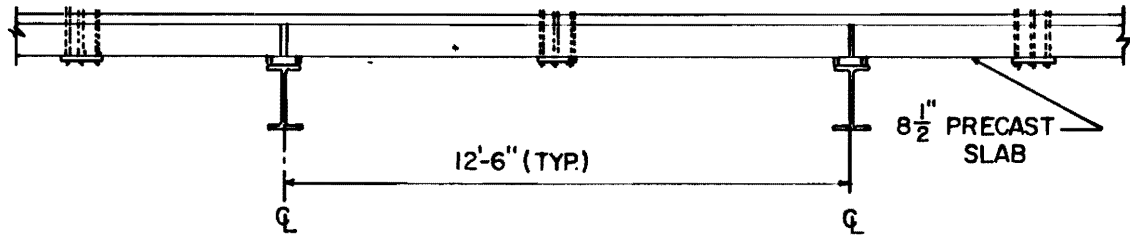


FIG. 10. Batchelerville Bridge, Saratoga County, New York.
New York State Department of Transportation.



TRANSVERSE SECTION



LONGITUDINAL SECTION

FIG. 11. Batchelerville Bridge Details, Saratoga County, New York. New York State Department of Transportation.

select either cast-in-place or precast concrete deck replacement. He selected the second option.

Pennsylvania Turnpike Commission

The Pennsylvania Turnpike Commission used precast concrete panels to rehabilitate the deteriorated deck of Clark's Summit bridge in Lackawanna County, Pennsylvania (8). This bridge is a 1627-ft-long girder structure. After removal of the old deck, the top flanges of the steel stringers were sandblasted. An epoxy coat was applied to the sandblasted steel to receive neoprene elastomeric strips. Epoxy mortar with a slight overfill was placed and retained between the elastomeric strips which served as a levelling device. Inserts and bolts were used to secure the precast panels to the stringers, as shown in Fig. 12. The panels were bolted longitudinally, and a nonshrink grout was placed in the shear key joints between adjacent panels. The precast concrete deck was not designed for composite action with the stringers, although it is very likely that some composite action may have developed because of the adhesive strength of the epoxy mortar (14).

Interstate 80 Overpass, Oakland, California

On this project from 60 to 80 ft of deteriorated concrete deck, 12 ft wide, was removed daily, leaving the girders bare (17). The new precast concrete panels, 30 to 40 ft long, were cast near the site and transported by truck to the installation area. Pocket holes were formed in the panels, and four shear steel stud connectors were welded to the steel girders through each hole. This connection is very similar to the one used by the New York Thruway Authority at Albany, New York, with the difference being that fast-setting sand cement grout was used instead of epoxy mortar. The levelling device for the precast panels was composed of bolts that were turned into threaded sockets cast in the panels. Traffic interference was minimal.

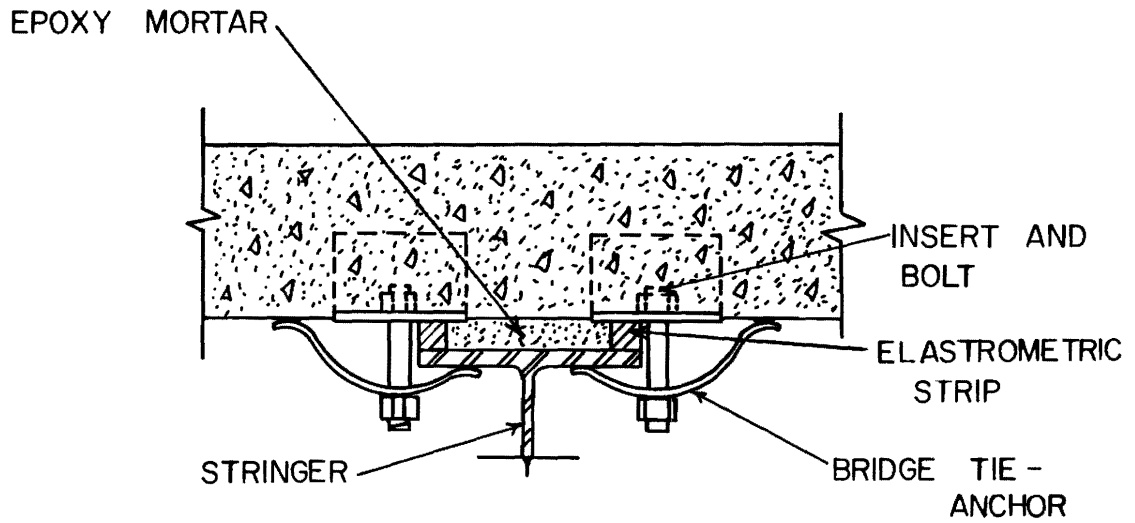


FIG. 12. Precast Panel Connection Details, Clark's Summit Bridge, Pennsylvania. Pennsylvania Turnpike Commission (8,17).

Maryland State Highway Administration-Federal Highway Administration

The Maryland State Highway Administration and the Federal Highway Administration awarded a contract in July, 1982, for the concrete deck replacement of the 5900-ft-long Woodrow Wilson Memorial bridge (5). This bridge is located over the Potomac River south of Washington, D.C.

This bridge mainly consists of four steel girder sections that are continuous over two, three and four spans. The individual spans vary in length from 62 ft to 184 ft. Floorbeams between girders are spaced between 16 ft and 26 ft and carry five rolled beam stringers per roadway continuous over the floorbeams.

The new deck consists of precast transversely post-tensioned lightweight concrete panels as illustrated in Fig. 13. The panels are supported on the exterior girders and the existing continuous stringer by pour-in-place polymer concrete bearing pads.

The new deck will yield two 44-ft roadways. The dimensions of the precast panels are 46 ft 7-1/4 in. wide, 10 to 12 ft long, 8 in. thick and have a 5 in. haunch at the exterior girder, as illustrated in Fig. 14. The panels are longitudinally post-tensioned in segments from 140 to 285 ft in length, which generally corresponds to the continuous girder unit length. The principal function of the longitudinal post-tensioning is the virtual elimination of transverse joints. The transverse post-tensioning is the primary component of the panels' structural design. The connection between adjacent panels is a transverse joint which is filled with polymer concrete immediately prior to longitudinal post-tensioning, as shown in Fig. 15.

The most significant aspect of this project is that traffic interference is minimized. Single-lane, two-way traffic is maintained on one roadway for the full length of the bridge during nighttime work periods, and six lanes of traffic are provided during peak hours. This construction started in December 1982 and completed in September 1983.

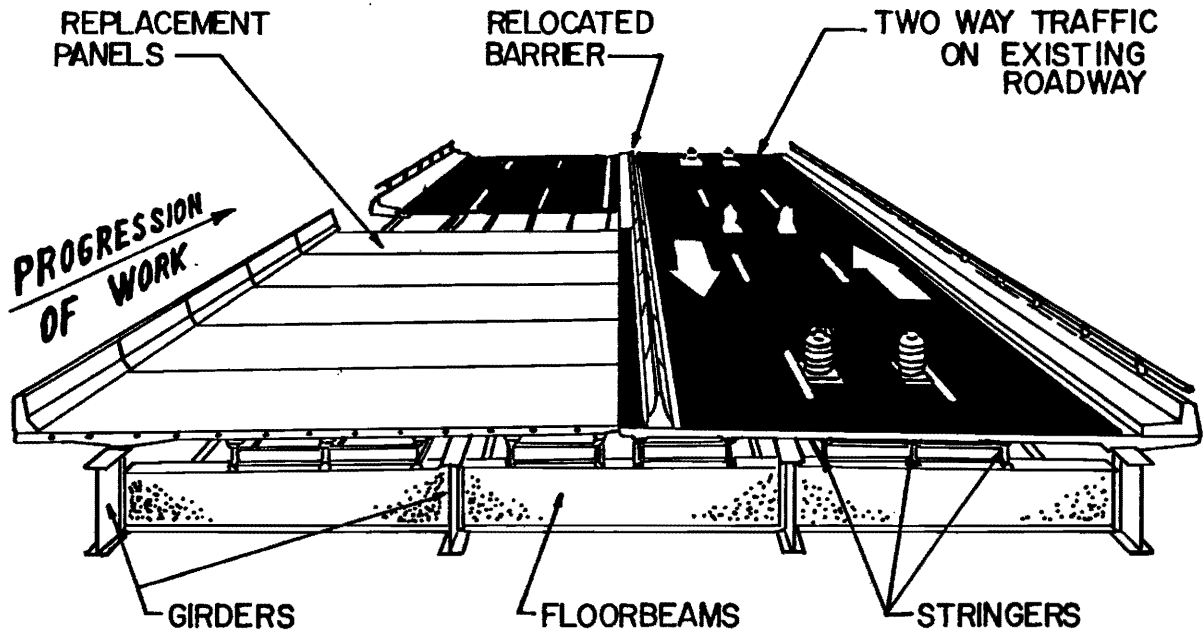


FIG. 13. Schematic of Woodrow Wilson Memorial Bridge Deck Replacement. Maryland State Highway Administration-Federal Highway Administration (5).

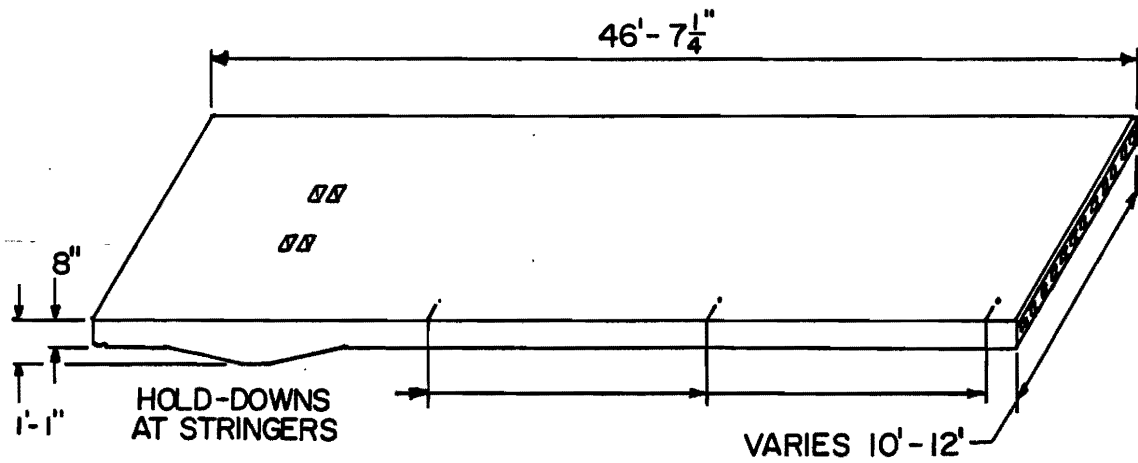


FIG. 14. Typical Panel, Woodrow Wilson Memorial Bridge (5).

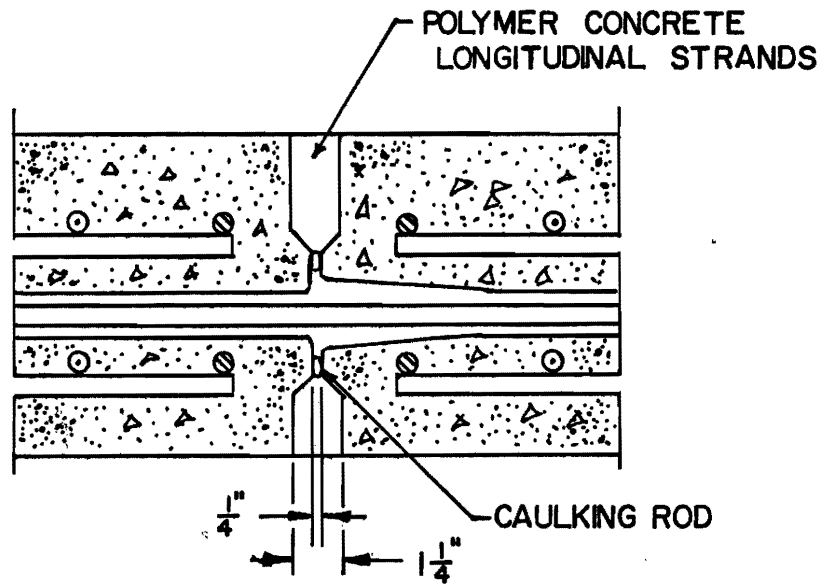


FIG. 15. Panel-to-Panel Joint Details, Woodrow Wilson Memorial Bridge (5).

Summary

Of the several projects using precast concrete panels on steel girders, some were designed so that the deck acts compositely with steel systems, and some were designed to be noncomposite. The New York Thruway projects are good examples of assuring composite action by means of mechanical shear connectors between the precast deck and steel stringers. The adhesive strength of epoxy mortar was neglected in their design. Although it has been reported by the Indiana State Highway Commission that composite action between panels and steel systems is developed by epoxy mortar (17), the composite action developed is something that cannot be relied upon, because of the extremely high quality control requirements in placing the epoxy mortar, especially under field conditions. Therefore, if the structure is required to develop composite behavior, mechanical shear connectors must be used. The additional strength of the epoxy mortar, if developed, can be taken into account only for additional safety.

Of the panel to panel connection designs reviewed, it seems that the most appropriate is the shear key joint used in the New York Thruway projects. No spalling has been reported in this type of joint, and it provides a means of transfer of normal forces between panels to assure full composite action between the precast deck and steel systems.

Objectives of Study

The objectives of this study were:

- 1) Evaluate the effectiveness of a number of structural details and construction procedures for precast concrete panels to be used in rapid bridge deck replacement.
- 2) Design and construct a structural model that simulates a steel stringer bridge with precast concrete panels connected to obtain composite interaction in the structure.
- 3) Obtain flexural strain distribution, shear strain distribution, and deflection data to quantify the amount of composite action achieved in the structural model under static loading.

Scope of Study

The experimental work of this study was limited to a scaled laboratory structural model. A total of three major static load tests were conducted without taking the structural model to yield or failure:

- 1) Static load test on the steel stringers of the model.
- 2) Static load test on the model with precast concrete panels grouted with epoxy mortar at the pocket connections.
- 3) Static load test on the model with the pocket connections and the shear keys grouted with epoxy mortar.

Dead load stresses are carried by the steel stringers and are not scaled. However, live load stresses, which are taken by a composite cross section, are scaled. Tests 2 and 3 were done 24 hours after the epoxy mortar was poured.

CHAPTER II

EXPERIMENTAL WORK

General

The experimental work involves the design and construction of a 1/3 scale structural model of a typical prototype bridge consisting of steel stringers and precast concrete panels. The bridge model was instrumented to obtain flexural strain, shear strain and deflection data under static loading.

Selection of Prototype Bridge

A typical prototype bridge was selected from the Texas highway system. The deteriorated deck would be replaced for precast concrete panels connected to act compositely with the steel stringers. The bridge is a 28-ft roadway, 60-ft-long steel stringer bridge built around the 1960's. The details were obtained from the Standard Drawings of Steel I-Beam Bridges of the Texas Highway Department (4) (now the State Department of Highways and Public Transportation). The bridge consists of four steel stringers spaced 8 ft apart. Each stringer is an old standard wide flange section 36 WF 150, with cover plates 3/4 in. thick, 10 in. wide, and 40 ft long welded in the middle portion of the beam to the top and bottom flanges. The actual span length is 58 ft 9 in. Details of the prototype bridge are shown in Fig. 16.

Because of the presence of the cover plates in the middle portion of the stringers, there are two different cross sections. The first cross section around midspan includes cover plates and has a moment of inertia of 14,032.7 in⁴. The second cross section near the supports does not include cover plates and has a moment of inertia of 9,012.1 in⁴ (10). Because of the significant difference in the inertia properties, both cross sections were considered in the study. Details and dimensions of both cross sections of the stringers are shown in Tables 1 and 2.

The stringers originally carry a 7-1/4 in. thick cast-in-place concrete slab that hypothetically is replaced with ten 6-ft long, 8 in. thick precast

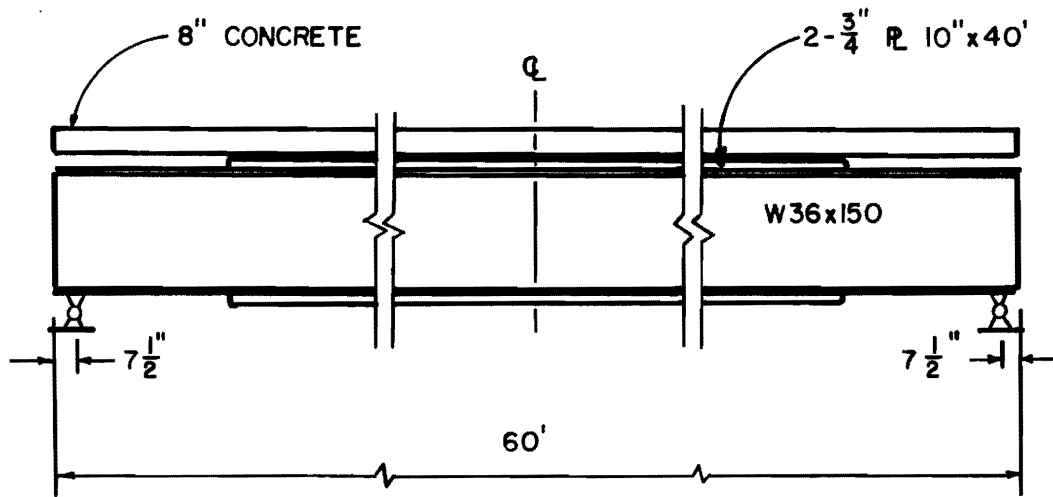
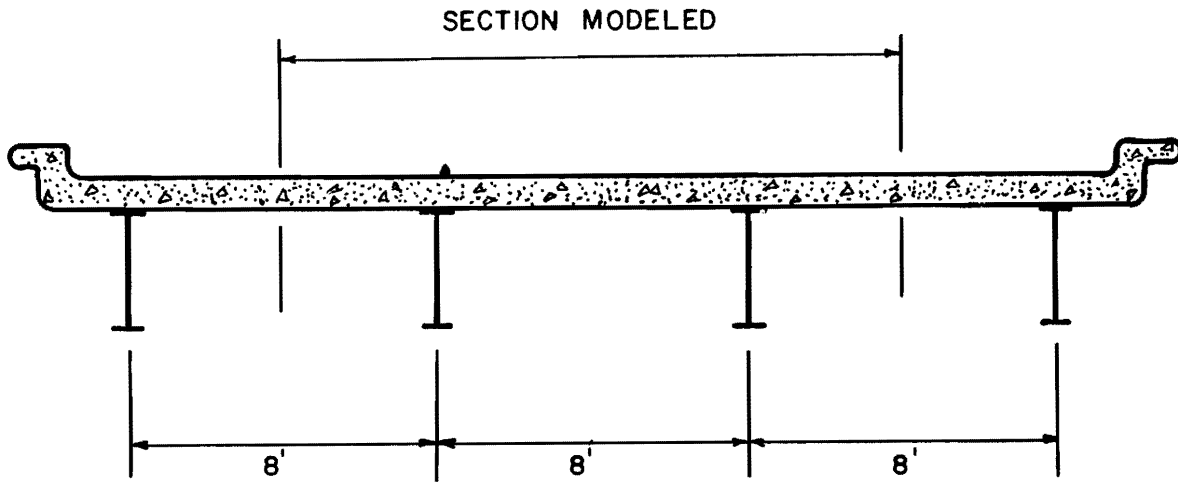


FIG.16. Details of Prototype Bridge. Texas Highway Department (4).

TABLE 1. Prototype Stringer Sectional Properties at Midspan,
36 WF 150 with Cover Plates (10).

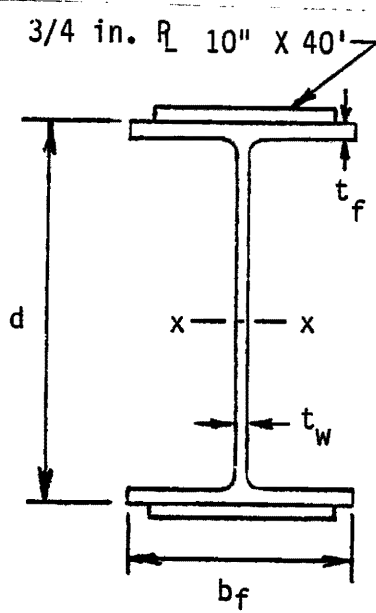
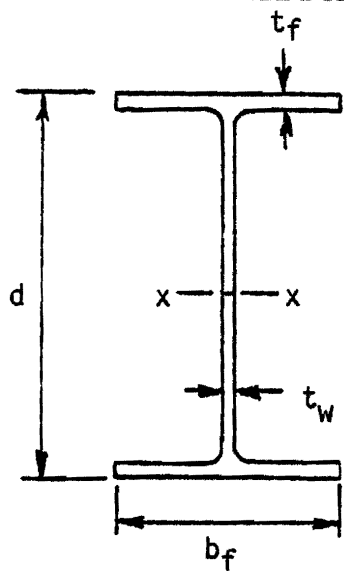
Stringer Cross Section Properties at Midspan (36 WF 150 with Cover Plates)	
 <p>3/4 in. PL 10" X 40'</p> <p>d</p> <p>t_f</p> <p>$x-x$</p> <p>t_w</p> <p>b_f</p>	<p>Area = 59.16 in²</p> <p>d = 35.84 in.</p> <p>b_f = 11.972 in.</p> <p>t_f = 0.940 in.</p> <p>t_w = 0.625 in.</p> <p>I_{x-x} = 14032.7 in⁴</p>

TABLE 2. Prototype Stringer Sectional Properties at Supports
36 WF 150 (10).

Stringer Cross Section Properties at Supports (36 WF 150)	
	<p>Area = 44.16 in²</p> <p>d = 35.84 in.</p> <p>b_f = 11.972 in.</p> <p>t_f = 0.940 in.</p> <p>t_w = 0.625 in.</p> <p>I_{x-x} = 9012.1 in⁴</p>

concrete panels. The bedding detail between the panels and the steel stringers typically forms a gap of 1/4 to 3/4 in. which is filled with epoxy mortar. This gap increases the inertia properties of the composite cross section.

The reinforcement of the prototype precast panels was designed to carry a 16,000-lb concentrated force equivalent to an HS20-44 truck wheel load according to the Standard Specifications of Highway Bridges of the American Association of State Highway and Transportation Officials (16). Table 3 summarizes the amount of steel required in the transverse and longitudinal directions at both the positive and negative moment regions.

Model Design

A structural model was designed based on the prototype described in the previous section using dimensional analysis. Appendix B shows the dimensional analysis. The model was designed so that strains and stresses in the model and prototype were equivalent. Two modified W 12 X 19 wide flange beams were used as stringers of the model. Welded wire fabric was used to simulate the steel reinforcement of the precast panels and a model concrete mix was designed to simulate the concrete mix used in the construction of bridge decks.

Table 4 lists the scale factors to obtain a true static model of the parameters considered in the prototype. Since the model and the prototype must be equivalent, the only independent scale factor is that of the linear dimensions. Mass densities were not considered because a composite section only carries live loads.

The materials used to fabricate the model were essentially the same materials found in a prototype bridge: steel, concrete and epoxy mortar.

Design of Model Stringers

In designing the steel beams of the model, priority was given to using standard wide flange beams. The option of having the beams fabricated with plates was considered, but the amount of welding involved would have made such fabrication impractical.

TABLE 3. Summary of the Reinforcement Meeting AASHTO Code Requirements.

	Transverse		Longitudinal	
	Top	Bottom	Top	Bottom
Area Required * $f_y = 60$ ksi	0.56	0.50	0.34	0.34
Gross Percent ρ_g	0.58	0.52	0.35	0.35
Percent of steel ρ	0.81	0.67	-	-
Spacing of # 4 bars, in inches	4-1/4	4-3/4	7	7

* in square inches per foot of slab

TABLE 4. Scale Factors for 1/3 Model Bridge.

Quantity	Dimensions	Scale Factors
Stress	FL^{-2}	1
Strain	-	1
Linear Dimension	L	3
Displacement	L	3
Reinforcing Steel Area	L^2	9
Shear Connector Area	L^2	9
Concentrated Load	F	9
Moment	FL	27
Moment of Inertia	L^4	81
Section Modulus	L^3	27
Young's Modulus	FL^{-2}	1

The procedures used in designing the steel beams were as follows:

1) The cross-sectional composite inertia properties of the prototype bridge were computed assuming a gap of 3/4 in. between the precast panels and the steel stringers, and a 5,000 psi strength concrete for the slab.

2) The composite inertia properties of the prototype were divided by their corresponding scale factors to obtain the ideal composite inertia properties for a true model.

3) The model steel stringers were designed to match the inertia properties desired for a true model.

It was realized that obtaining a true model and simulating all composite cross-sectional property requirements was impractical. Therefore, priority was given to obtain similitude in those parameters that control the design of the prototype bridge and precast panels.

Those cross-sectional parameters considered were:

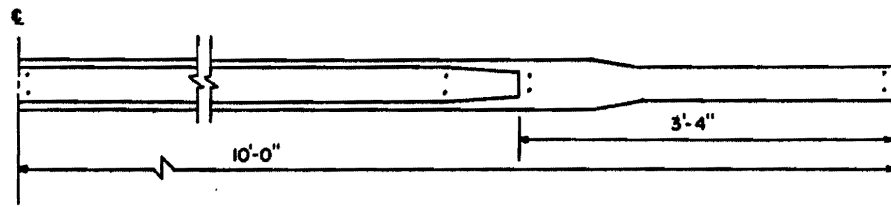
1) The moment of inertia of the transformed composite section I , which controls deflections, stresses and strains.

2) The first moment of area, Q , about the neutral axis of the composite section of the transformed compressive area which controls the horizontal shear forces at the level of the shear connectors.

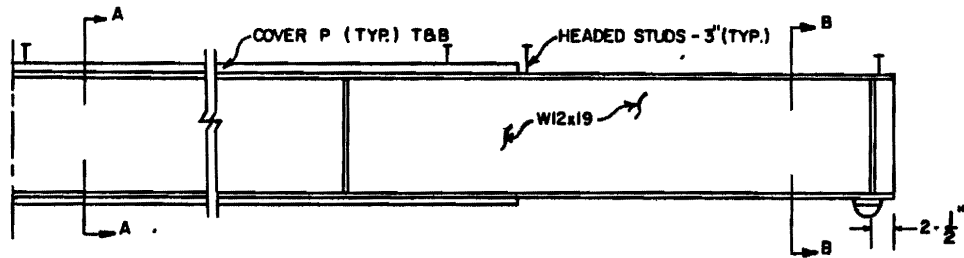
3) The composite section modulus at the top surface of the panels, S_{top} , which is critical for the flexural stresses and strains at this surface.

4) The composite section modulus at the bottom surface of the steel stringers, S_{bot} , which controls the design of the steel stringer in the prototype.

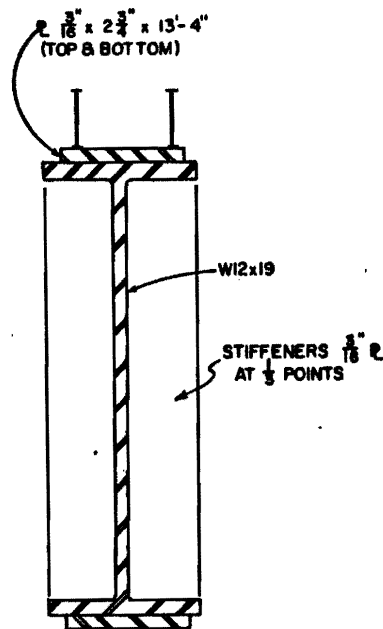
Because of the problems anticipated in fabricating the steel beams from plates, modified standard W 12 X 19 wide flange beams were selected. The final design calls for 3/16 in. thick, 2-3/4 in. wide, 13 ft 4 in. long cover plates welded to the top and bottom flanges, and a 3/8 in. wide, 34-1/2 in. long strip removed from the four edges of the flanges at the end sections. Details of the design are illustrated in Fig. 17. The calculations of the design inertia properties of the prototype and model are shown in Appendix C. The values of the composite cross-sectional properties of the prototype, the ideal model and the design model are tabulated in Table 5.



(a) HALF-PLAN

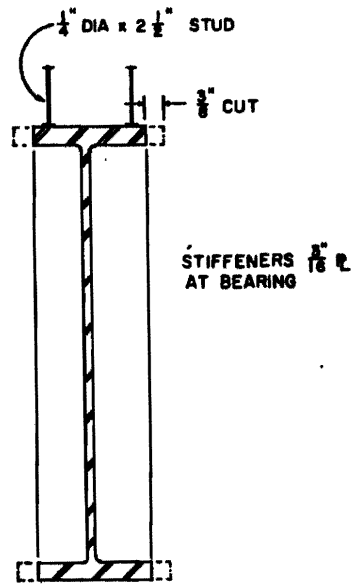


(b) HALF-ELEVATION



SEC-A

(c)



SEC-B

(d)

FIG. 17. Details of Model Stringers.

TABLE 5. Composite Sectional Properties of Prototype, 1/3 Ideal Model, and 1/3 Design Model at the Middle and End Sections.

	Composite Sectional Parameter	Prototype	1/3 Ideal Model	1/3 Design Model
M I D S E C T I O N S	I, in inches ⁴	34370.	424.32	424.06
	Q, in inches ³	871.32	32.27	32.55
	S _{top} , in inches ³	2878.08	106.04	105.92
	S _{bot} , in inches ³	1029.1	38.11	37.87
	I/Q, in inches	39.45	13.15	13.03
E N D S E C T I O N S	I, in inches ⁴	25778.7	318.26	324.78
	Q, in inches ³	713.77	26.43	27.08
	S _{top} , in inches ³	2453.7	90.88	91.37
	S _{bot} , in inches ³	756.32	28.01	28.34
	I/Q, in inches	36.12	12.038	11.99

The values of the ideal model were obtained by dividing the values of the section properties of the prototype by their respective scaling factors. The design of the model was performed to try to match the inertia properties of the ideal model.

Design of Shear Connectors

Standard shear connectors were provided to connect the precast panels to the model stringers. Normally, the shear connectors provided in a bridge shall be designed on the basis of fatigue and then checked on the basis of ultimate strength. The amount of mechanical shear connectors to be placed in the models do not comply with either fatigue or ultimate strength requirements called by the AASHTO bridge specifications (16).

These specifications, although shall be rigorously met for all composite bridges, do not consider composite interaction achieved by means of adhesion. For the purpose of this experiment, it was determined that the amount of shear connectors would not be critical for the test results because most of the horizontal shear forces would be transmitted by the epoxy mortar that would be placed in the concrete-stringer interface and not by the steel connectors.

Furthermore, it was also decided that, for a planned subsequent ultimate load experiment on the same model, it would be more appropriate to force an overall failure by first fracturing the interface bond and second yielding the shear connectors. These data could then be compared to data gathered with push-out experiments.

Therefore, considering the above discussions, 1/4-in. diameter by 3-1/2 in. long standard headed stud connectors were selected. These connectors are to be placed in pairs, 1.75 in. apart and spaced every six inches. Nonetheless, neglecting the interface adhesive bond, the ultimate load capacity provided by the shear connectors alone in a third-point loading condition, is expected to be higher than the loads to be applied in this experiment.

Design of Precast Panels

The design of the precast concrete panels of the model called for a nominal length of 2 ft, a thickness of 2.67 in. and a width of 64 in. These were 1/3 scale dimensions of the precast panels of the prototype bridge. Typical length dimensions of precast concrete panels that have been used in replacement of decks vary from 4 ft to 12 ft. The selected 6 ft. wide prototype panels are realistic, falling within the range of width dimensions that have already been used by some highway agencies.

The details of the precast panels of the model are related to connections to the steel systems and to adjacent slabs. Each panel has four molded tapered pocket holes per stringer, spaced 6 in. apart, to allow room for the shear connectors as illustrated in Fig. 18. The panel also has a groove at the long sides of the panel, so that when two panels are placed adjacent to each other, they form the 3/8 in. shear key joint shown in Fig. 19, which is filled with epoxy mortar. The geometry of this shear key joint

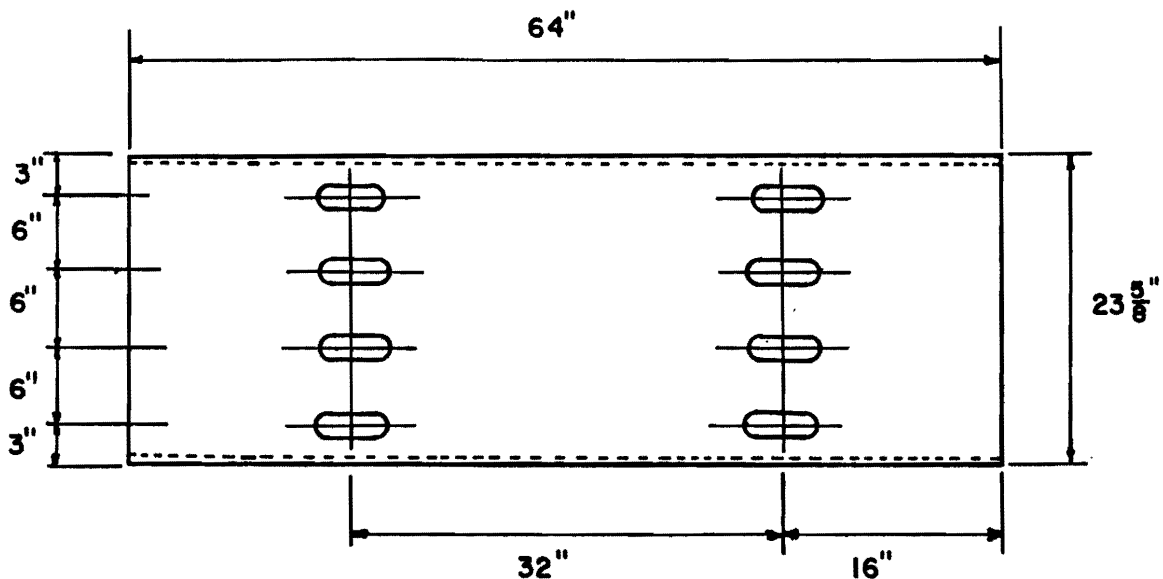


FIG. 18. Model Precast Concrete Panel Details.

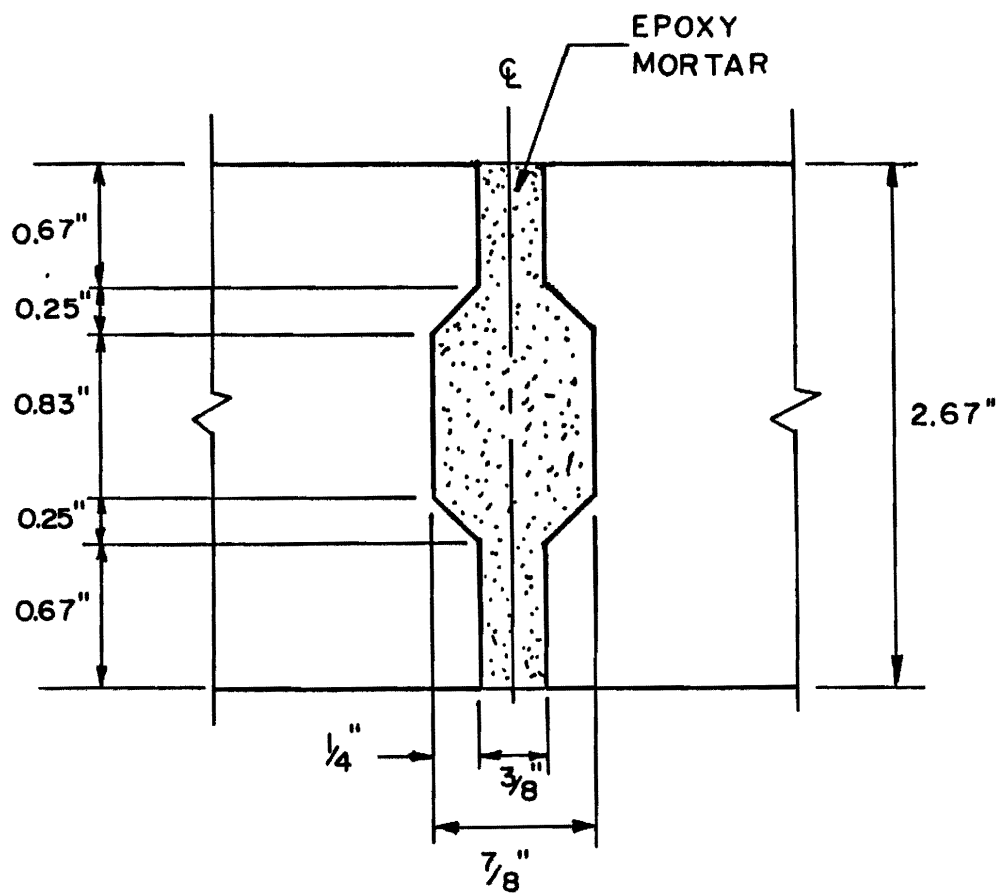


FIG. 19. Model Shear Key Joint Details.

was slightly varied from that of the prototype. The shear key of the prototype usually has a wider gap at the top surface of the panels to facilitate pouring of the epoxy mortar, and a narrower gap at the bottom surface to hold the epoxy in place. Because of difficulties in forming, the dimension of this gap in the model is the same at the top and bottom surfaces.

Design of Reinforcing Steel

The amount of reinforcing steel in the panels was designed to scale the longitudinal reinforcement required by the AASHTO specifications.

Instead of simulating every single reinforcing bar of the prototype, the gross area of reinforcement was scaled. This was done by dividing the amount of reinforcing steel required in the longitudinal direction by its corresponding scale factor to obtain the amount of reinforcement to be provided in the model. The area of steel reinforcement required in the longitudinal direction in the prototype is 0.36 in.² per foot of slab. The area of reinforcing steel provided in the model is 0.12 in.² per foot of slab.

The steel reinforcement in the model was provided in the form of welded wire fabric. The mesh selected was a 3.X 3.-D3 X D3 that consists of 60-ksi deformed steel wires, 0.195 in. in diameter, spaced at 3 in. both longitudinally and transversely.

The amount of steel reinforcement provided in precast panels of the model is the same in the transverse and longitudinal direction. The percentage of steel with respect to the gross area of concrete in the model is 0.38 percent. The percentage of steel in the transverse direction did not simulate the transverse prototype reinforcement meeting the AASHTO Specifications. However, it exceeded the requirements of a more liberal design code, the Ontario Highway Bridge Design Code (12). Table 6 shows the percent of reinforcing steel designed for the model compared to the percentages required by the AASHTO and Ontario Codes.

TABLE 6. Reinforcement Provided in the 1/3 Model Compared to AASHTO and Ontario Bridge Codes Requirements.

		Design meeting AASHTO Code $f_y=60$ ksi, 8-inch slab	Design meeting Ontario Code $f_y= 60$ ksi, 8-inch slab	1/3 Model, Welded Wire Fabric 3 X 3-D3 XD3
Transverse Top	A_s^*	0.56	0.30	0.12
	ρ_g	.0058	.0031	.0038
	Reinf.	#4 @ 4-1/4"	#4 @ 8"	D3 @ 3"***
Transverse Bottom	A_s	0.50	0.30	0.12
	ρ_g	.0052	.0031	.0038
	Reinf.	#4 @ 4-3/4"	#4 @ 8"	D3 @ 3"
Longitudinal Top	A_s	0.38	0.30	0.12
	ρ_g	.0039	.0031	.0038
	Reinf.	#4 @ 6-1/4"	#4 @ 8"	D3 @ 3"
Longitudinal Bottom	A_s	0.34	0.30	0.12
	ρ_g	.0035	.0031	.0038
	Reinf.	#4 @ 7"	#4 @ 8"	D3 @ 3"

* in square inches per foot of slab

** Area of a D3 bar is 0.03 square inches

Design of Model Concrete

A concrete mix for the precast panels of the model was designed to meet geometric and material requirements for similitude. The geometric requirement is satisfied by scaling the aggregate sizes. The material requirement is that the moduli of elasticity of the materials used in the prototype must be equivalent to those of the materials used in the model. This can be easily accomplished in steel; but, in concrete, the modulus of elasticity is a function of many variables, making scaling difficult. For this reason it was satisfactory to obtain a modulus of elasticity between 3.0×10^6 and 4.0×10^6 psi in the concrete, which is the typical range frequently encountered in concrete mixes.

To scale the size of the aggregates in the prototype, the grading requirements for coarse and fine aggregates for concrete mixes were obtained from the AASHTO Specifications for Transportation Materials (15). The top size of the coarse aggregate was selected to be 3/4 in. Such gradation requirements are tabulated in Table 7.

The grading requirements yield two envelopes, and the grading of the specific coarse and fine aggregates must lie within its respective envelope.

Instead of having specific aggregates to simulate, the sieve linear dimensions in the grading charts were divided by the geometric scale factor of three to generate two shifted envelopes that represent the grading limits of the aggregates of the model concrete mix. Consequently, coarse and fine aggregates falling within these shifted envelopes needed to be located.

The coarse aggregate that was found the closest to the grading limits of the model was a 3/8-in. Bryco pea gravel after passing through a 3/8 in. sieve to remove large particles.

After the removal of the larger particles, five samples were taken to obtain an average gradation for this gravel. The results of the sieve analyses are shown in Table 8. The average grading was plotted and is shown in Fig. 20. It can be observed that the grading curve for the coarse aggregate selected for the model fell closely within the required scaled limits.

TABLE 7. AASHTO Grading Requirements for 3/4 in. Coarse Aggregate, and Fine Concrete Sand (15).

Sieve No. or size	Percent Passing by weight	
	3/4" Coarse Aggregate	Fine Aggregate
1 in.	100	-
3/4 in.	90-100	-
3/8 in.	20-55	100
No. 4	0-10	95-100
No. 8	0-5	-
No. 16	-	45-80
No. 50	-	10-30
No. 100	-	2-10

TABLE 8. Gradation Data for the 3/8 in. Bryco Pea Gravel.

Sample	Cumulative Percent Passing					
	No. 3/8	No. 1/4	No. 4	No. 8	No.16	No.20
1	100.0	96.52	70.68	6.26	1.26	.62
2	100.0	97.11	70.43	6.81	1.19	.63
3	100.0	96.40	71.11	6.01	1.20	.61
4	100.0	96.12	69.82	6.23	1.29	.59
5	100.0	96.70	70.60	6.24	1.25	.55
Average	100.0	96.57	70.52	6.31	1.24	.60

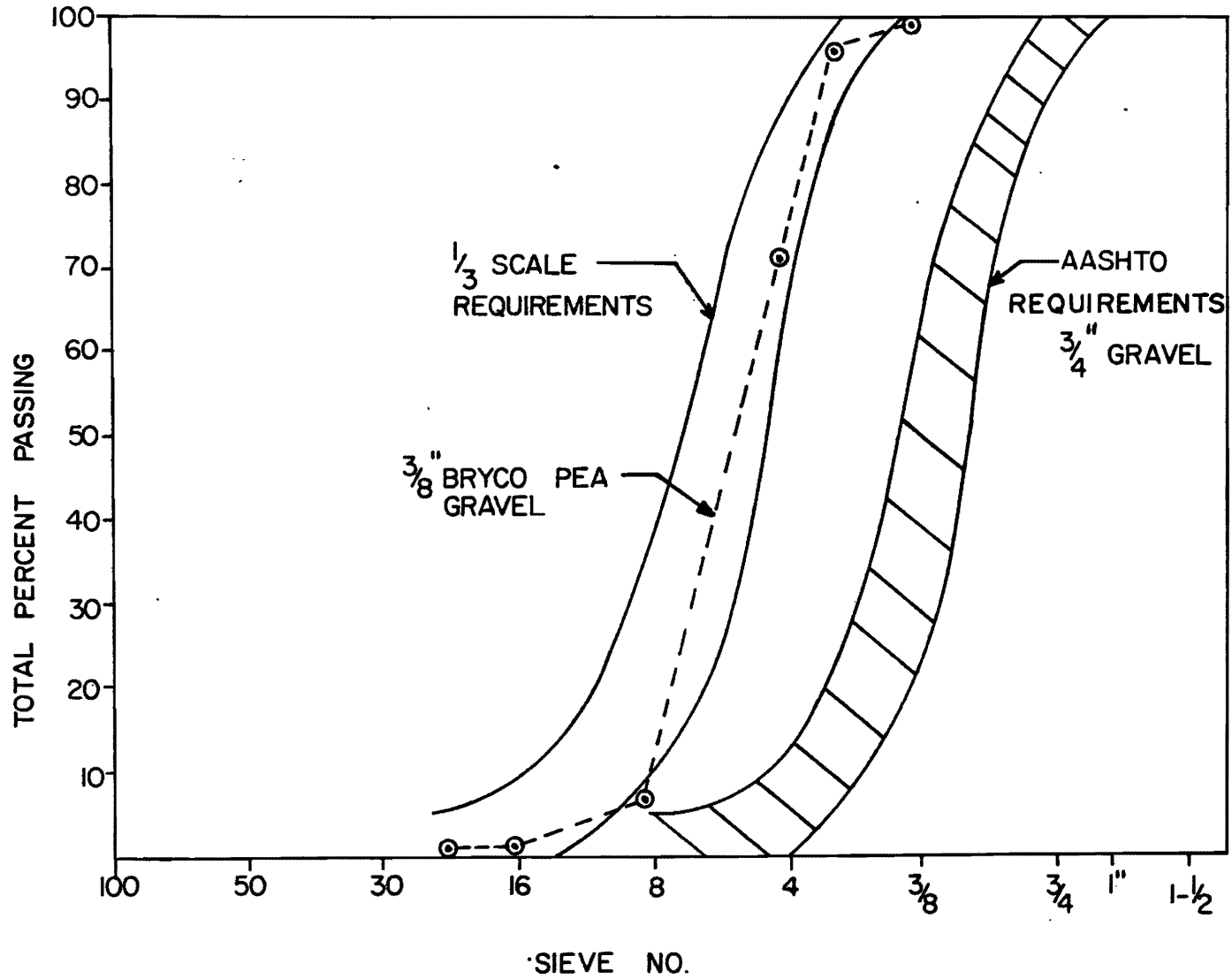


FIG. 20. Gradation Chart of 3/8 in. Bryco Pea Gravel.

The fine aggregate that was selected to be used in the model satisfies the scaled grading limits only for larger particles. The finer particles fell outside, to the right, of the gradation requirements. However, this aggregate was very satisfactory because had the grading limits been completely met, the amount of finer particles would have been large enough to increase the water requirements in the concrete mix of the model. The sand selected was a fine masonry Bryco sand. The gradation data for the sieve analyses of this sand is tabulated in Table 9, and is also shown in Fig. 21 along with the scaled grading limits.

After the aggregates for the model concrete were selected and obtained, laboratory batches were performed to determine the desired mix proportions of the model concrete in terms of workability. To fully satisfy similitude requirements, the same volume mix proportions need to be used in the prototype and in the model concrete. However, because of the reduced size of the aggregates in the model concrete, a higher water content was required to obtain a good workability; consequently, a higher cement factor was also required. Therefore, the mix proportions of the model concrete were determined in terms of workability. The mix proportions obtained from the laboratory are tabulated in Table 10. The cement factor for this model mix was quite high, 9.0 bags of cement per cubic yard of concrete.

Model Construction

The construction of the 1/3 scale model started with the casting of the precast concrete panels in plexiglass forms. The two model steel stringers were obtained from a steel fabricator.

Forms

In the fabrication of structural models, tolerances must be reduced in proportion to the scale utilized. This requires careful forming techniques. The forming methods that have been used in casting full scale panels were judged undesirable. Instead, plexiglass forms were used for the following reasons:

- 1) The transparency of plexiglass facilitates placement and visual inspection of the reinforcing steel and of the model concrete.

TABLE 9. Fine Masonry Sand Gradation Data.

Sample	Cumulative Percent Passing						Modulus
	No. 4	No. 8	No. 16	No. 30	No. 50	No. 100	
1	100.0	99.70	94.51	76.20	25.90	5.51	1.982
2	100.0	99.62	94.30	76.31	25.83	5.42	1.985
3	100.0	99.72	94.47	76.28	25.92	5.54	1.981
4	100.0	99.71	94.61	76.22	25.98	5.49	1.980
5	100.0	99.66	94.48	76.24	25.87	5.43	1.983
Average	100.0	99.68	94.47	76.25	25.90	5.48	1.982

TABLE 10. Design Volume Mix Proportions of Model Concrete.

Material	Design Percent Absolute Volume	Specific Gravity
Cement	16.1	3.15
Water	22.85	1.0
Fine Masonry Sand	34.9	2.62
3/8 in. Pea Gravel	23.1	2.6
Air	3.0	-

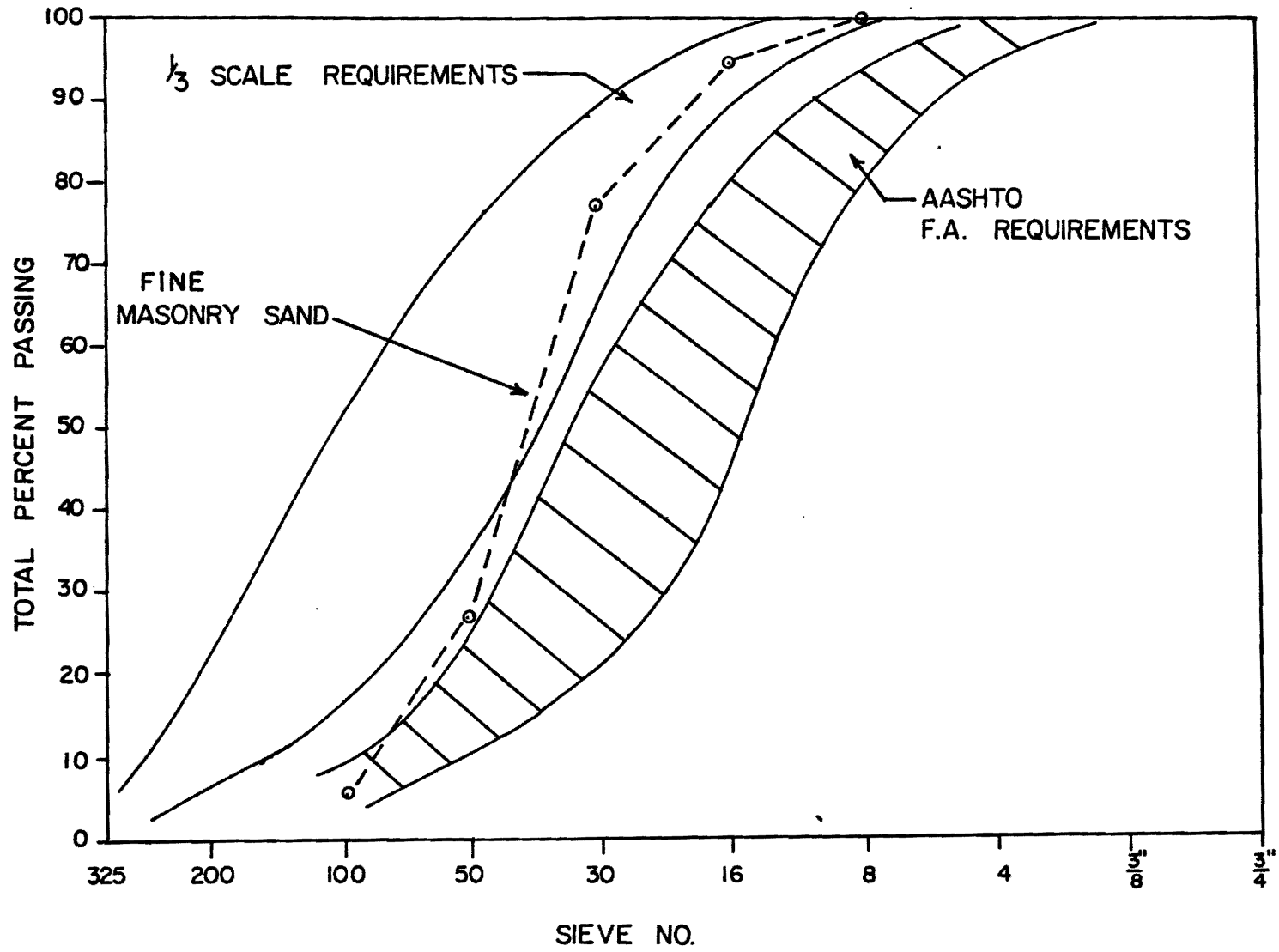


FIG. 21. Gradation Chart of Bryco Fine Masonry Sand.

2) No bond release agent is required as the concrete does not adhere to plexiglass. This is important because forming oil may be detrimental for proper subsequent bonding of epoxy mortar to concrete surfaces.

3) The plexiglass does not absorb water from the mixture, and the joints can be adequately sealed to avoid any bleeding of water.

Three forms consisting of 1/4 in. thick plexiglass sheets were manufactured. Because of the flexibility of the plexiglass, the forms were strengthened with plexiglass ribs bonded to the bottom surface form to add rigidity and to keep the forms flat during casting.

To form the connection details in the panels, solid wood molds were manufactured and bonded to the bottom of the forms using silicon rubber to form the pocket holes in the panels, and two identical 64 in. long, 1/4 in. thick, 7/8 in. wide trapezoidal shaped pieces of plexiglass were bonded to the inside of the forms to mold the groove for the shear key joints.

Reinforcing Steel

Steel reinforcing cages were fabricated by cutting the welded wire fabric to the desired size. The welded wire fabric facilitated the handling and fabrication of the reinforcing cages. If single reinforcing bars had been utilized fabrication would have required hand-tying of the bars.

Special steel chairs were obtained to control the cover distances in the panels when casting. The required cover distances were 1/2 in. at the bottom and 0.67 in. at the top. These covers simulate the 1-1/2 and 2 in. bottom and top covers currently used in bridge decks by the Texas State Department of Highways and Public Transportation.

Additionally, four coil inserts were attached to the bottom layer of the reinforcement to facilitate handling of the panels. Each panel weighed approximately 350 lbs.

Panel Casting

The casting of the precast concrete panels was performed using a 6 cu ft concrete mixer. The panels were cast using a batch size of 3 cu ft, which was enough for one panel and the cylindrical samples. The predetermined mix

proportions were used. The mix was harsh and stiff. Thus, a good vibration system was required to consolidate the model concrete.

The plexiglass forms were placed on the top of a 2-1/2 by 6 ft sheet of plywood which was sitting on a 20 by 20 in. shaking table. A trial panel was cast to test the vibration system. Proper consolidation of the model concrete was obtained only in the middle portion of the panel, right above the shaking table. Severe honeycombs formed in the end sections. Therefore, to provide proper and uniform consolidation, two additional air driven vibrators, each delivering a 150 lb force at 12,000 rpm, were attached to the overhangs of the plywood.

The concrete panels were manufactured at a rate of one panel every three days. For this reason, it was expected that some concrete model panels would have a greater concrete strength than others because of age.

Fig. 22 shows a form prior to casting and one panel after casting. The main components are the reinforcing steel cages, the wood molds to form the pockets in the panels, coil inserts, and strain gages. The concrete panels were left two days in the forms to allow time for strength development for handling. The panels were lifted using a crane with steel chains connected to four 1/2 in. diameter eye-bolts. The panels were individually wrapped with burlap and stacked on top of each other inside the laboratory. The burlap was kept wet at all times until proper curing was finished. For this reason, the panels that were cast first received longer curing time than those that were cast last.

Steel Stringers

The model steel stringers were ordered from a steel fabricator. The cover plates were continuously welded to the flanges of two W12x19 I-beams. Additionally, half round steel cylinders, 2 in. in diameter, were welded to the bottom flanges at 2-1/2 in. from each end of the two beams to simulate the rocker connection of the prototype.

The model steel stringers, as delivered, were carefully measured to determine if there were any differences in dimension with the design. The measurements revealed the existence of dimensions smaller than those

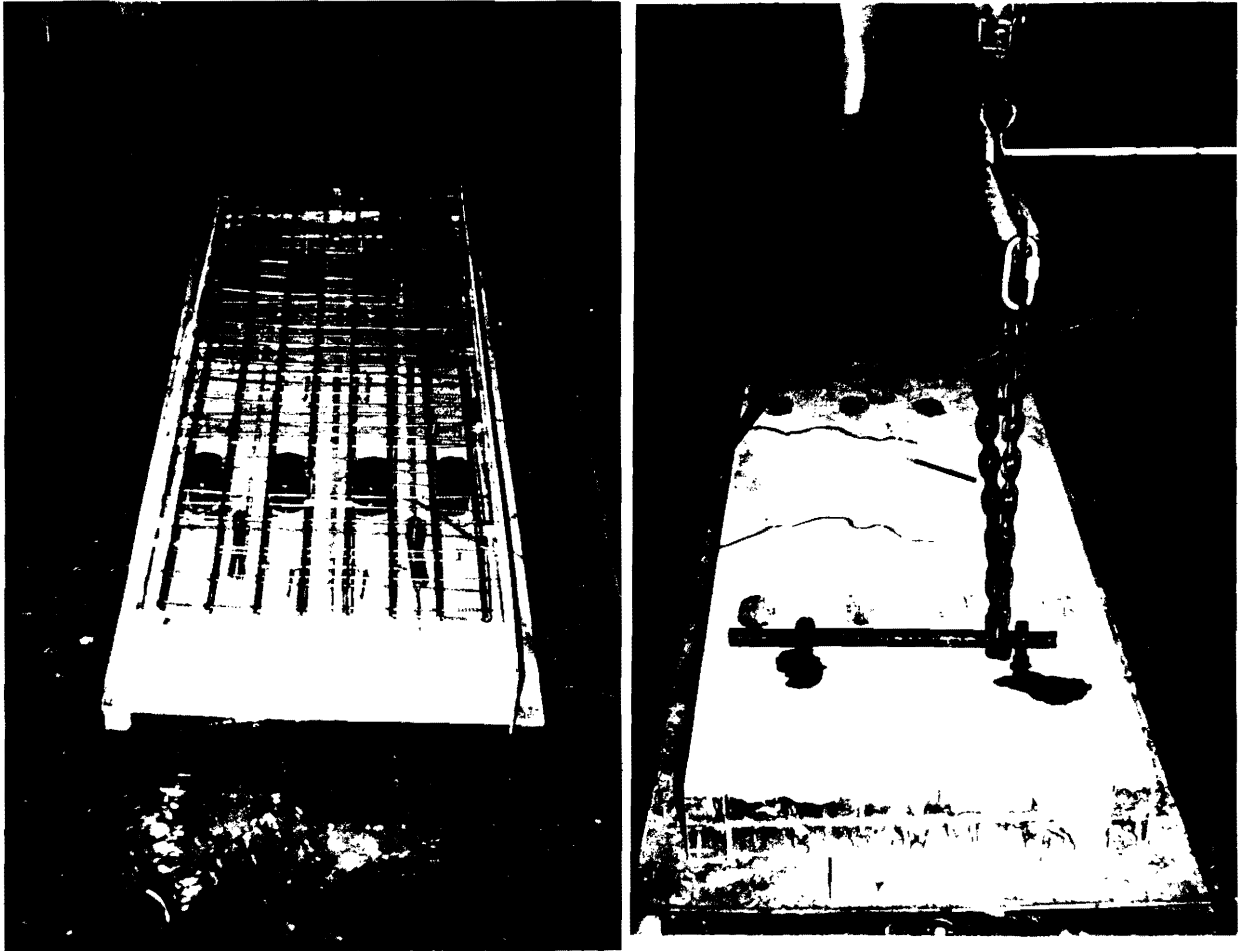


FIG. 22. Plexiglass Form Before Casting and Concrete Panel After Casting.

specified in the Manual of Steel Construction of the American Institute of Steel Construction (9). This was normal in the sense that certain errors in dimensions are expected due to tolerances in manufacturing hot-rolled structural steel sections. Measurements of the flange width, flange thickness, and depth of the beams were taken every 6 in. along the beam. The web thickness was also measured but only at the end of the beams.

Despite the fact that the dimensions were smaller than expected, consistency of the measurements was found in the uncut portions. On the end portions, on which the 3/8 in. cuts were made, the flange width was variable because the cuts were made by grinding the edges of the flanges. The measurements of those portions are tabulated in Table 11. The actual average moments of inertia of the model stringers are compared to those of the design in Table 12.

The steel shear connectors were welded in pairs, 1-3/4 in. apart, every 6 in. along both model stringers. A 100 amp stud welding machine was used.

Compression Tests on Model Concrete

Compression tests were performed on 2 by 4 in. cylinder samples of the model concrete of the precast concrete panels. These tests revealed that the strength of the model concrete varied significantly, probably because some panels received longer curing time than others and also because the age at which the samples were tested varied from panel to panel. The tests were run 30 days after the last panel was cast. Table 13 shows the average strength values obtained for the panels.

Design of Epoxy Mortar

The design of the epoxy mortar to grout all connections of the precast panels was done in terms of workability. Laboratory trial mixes were made to determine the proportions of aggregate and epoxy. The aggregate was designed to meet recommended grading limits.

The quick-setting epoxy used in this study was the Texas Highway Department Epoxy Binder B-102 which is intended to be mixed with selected

TABLE 11. Flange Width Measurements of Model Stringers.

Distance From Left End, in feet	Beam No. 1 Flange Width, in inches		Beam No. 2 Flange Width, in inches	
	Bottom	Top	Bottom	Top
0.5	3.231	3.275	3.153	3.312
1.0	3.270	3.224	3.190	3.273
1.5	3.258	3.238	3.209	3.205
2.0	3.235	3.296	3.273	3.140
2.5	3.311	3.268	3.200	3.107
3.0	3.946	3.934	3.902	2.898
3.5 - 16.5	3.947	3.947	3.947	3.947
17.0	3.944	3.916	3.932	3.940
17.5	3.274	3.143	3.222	3.247
18.0	3.272	3.284	3.293	3.267
18.5	3.271	3.239	3.271	3.235
19.0	3.234	3.245	3.244	3.275
19.5	3.270	3.268	3.261	3.218

TABLE 12. Average Moment of Inertia of the Model Steel Stringers and Design Moment of Inertia.

Section	Model Stringer 1 Average Moment of Inertia, in inches ⁴	Model Stringer 2 Average Moment of Inertia, in inches ⁴	Design Moment of Inertia, in inches ⁴
Left End	108.13	107.55	111.69
Middle	167.31	167.21	169.31
Right End	108.09	108.67	111.69

TABLE 13. Compression Test Results of Model Concrete of
Precast Panels.

Panel No.	Compressive Strength of the Model Concrete, in pounds per square inch	
	4 by 8 in. samples	2 by 4 in. samples
3	7510	-
4	6400	-
5	6960	-
6	-	6210
7	6890	-
8	-	8640
9	6370	6480
10	7160	7352

aggregate. The customary use of this epoxy binder is to repair holes or spalled areas in existing concrete structures.

There are temperature recommendations for placing this epoxy (7):

- 1) The concrete temperature should be between 60 and 120 degrees F.
- 2) The ambient temperature must be between 60 and 105 degrees F.

Aggregates

The aggregate recommended for this epoxy is as defined by the Texas Highway Department for grade No. 1. Such aggregate must be free of moisture and free of fines. The grading limits of the THD grade No. 1 are presented in Table 14. To obtain an aggregate meeting these grading limits, commercially available sandblasting dry sands were obtained.

Three different grades of sandblasting sand were obtained and investigated: Texblast grades No. 2, No. 3 and No. 4. Samples of these sands were used to run sieve analyses. Table 15 shows the results of the analyses and the results of a sieve analyses of a 50-50 percent blend of Texblast grades No. 2 and No. 4. This blend was found to be the closest in meeting the Texas Highway Department Grade No. 1 grading limits. The gradation of the selected aggregate is shown in Fig. 23 along with the grading limits.

Trial Mixes

Four different trial mixes were made by varying the aggregate-epoxy binder ratio by weight to make observations of the workability of the mixes and to obtain 2 by 4 in. cylindrical samples. The aggregate-epoxy binder ratio was varied from 2.75 to 3.50 in increments of 0.25. The laboratory mixes were blended with a paint mixer attached to a variable speed 3/8 in. hand drill. The following useful observations were made during mixing:

- 1) The workability of the epoxy mortar mix decreased as the aggregate-epoxy ratio increased.
- 2) Bleeding was more severe in the lower aggregate-epoxy ratios. The particles of sand in the epoxy mortar mix had the tendency to settle down, causing the epoxy binder to bleed to the top.

TABLE 14. Grading Limits for the Texas Highway Department
Grade No. 1 Aggregate (7).

Sieve No.	Cumulative Percent Retained
No. 4	0 - 5
No. 8	0 - 20
No. 16	15 - 50
No. 30	40 - 75
No. 50	70 - 90
No. 100	90 - 100

TABLE 15. Gradation Data of the Texblast Sandblasting Sands No. 2, No. 3, No. 4, and a 50-50% Blend of No. 2 and No. 4.

Sieve No.	Cumulative Percent Retained			
	Texblast No. 2	Texblast No. 3	Texblast No. 4	50% Texblast No. 2-50% Texblast No. 4
No. 4	0.0	0.0	0.0	0.0
No. 8	0.0	0.0	0.0	0.0
No. 16	21.3	2.9	0.0	10.6
No. 30	81.9	14.8	1.0	41.5
No. 50	99.8	86.7	82.2	91.5
No. 100	100.0	99.3	98.5	99.7

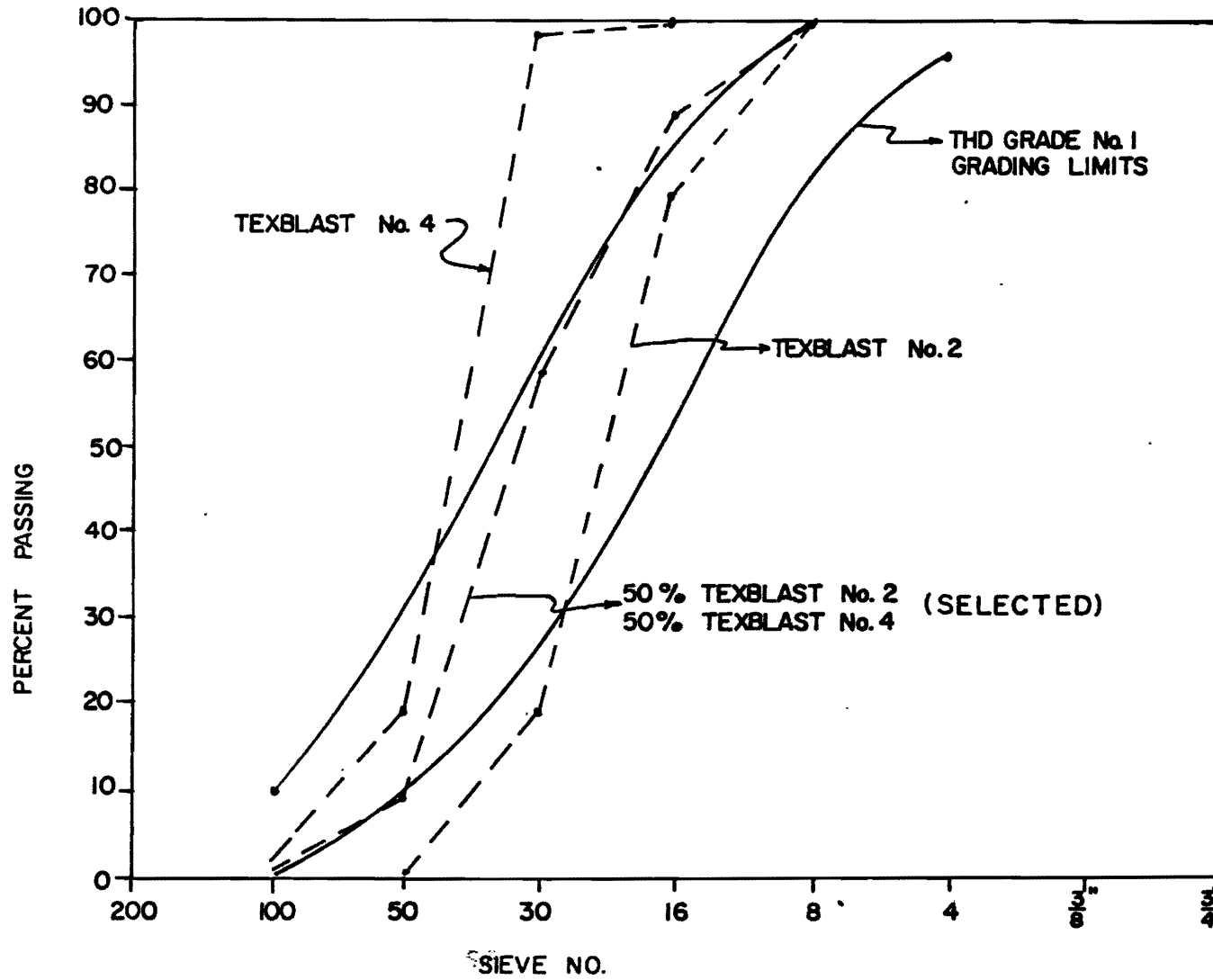


FIG. 23. Gradation Chart of Sandblasting Sand for Epoxy Mortar.

3) Consolidation was good in all the trial mixes. However, for higher aggregate-epoxy binder ratios, rodding was required to ensure proper consolidation and to get rid of trapped air in the mix.

Four 2 by 4 in. samples were cast from every mix to perform split tensile tests and uniaxial compression tests.

Split Tensile Tests

Split tensile tests were performed on two samples of every mix 24 hours after the mixes were made. A Universal 60-kip testing machine was used. The tensile strength of epoxy mortar, σ_t , was computed using the following formula:

$$\sigma_t = \frac{2 P}{\pi D l}$$

where:

P = the force required to fail specimens,

D = the diameter of the cylindrical sample, and

l = the length of the cylindrical sample.

The results of the split tensile test are shown in Table 16 . According to the values obtained, the tensile strength of the epoxy mortar was not affected very much as the aggregate epoxy binder ratio was varied. However, no conclusion can be drawn other than the fact that the tensile strength of the epoxy mortar was about three times that of the concrete.

Compression Tests

Compression tests were also performed approximately 24 hours after the samples were cast. A 60-kip loading machine was used. The results of the compression tests on the epoxy mortar sample are shown in Table 17. These results are believed to be very conservative because of the capping of the samples. Plaster cappings were used. The plaster did not bond to the epoxy mortar samples, and the strength of the plaster is believed to be much smaller than that of the epoxy. However, despite all the problems in the cappings, the values obtained are still much higher than the normal strength of concrete.

TABLE 16. Laboratory Split Tensile Test Results of Epoxy Mortar at 24 hours.

Sample	Aggregate-Epoxy Binder Ratio by Weight	Force P, in pounds	Tensile Strength in (psi)
A-1	2.75	13,550	1,078
A-2	2.75	15,100	1,201
B-1	3.00	16,500	1,313
B-2	3.00	16,200	1,289
C-1	3.25	16,100	1,281
C-2	3.25	16,500	1,313
D-1	3.50	15,500	1,233
D-2	3.50	17,400	1,384

TABLE 17. Laboratory Compression Test Results of Epoxy Mortar at 24 hours.

Sample	Aggregate-Epoxy Binder Ratio by Weight	Compressive Force P, in pounds	Compressive Strength (psi)
A-3	2.75	30,850	9,820
A-4	2.75	29,900	9,517
B-3	3.00	24,000	7,640
B-4	3.00	30,400	9,676
C-3	3.25	25,800	8,212
C-4	3.25	25,500	8,116
D-3	3.50	26,500	8,435
D-4	3.50	25,000	7,957

Loading System

A loading system was designed to apply four equal concentrated forces at approximately the third point of each of the model stringers. An existing loading frame was adapted to support four identical hydraulic rams. The hydraulic system was designed to provide equal hydraulic pressure to each of the rams.

Loading Frame

The loading frame to apply the static load on the model consisted of an existing rectangular frame and a steel adaptor fabricated from wide flange sections. The existing frame had a clearance of 12 ft wide and 3 ft 8 in. high and was anchored to a reaction floor. The frame adaptor consisted of a W 12 X 65, 4 ft long section bolted longitudinally to the top of the existing frame and two W 12 X 40, 7 ft long, were bolted 32 in. apart transversely to the existing frame. The two W 12 X 40 sections were braced using W 18 X 35 sections. Steel cylinders with a slot were welded to the bottom of the overhangs to place the hydraulic rams.

Hydraulic System

The hydraulic system consisted of four identical RC-250 Blackhawk rams connected to a four-way manifold and an electrical hydraulic pump. Hoses were attached to each of the outlets and connected to each of the hydraulic rams. The main purpose of the hydraulic system was to provide equal pressure to the rams; thus, since the same size of rams was used, equal forces were applied.

Instrumentation

The objective of the instrumentation was to provide a means of obtaining data regarding the structural behavior of the model under static loading. The following data was required:

- 1) the static loads applied to the model,
- 2) the flexural strain distribution,

- 3) the shear strain distribution,
- 4) the deflection of the model stringers, and
- 5) the relative slip displacement of the precast concrete panels and the model stringers.

To accomplish these requirements, load cells were installed under the rams to accurately measure the loads applied. Longitudinally oriented uniaxial strain gages were bonded to eight different cross sections to monitor the flexural deformations of the model under bending. Three-element strain gage rosettes were also bonded to the model stringers at four cross sections near the supports to obtain shear strain distributions. Mechanical dial indicators were used to measure deflections, and electrical displacement transducers were used to measure the relative slip displacements of the precast panels and the model stringers at four locations close to both supports of each model stringer.

Load Cells

Four load cells were installed under each of the hydraulic rams. Two 100-kip load cells and two 50-kip load cells were used. Three of the load cells were connected to a 10 channel switch and balance unit monitored with a strain indicator. The other load cell was connected to a digital readout and was used to control the loading of the model. The load cell connected to the digital readout was calibrated against a loading machine of the National Bureau of Standards. The remaining load cells were calibrated against a mechanical beam loading machine accurate to the nearest 10 lb.

Strain Gages

The objective of the strain gages was to obtain flexural and shear strain distributions at different sections of the model under static loading. Ninety-three strain gages were installed either in the concrete panels or on the model stringers. Uniaxial strain gages were used to monitor eight cross sections for flexure and three-directional strain

rosettes to monitor four cross sections near the supports for shear strain distributions.

Fig. 24 shows the location of the cross sections where strain gages were installed. The cross sections 1-1 to 8-8 were monitored for flexure, and cross sections A-A to D-D were monitored for shear strain distribution.

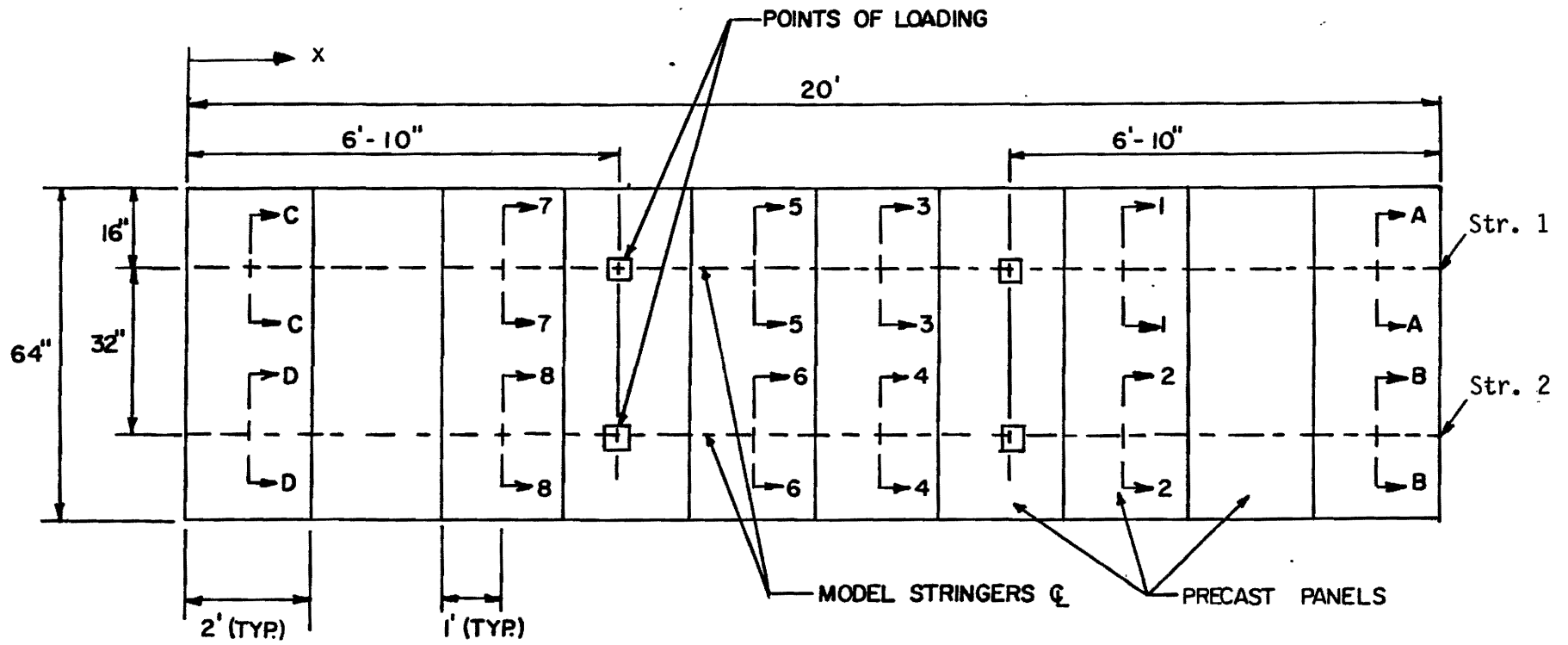
Eight uniaxial strain gages were installed in each of the cross sections monitored for flexure, four in the model stringers and four in the concrete panels. The location of the uniaxial strain gages are as follows: two strain gages were installed on the flanges of the beam, one at the top and one at the bottom; two were bonded to the web at approximately 4-1/2 in. from the neutral axis of the stringer cross section; one was bonded to the bottom surface of the panel; two were bonded to pieces of reinforcement that were tied to both layers of reinforcement, top and bottom; and one was embedded in the concrete. Details of the location of the strain gages of a cross section monitored in flexure are illustrated in Fig. 25.

The cross sections that were investigated for shear strains were located about one foot from the supports. Cross section A-A had three strain rosettes installed, one at the neutral axis of the steel cross section, one 4-1/2 in. to the top of the neutral axis, and another 4-1/2 in. to the bottom. Cross sections B-B, C-C, and D-D had only two strain rosettes installed in each. One of them was bonded at the neutral axis of the steel cross section and the other at 4-1/2 in. to the top of the neutral axis. Details of cross section A-A are shown in Fig. 26.

Dial Indicators

Six dial indicators were mounted on the model to measure the deflections at quarter-points of each of the model stringers. The model was supported by steel sections sitting outside the reaction floor of the frame; but settlement of the supports was considered likely. Thus, deflections could not have been measured accurately.

To obtain accurate deflections, the dial indicators were attached to a beam that was simply-supported at the two model supports without making contact with the reaction floor; therefore, the deflections were measured



PLAN

FIG. 24. Location of Instrumented Cross Sections.

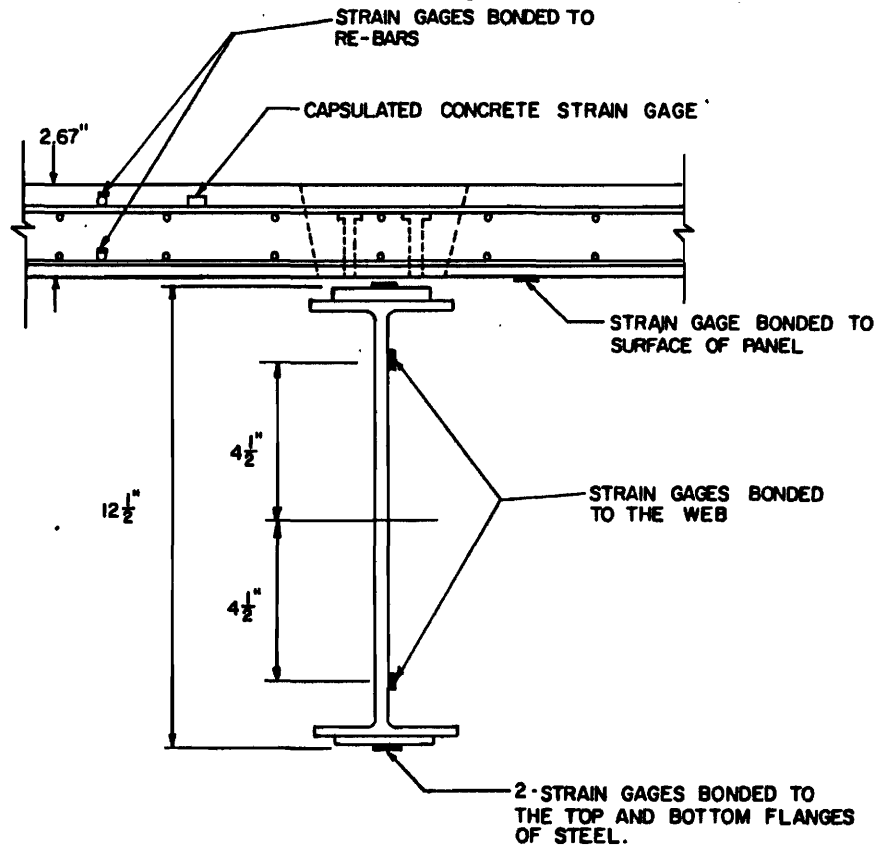


FIG. 25. Typical Cross Section Instrumented for Flexure.

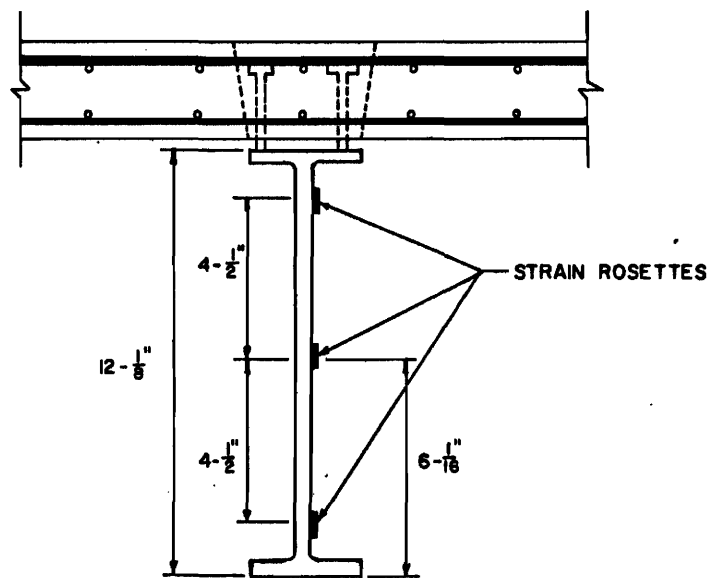


FIG. 26. Typical Cross Section Instrumented for Shear.

relative to the same reference line at all times independent from any support settlement.

Displacement Transducers

Four electrical displacement transducers were installed to measure the relative displacement of the precast concrete panels and the model stringers. The transducers were attached close to the supports where the shear is greatest. Each transducer consists of a steel cantilever beam with strain gages bonded to it. It directly measures bending strain when displaced. This transducer, when connected to the strain indicator, was capable of detecting displacements as small as 6×10^{-5} in. per microstrain of readout. The displacement transducers were connected to the same 10-channel switch and balance unit used for the load cells. Details of a displacement transducer are illustrated in Fig. 27.

Assembly of Model

The 1/3 model was assembled directly underneath the loading frame. The two model stringers were spaced 32 in. apart and supported on two transverse W 16 X 26 steel sections. After the model stringer instrumentation was installed, Test No. 1 was performed applying static loads to the plain model stringers to test the instrumentation and the loading system. After the proper function of the instrumentation was verified, the precast panels were placed on the top of the stringers.

The panels were actually laid on bearing devices shown in Fig. 28 that were also used to retain the epoxy mortar only around the pocket connections and not between pockets. The panels were properly aligned and uniformly spaced. This was very important because of the tolerances of the shear key joints.

Epoxy mortar was poured into the pockets, and 24 hours later, Test No. 2 was run. Immediately after Test No. 2 was completed, the shear key joints were grouted with epoxy mortar. Test No. 3 was run 24 hours later.

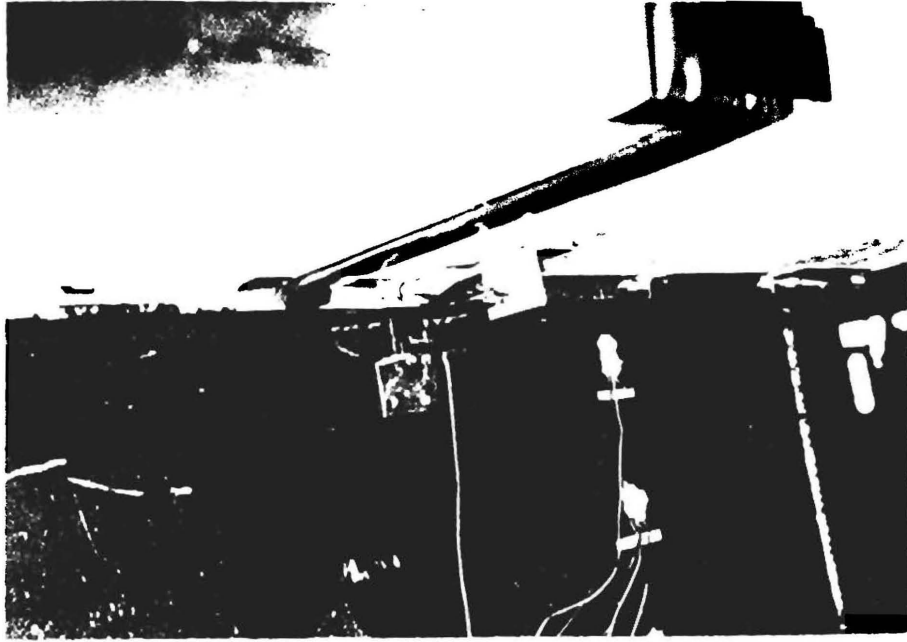


FIG. 27. Electrical Displacement Transducer to Measure Slip Displacements.

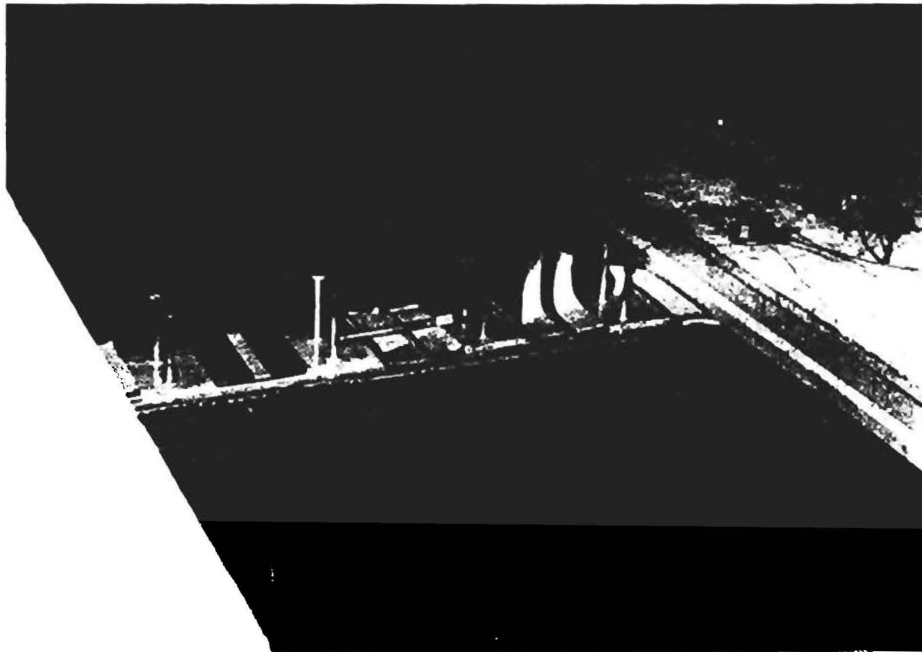


FIG. 28. Bearing Devices for Panels.

Grouting of the Pocket Connections

The pocket connections of the model were grouted using a mix of one part Epoxy Binder B-102 and 3 parts of the selected aggregate by weight. Because the flowability of the epoxy mortar, all possible leaks were sealed.

All gaps around the pockets that were caused by the bearing device were sealed using a foam tape adhered to strips of wood. The wood strips were supported from the floor, as shown in Fig. 29.

The mixing equipment consisted of a mortar mixer driven by a 1/2 in. variable speed drill. The mortar was mixed in a five-gallon bucket. The inside of the bucket was first coated with the epoxy binder, and then the excess was removed. The epoxy resin was blended with the specified curing agent. When a uniform blend was obtained, the pre-weighed amounts of the selected aggregate were slowly poured into the mixing bucket. When mixing the aggregate and the epoxy, the drill was run at low speeds to avoid any intrusion of air bubbles into the mortar mix.

After the mortar was uniformly blended, aggregate scoops were used to pick up the mortar and pour it into the pocket connections. The in-place epoxy mortar was rodded to displace the trapped air. Three batches were required to fill the pockets and 2-by 4-in. cylindrical samples. Fig. 30 shows the placement of the mortar into the pockets. Test No. 2 was run 24 hours after the grouting was completed.

Grouting of the Shear Key Joints

The shear key joints were grouted using the same mixing techniques as those used in the grouting of the pockets. The epoxy mortar mixed was different; for the key joints, a more flowable mix was required because the pouring was done through 3/8 in. gaps. Therefore, 2.75 parts of aggregate and 1 part Epoxy Binder B-102 were used instead. The same mixing equipment was used, with the exception that a trapezoidal funnel was used to facilitate the pouring from the top.

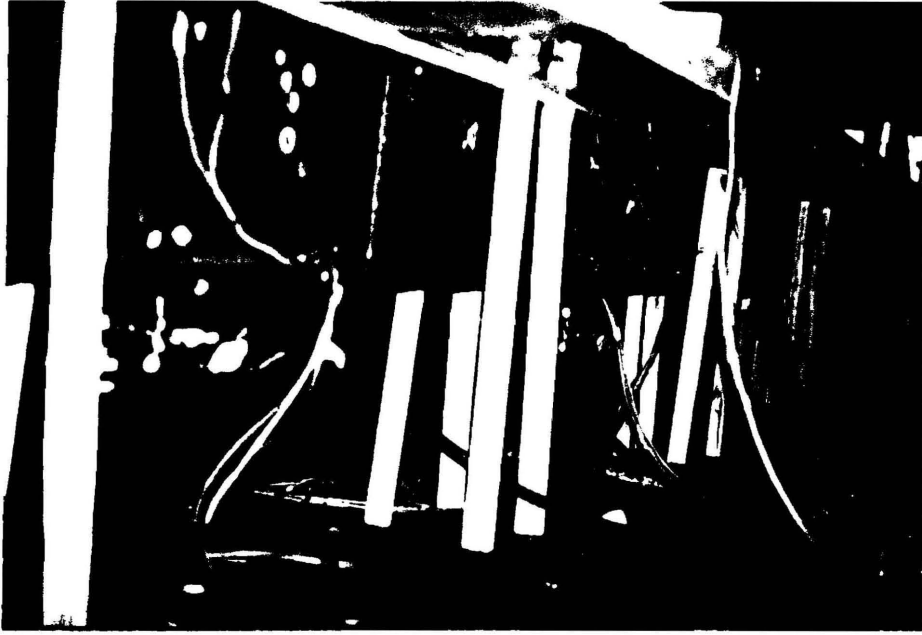


FIG. 29. Sealing Devices Supported from Floor.



FIG. 30. Grouting of Pocket Connections.

The bottom gaps of the shear key joints were formed using wood supports. Cylindrical samples were also cast from this mortar mix. Fig. 31 shows the model after the grouting of the connections was completed. Test No. 3 was run 24 hours after the shear key joints were grouted.

Cylinder Tests on Epoxy Mortar of Connections

Cylinder tests were performed on samples of epoxy mortar used in the pocket and shear key connections. Three types of cylinder tests were performed on the samples: compression tests, split tensile test, and tangent moduli tests.

Compression Tests

Compression tests were performed on the 2-by 4-in. cylindrical samples. Four samples of each epoxy mortar were tested. The age of the specimens was approximately 24 hours.

The results of the compression tests are tabulated in Table 18. Consistency of the results was obtained because sulphur capping was used instead of plaster. The epoxy mortar poured in the pocket connections exhibited an average compressive strength of 12,440 psi at 24 hours. The aggregate-epoxy ratio was 3.0. The epoxy poured in the shear key joints developed a compressive strength of 11,790 psi at 24 hours. The aggregate-epoxy ratio was 2.75. These compressive strengths are higher than those reported in Table 17 because of the different cappings.

Split Tensile Tests

Split tensile tests were done on two samples only. The results of the split tensile tests are shown in Table 19.

The epoxy mortar used in the pocket connections exhibited a 24-hour split tensile strength of 1,670 psi, and that used in the shear key joints exhibited a strength of 1,510 psi.



FIG. 31. One-Third Model After All Grouting was Completed.

TABLE 18. Compressive Strength of Epoxy Mortar of Connections at 24 hours.

Compressive Strength of Epoxy Mortar of Connections at 24 hours, in pounds per square inch			
Sample	Pocket Connections (3 parts Aggregate, 1 Epoxy)	Sample	Shear Key Joints (2.75 parts Aggregate, 1 Epoxy)
P-1	12,320	S-1	12,130
P-2	12,450	S-2	11,170
P-3	12,570	S-3	11,840
P-4	12,410	S-4	12,030
Ave.	12,440	Ave.	11,970

TABLE 19. Tensile Strength of Epoxy Mortar of Connections at 24 hours.

Tensile Strength of Epoxy Mortar used in Connections at 24 hours, in pounds per square inch			
Sample	Pocket Connection (3 parts Aggregate, 1 Epoxy)	Sample	Shear Key Joints (2.75 parts Aggregate, 1 Epoxy)
P-5	1,530	S-5	1,352
P-6	1,810	S-6	1,655
Ave.	1,670	Ave.	1,510

Determination of the Tangent Moduli

The initial tangent moduli of samples of epoxy mortar used in the connections were experimentally determined. Each individual sample was carefully measured in length. The diameter was measured at three different points of the sample and the average diameter was computed.

After the samples were carefully measured, they were placed in a 20 kip Universal Instron machine. A dial indicator with a resolution of one 0.0001 in. was used to measure the deformation of the sample under axial loading. The loads were directly read from the Instron machine.

Thus, knowing the axial deformations, the load applied, the length and the diameter of the sample, the uniaxial strain and the axial stress were computed.

Stress-strain plots were made for each of the samples tested. The initial tangent moduli were obtained graphically. The results are tabulated in Table 20.

TABLE 20. Tangent Moduli of Epoxy Mortar of Connections.

Tangent Moduli of Epoxy Mortar of Connections, in pounds per square inch			
Sample	Pocket Connections	Sample	Shear Key Joints
P-7	1.20×10^6	S-7	1.37×10^6
P-8	1.37×10^6	S-8	1.65×10^6
P-9	1.19×10^6	S-9	1.45×10^6

C H A P T E R I I I

STATIC LOAD TEST RESULTS

General

Static load tests were performed on the 1/3 full-scale model bridge. Three major tests were conducted to investigate three different structural behaviors that may be encountered:

1) Noncomposite behavior that may result from a lack of structural interaction between precast panels and steel stringers.

2) Partial composite behavior that may result from an interaction at the pocket connections only.

3) Full composite behavior that may result from having the pocket and shear key joints grouted; that is, not only is there a transfer of shear between the precast panels and the steel stringers, but there is also a transfer of normal forces between adjacent panels that leads to the development of full composite behavior.

Test No. 1. Noncomposite Test

Static load tests were performed on the model stringers to obtain flexural strain distribution data, shear strain distribution data and deflections. Other objectives of this test were to verify the accuracy of the instrumentation and strain gages installed in the model stringers and to test the loading system.

Description of Test No. 1

Static loads were applied with four hydraulic rams at the two third points of each of the two model stringers. A maximum point load of 5 kips was applied quasi-statically in one-kip increments. The deck panels directly beneath the loading rams were set in place to help to transfer the applied loads to the stringers. Neoprene pads were placed between the panels and the stringers to avoid any spalling in the concrete.

A total of 32 uniaxial strain gages was used to monitor eight cross sections for flexural strain distribution and nine strain rosettes to monitor four cross sections for shear strain distributions. Six dial indicators were used to measure deflections at the quarter points of each of the model stringers.

Flexural Strain Distribution

The flexural strain data was reduced. The strain readouts were obtained with the gage factor set at 2.00 at the strain indicator. The gages had a gage factor of 2.11. Therefore, the recorded strains were multiplied by a correction factor of the ratio of 2.11 to 2.00.

To verify the accuracy of the strain gages, the data was reduced and correlated with the theory to obtain a theoretical correlation factor. Using the measured inertia properties of the model stringers, the distance of each of the gages to the neutral axis of the stringer cross sections, and the moment acting on every cross section, the theoretical flexural strains, ϵ_{th} , were computed using the formula:

$$\epsilon_{th} = \frac{M y}{I E_s}$$

where

M = the moment applied at any cross section,

y = the distance from the neutral axis of the steel cross section to the location of the strain strain gages,

I = the moment of inertia of the stringer cross section, and

E_s = the modulus of elasticity of steel, 29×10^6 psi.

After the theoretical strains were computed for every gage and every loading, the theoretical correlation factor, T.C.F., was computed for every gage to determine the accuracy of the results using the following formula:

$$T.C.F. = \frac{\sum \frac{\epsilon_{th}}{\epsilon_{mea}}}{n}$$

where

ϵ_{mea} = the measured flexural strain by a particular gage, and
 n = the number of strain measurements.

Using the above procedure, the theoretical correlation factors were computed for every uniaxial strain gage at every one of the eight cross sections monitored for flexure. The results are summarized in Table 21. The theoretical correlation factors were not used in any further tests, they were only used to verify the data obtained by the strain gages bonded to the model stringers with the theoretical values to build up confidence in the results. The absence of errors is reflected when the theoretical correlation factor equals one. They were also a means of measuring the average percent error of the strain measurements. The maximum average percent error was 5.7% in cross section 1-1 at the gage bonded to the bottom flange. Most of the strain gages had very small percent errors. After observing the results, high confidence was gained on the strain measurements.

The flexural strains were plotted and correlated against the theory as illustrated in Fig. 32 through Fig. 39 for cross sections 1-1 to 8-8, respectively.

Shear Strain Distribution

Shear strain distribution data was computed from the measurement of uniaxial strains along three planes by means of strain rosettes. Each rosette was oriented at 45° , 90° , and 135° from the horizontal axis of the model stringer.

The horizontal shear strain, ϵ_{xy} , was solved using the following system of equations:

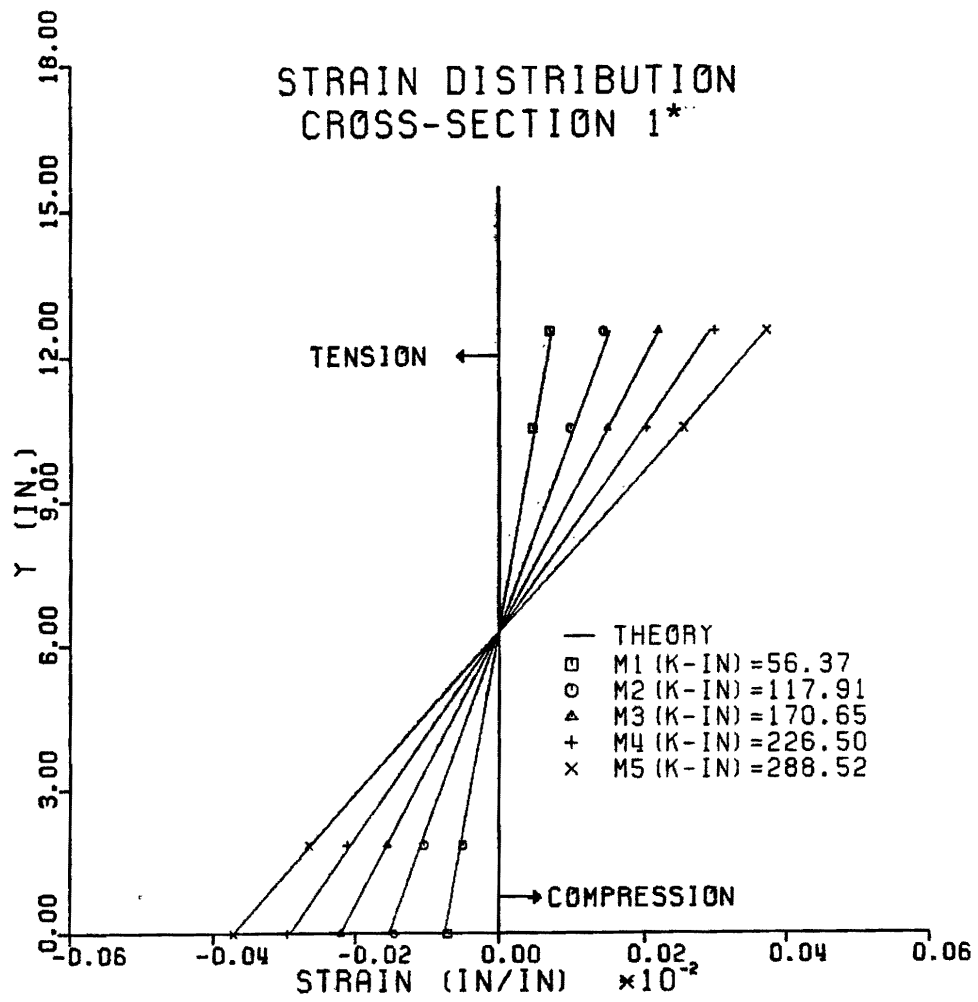
$$\begin{aligned}\epsilon_a &= \epsilon_{xx} \cos^2\theta_a + \epsilon_{yy} \sin^2\theta_a + \epsilon_{xy} \cos\theta_a \sin\theta_a \\ \epsilon_b &= \epsilon_{xx} \cos^2\theta_b + \epsilon_{yy} \sin^2\theta_b + \epsilon_{xy} \cos\theta_b \sin\theta_b \\ \epsilon_c &= \epsilon_{xx} \cos^2\theta_c + \epsilon_{yy} \sin^2\theta_c + \epsilon_{xy} \cos\theta_c \sin\theta_c\end{aligned}$$

TABLE 21. Theoretical Correlation Factors of Flexural Strain Gages.

Cross Section*	Strain Gage** Location	Correlation Factor
1-1 Stringer 1 x=15 ft	Top Flange	1.053
	Top Web	1.055
	Bottom Web	1.055
	Bottom Flange	1.057
2-2 Stringer 2 x=15 ft	Top Flange	1.029
	Top Web	1.025
	Bottom Web	1.025
	Bottom Flange	1.022
3-3 Stringer 1 x=11 ft	Top Flange	1.016
	Top Web	1.028
	Bottom Web	1.028
	Bottom Flange	1.029
4-4 Stringer 2 x=11 ft	Top Flange	1.017
	Top Web	1.011
	Bottom Web	1.010
	Bottom Flange	1.004
5-5 Stringer 1 x= 9 ft	Top Flange	1.024
	Top Web	1.031
	Bottom Web	1.031
	Bottom Flange	1.038
6-6 Stringer 2 x= 9 ft	Top Flange	1.017
	Top Web	1.005
	Bottom Web	1.005
	Bottom Flange	0.995
7-7 Stringer 1 x= 5 ft	Top Flange	1.024
	Top Web	1.026
	Bottom Web	1.025
	Bottom Flange	1.027
8-8 Stringer 2 x= 5 ft	Top Flange	1.037
	Top Web	1.028
	Bottom Web	1.028
	Bottom Flange	1.020

* See Figure 24

** See Figure 25



* Stringer 1, 15 ft from left end

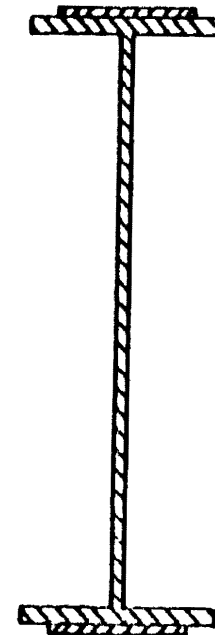
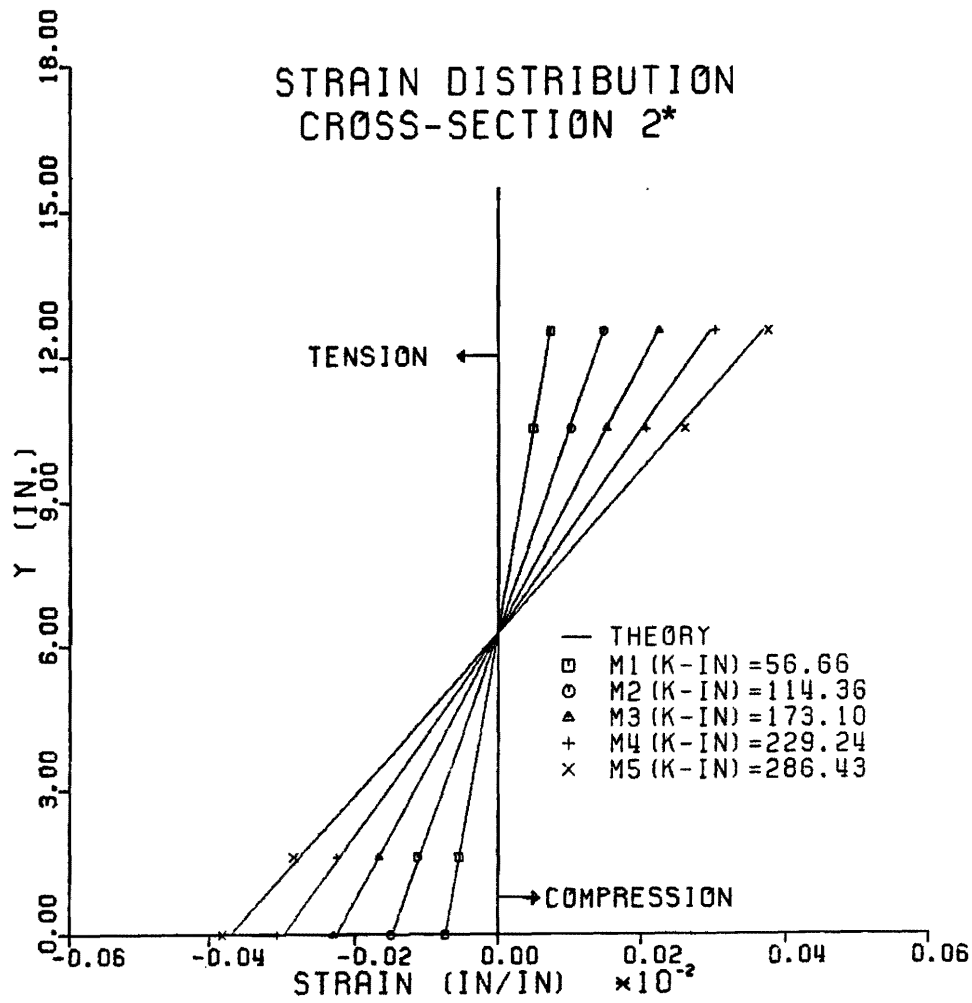


FIG. 32. Flexural Strain Distribution, Cross Section 1-1, Test No. 1.



* Stringer 2, 15 ft from left end

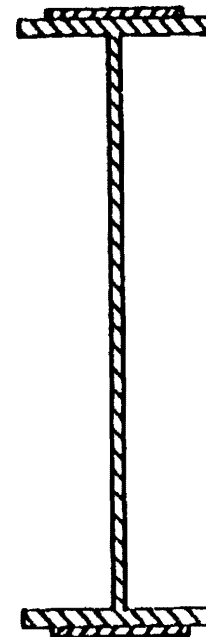
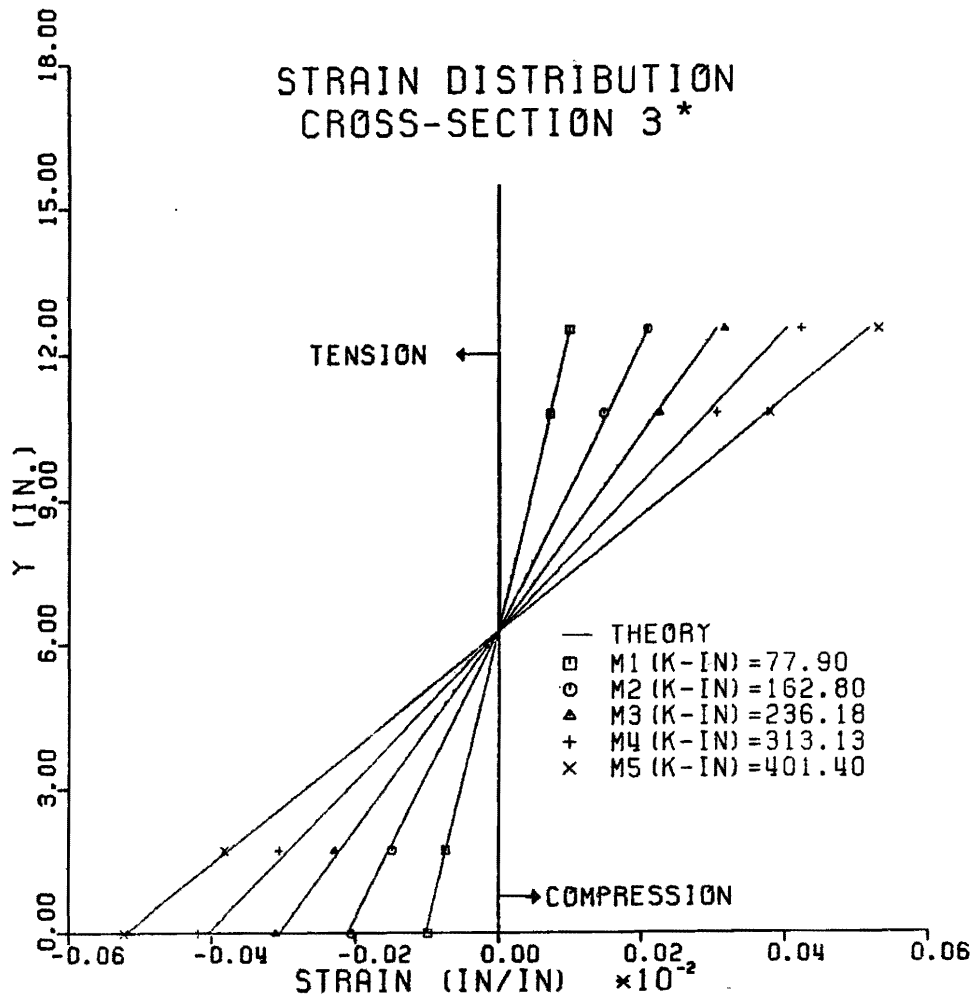


FIG. 33. Flexural Strain Distribution, Cross Section 2-2, Test No. 1.



* Stringer 1, 11 ft from left end

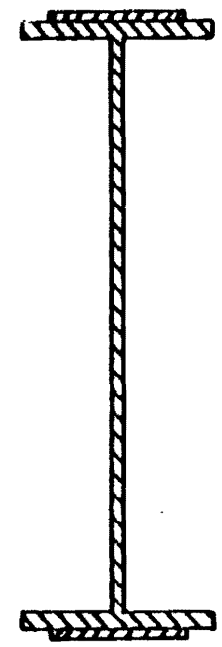
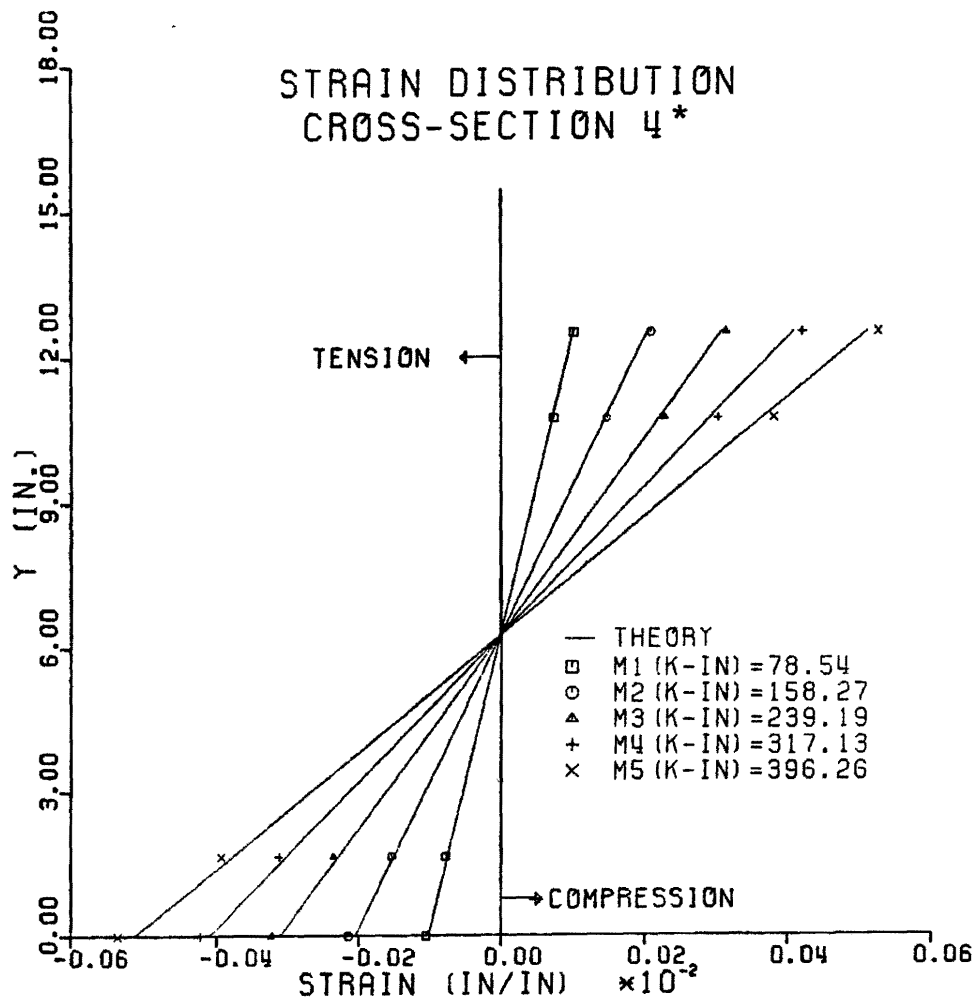


FIG. 34. Flexural Strain Distribution, Cross Section 3-3, Test No. 1.



* Stringer 2, 11 ft from left end

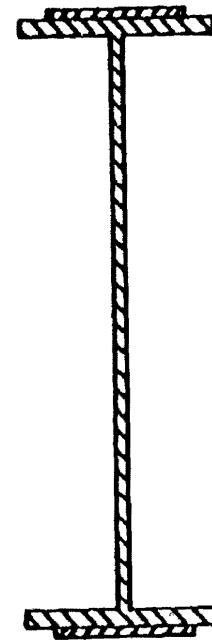
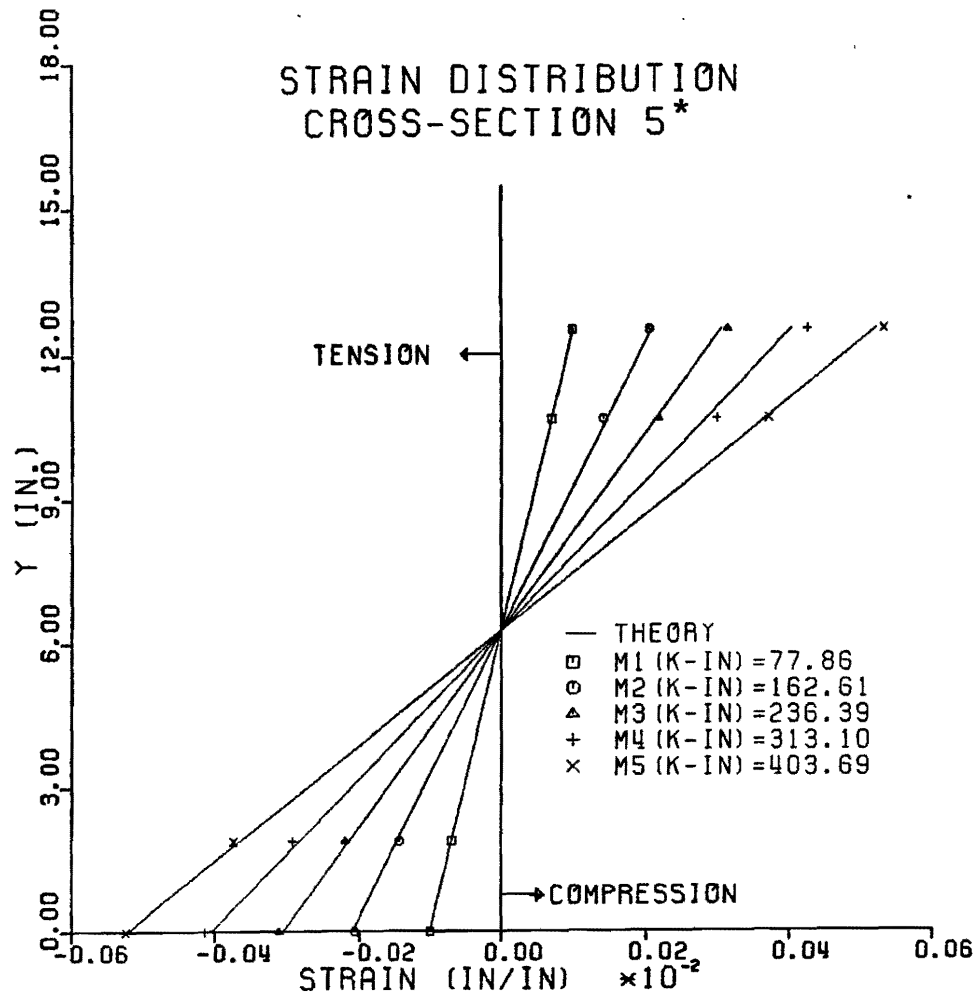


FIG. 35. Flexural Strain Distribution, Cross Section 4-4, Test No. 1.



* Stringer 1, 9 ft from left end

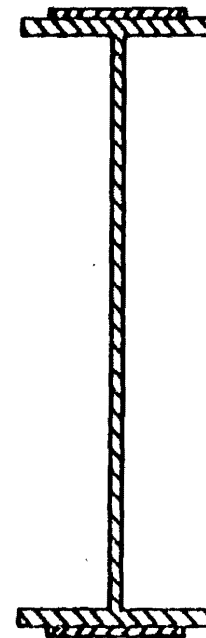
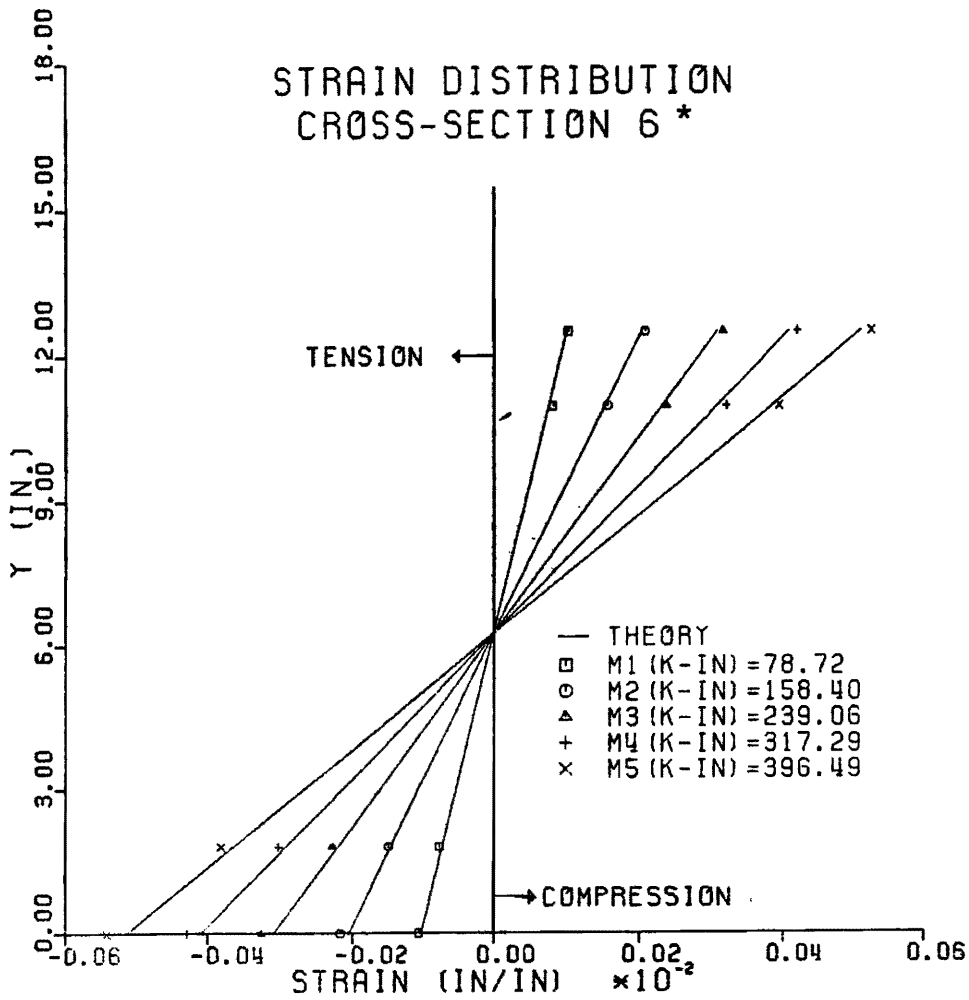


FIG. 36. Flexural Strain Distribution, Cross Section 5-5, Test No. 1.



* Stringer 2, 9 ft from left end

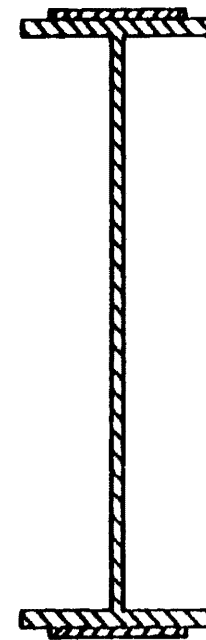
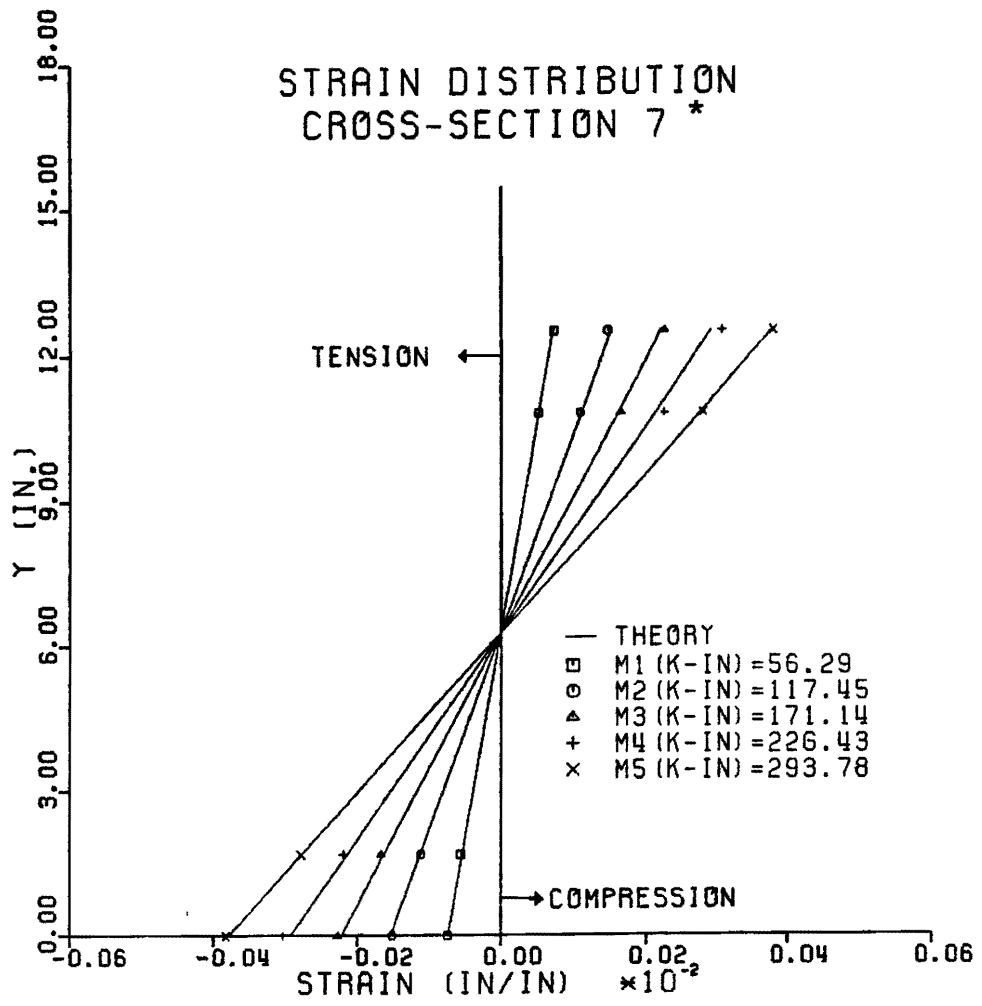


FIG. 37. Flexural Strain Distribution, Cross Section 6-6, Test No. 1.



* Stringer 1, 5 ft from left end

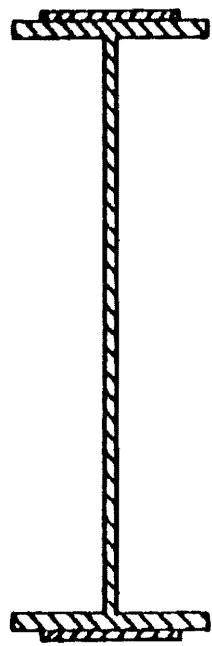
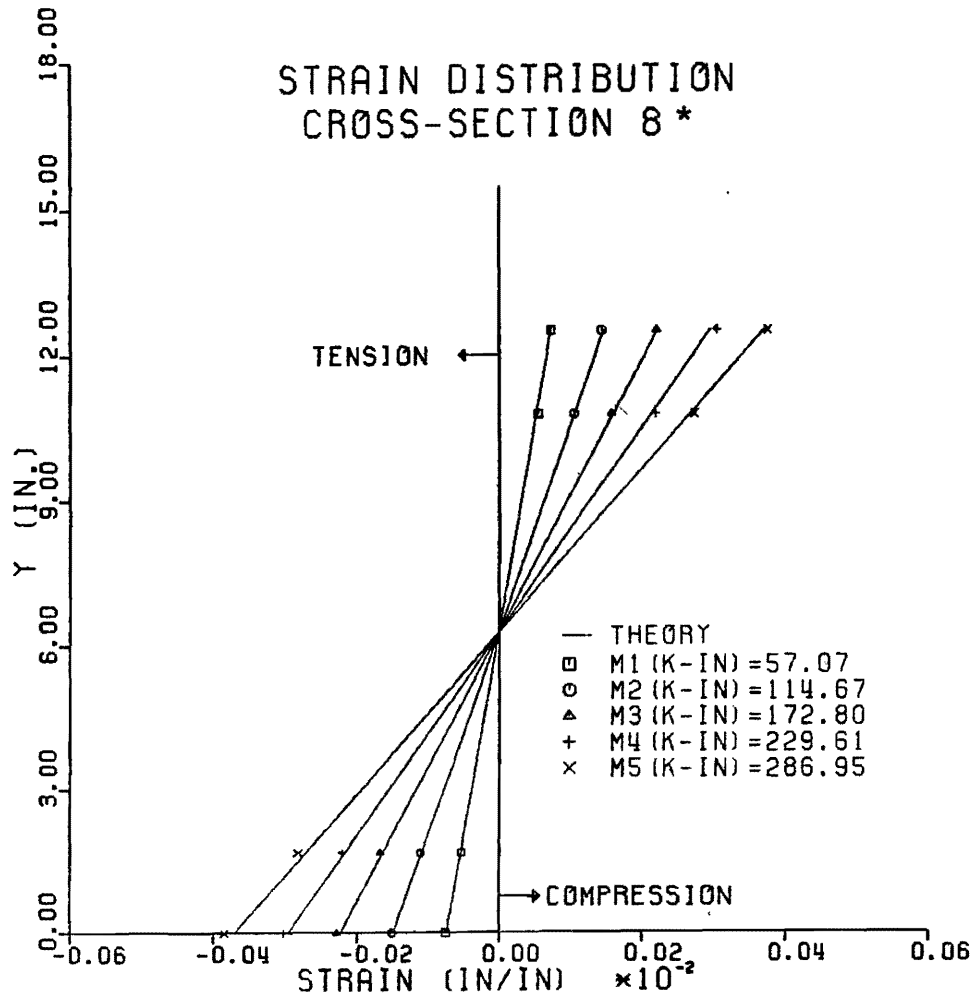


FIG. 38 Flexural Strain Distribution, Cross Section 7-7, Test No. 1.



* Stringer 2, 5 ft from left end

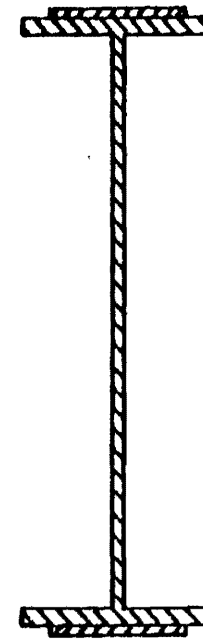


FIG. 39. Flexural Strain Distribution, Cross Section 8-8, Test No. 1.

where

- ϵ_a = the measured normal strain in direction A,
- ϵ_b = the measured normal strain in direction B,
- ϵ_c = the measured normal strain in direction C,
- ϵ_{xx} = the strain in the horizontal axis,
- ϵ_{yy} = the strain in the vertical axis,
- ϵ_{xy} = the horizontal shear strain,
- θ_a = angle of gage A with respect to the horizontal axis, 45° ,
- θ_b = angle of gage B with respect to the horizontal axis, 90° , and
- θ_c = angle of gage C with respect to the horizontal axis, 135° .

To verify the accuracy of the results, the measured horizontal shear strains, ϵ_{xy} , were correlated to the theoretical strains, $\epsilon_{xy th}$, computed using the following formula:

$$\epsilon_{xy th} = \frac{V Q}{I t G}$$

where

- V = the shear force acting on the section,
- Q = the first moment of area about the neutral axis of the stringer cross section of the area outside the gage,
- I = the moment of inertia of the stringer cross section,
- t = the thickness of the plane under investigation, and
- G = the modulus of rigidity of steel.

The average percent errors, APE, were computed for every strain rosette using the following formula:

$$APE = \frac{\sum \left| \frac{\epsilon_{xy th} - \epsilon_{xy}}{\epsilon_{xy th}} \right| \times 100\%}{n}$$

where

- ϵ_{xy} = the measured horizontal shear strain,
- $\epsilon_{xy th}$ = the theoretical horizontal shear strain, and
- n = number of loading

The average percent errors are tabulated in Table 22. It can be observed that a good correlation was obtained for cross sections A-A, B-B, and C-C. The average percent errors obtained for the strain rosettes of cross section D-D were extremely high. The errors were attributed to bad bonding of the strain gage rosettes, therefore, these rosettes were not utilized for further tests.

The results of the shear strain deformations at cross sections A-A, B-B, and C-C are illustrated in Figs. 40 through 42, respectively. It can be noticed that the data was extremely close to the theory.

Deflections

Deflections were measured at the quarter points of each of the model stringers at every load interval. To verify the accuracy of the measurements, the deflections measured were compared to the theory.

The area moment method was used to determine the theoretical deflections at the points where deflections were measured. The theoretical values were compared, and the percent errors were computed. Tables 23 and 24 show the deflection measurement along with the theoretical values and percent errors.

It is observed that the calculated percent errors obtained are relatively low for all dial indicators. The dial indicators placed at the midspan of each model stringer exhibited the lowest errors. The load-deflection curves for the midspan indicators were plotted and are shown in Fig. 43. The model stringers were deflecting at an average rate of 0.094 in. per 1 kip of third point load.

Test No. 2 - Static Load Test with Pocket

Connections Grouted

Static load tests were performed on the model 24 hours after the pocket connections were grouted to obtain flexural and deflection data. The main objective of these tests was to determine the extent of structural

TABLE 22. Average Percent Error of Shear Strain Rosettes

Cross Section *	Rosette ** Location **	Percent Error
A-A Stringer 1 x=19 ft	Top Web Neutral Axis Bottom Web	6.63 4.09 4.96
B-B Stringer 2 x=19 ft	Top Web Neutral Axis	4.03 3.00
C-C Stringer 1 x= 1 ft	Top Web Neutral Axis	8.53 5.21
D-D Stringer 2 x= 1 ft	Top Web Neutral Axis	46.91 33.83

* See Figure 24

** See Figure 26

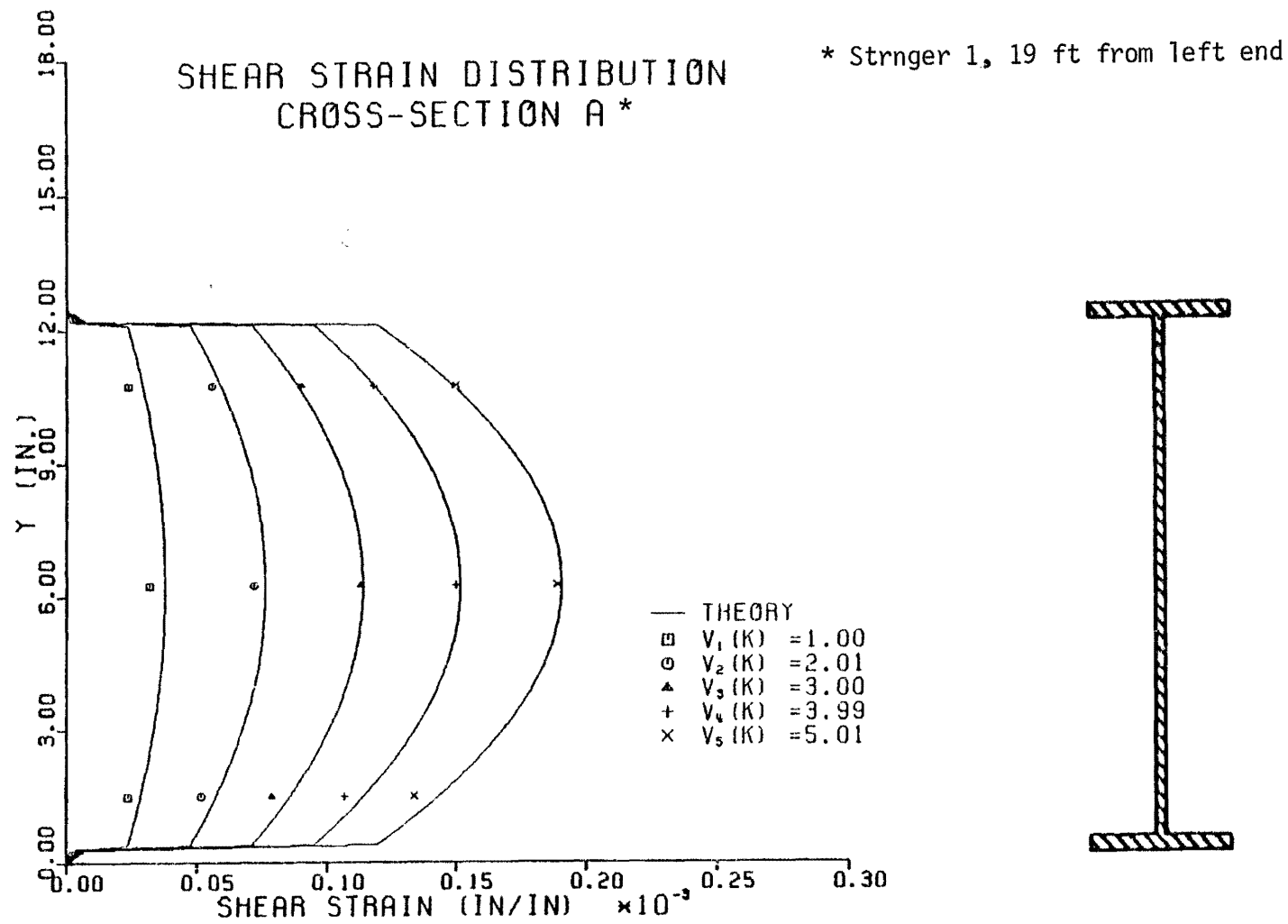
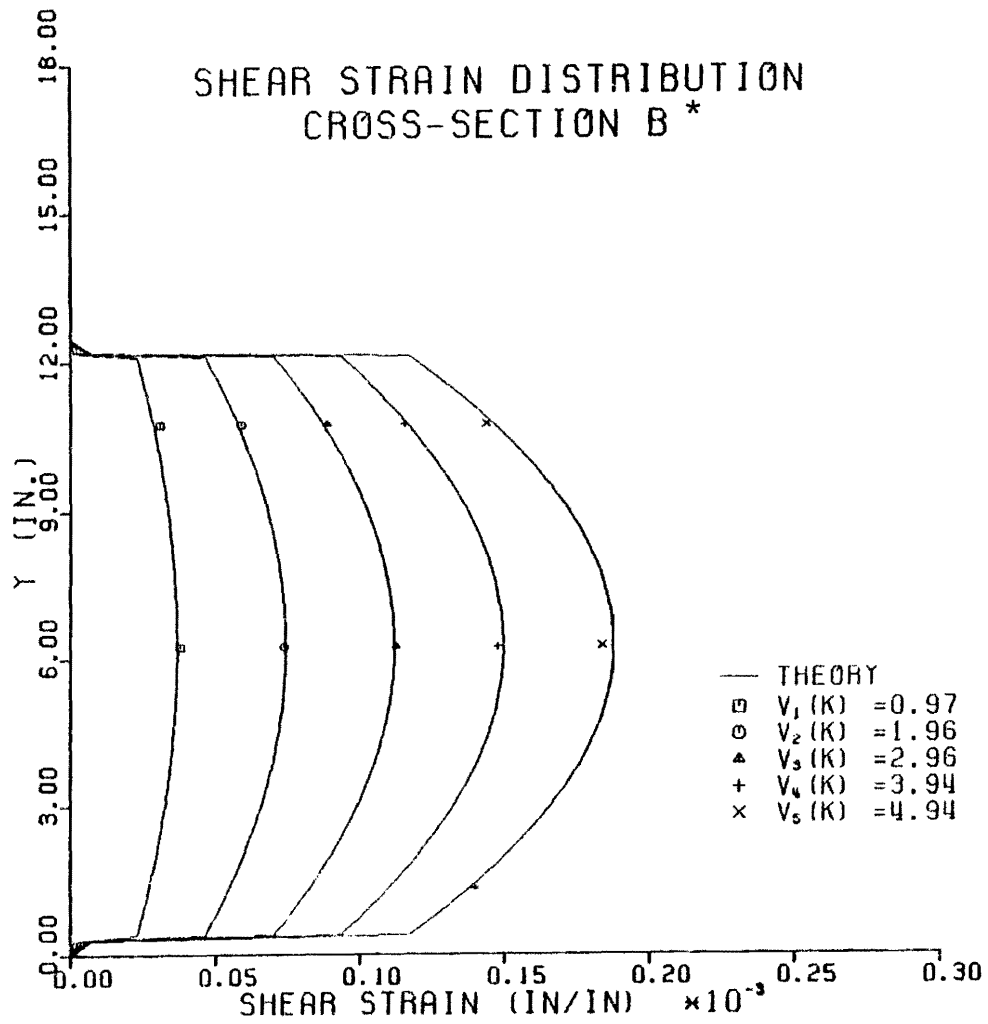


FIG. 40. Shear Strain Distribution, Cross Section A-A, Test No. 1.



* Stringer 2, 19 ft from left end

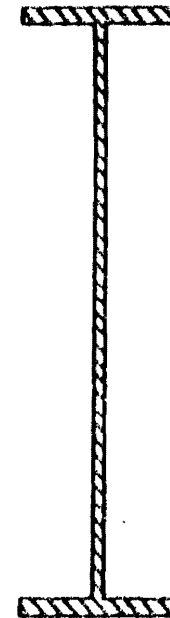
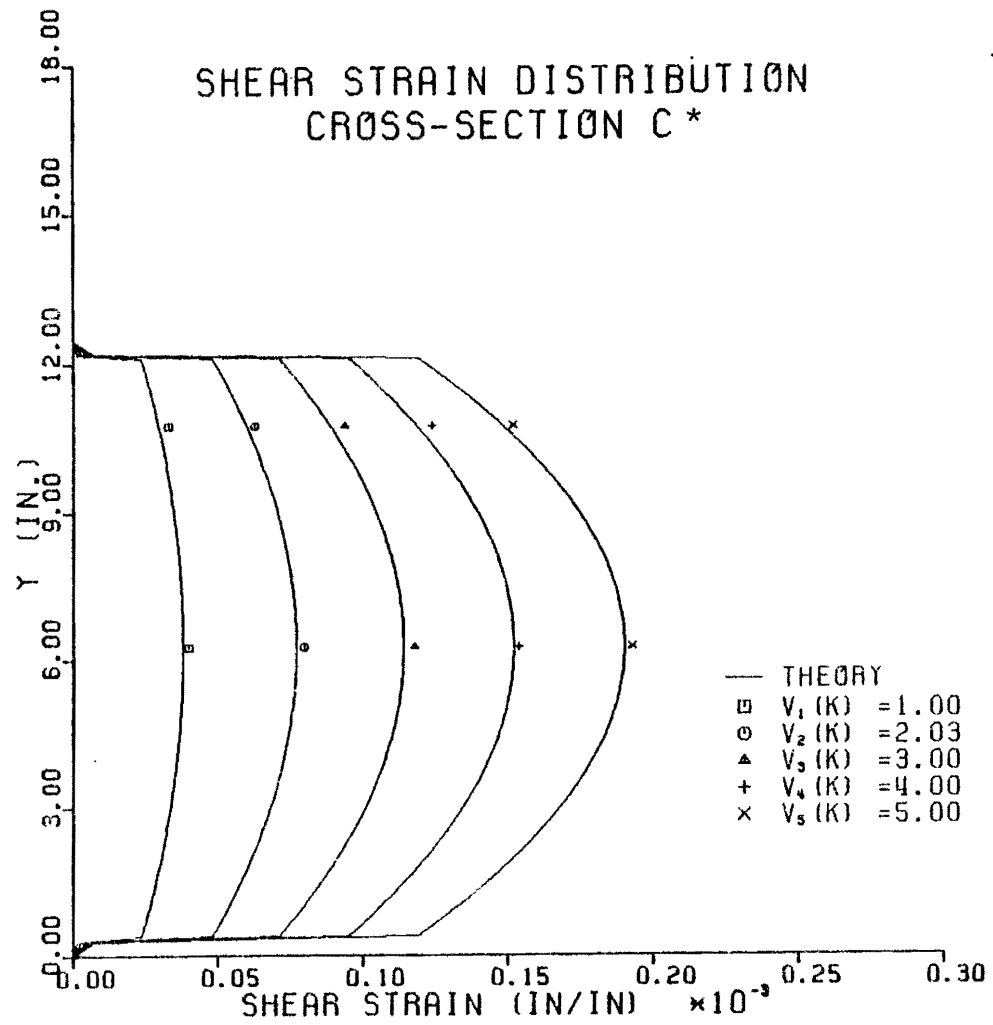


FIG. 41. Shear Strain Distribution, Cross Section B-B, Test No. 1.



* Stringer 1, 1 ft from left end

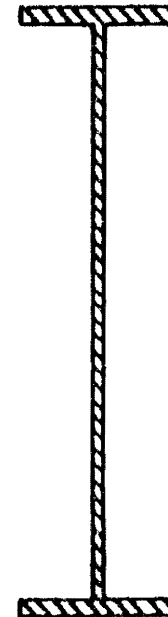


FIG. 42. Shear Strain Distribution, Cross Section C-C, Test No. 1.

TABLE 23. Deflections of Model Stringer 1, Test No. 1.

Deflections of Model Stringer 1 Test No. 1 in inches									
Average Loading in pounds	Dial Indicator #1 Quarter-Point			Dial Indicator #2 Midspan			Dial Indicator #3 Quarter-Point		
	Theory	Meas.	% Error	Theory	Meas.	% Error	Theory	Meas.	% Error
1000	.0675	.0622	- 7.85	.0922	.090	- 2.38	.0673	.061	- 9.36
2000	.1410	.130	- 7.80	.1945	.186	- 4.37	.1406	.113	-19.63
3000	.2046	.1964	- 4.01	.2796	.279	- 0.21	.2044	.182	-10.96
4000	.2712	.2633	- 2.91	.3705	.373	+ 0.67	.2707	.254	- 6.17
5000	.3479	.3301	- 5.11	.4763	.469	- 1.53	.3488	.324	- 7.11

TABLE 24. Deflections of Model Stringer 2, Test No. 1.

Deflections of Model Stringer 2 Test No.1 in inches									
Average Loading, in pounds	Dial Indicator #4 Quarter-Point			Dial Indicator #5 Midspan			Dial Indicator #6 Quarter-Point		
	Theory	Meas.	% Error	Theory	Meas.	% Error	Theory	Meas.	% Error
1000	.0684	.063	- 8.21	.0934	.089	- 4.71	.0682	.0734	+ 7.62
2000	.1377	.130	- 5.55	.1880	.187	- 0.53	.1373	.1449	+ 5.53
3000	.2079	.202	- 2.83	.2840	.287	+ 1.06	.2076	.2146	+ 3.37
4000	.2753	.273	- 0.84	.3766	.379	- 0.64	.2752	.2830	+ 2.83
5000	.3447	.340	- .08	.4708	.474	+ 0.68	.3439	.3528	+ 2.58

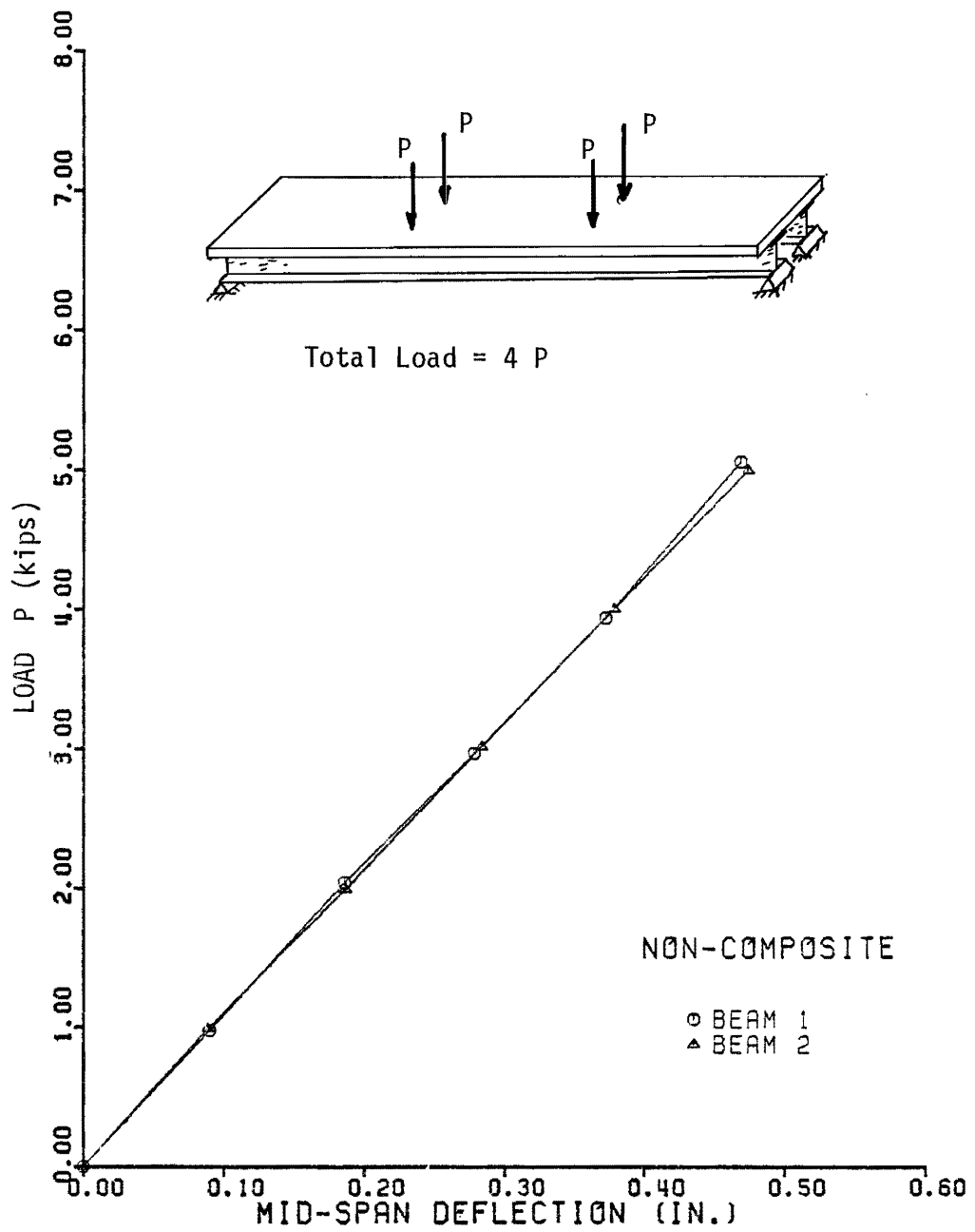


FIG. 43 Mid-Span Deflections, Test No. 1.

interaction between the precast panels and the model stringers due to the pocket connections alone.

Description of Test No. 2

In this test, all ten precast panels were in place, but were only grouted at the pocket connections as shown in Figure 44. There was a gap at the panel-stringer interface located between pockets. Point loads were applied at the third points over each of the two stringers. The model was loaded quasi-statically, and each point load incremented by one-kip up to a maximum of 5 kips. The same cross sections monitored in Test No. 1 were investigated for flexure. Some concrete gages were also monitored in some cross sections but in general, no good correlation was obtained with the data provided by these gages. Deflection readings were also taken at all six quarter points of the model stringers.

Flexural Strain Distribution

The flexural strain data obtained in this test was reduced by multiplying the strain readings of every strain gage by its corresponding correction factor. These data were not correlated with the theory because of difficulty in formulating an analytical solution; instead, a linear fit was used. Each of the cross sections monitored was located at the same place reference to the panel geometry, 1-ft from the centerline of the shear key joints as illustrated in Fig. 44. Therefore, the moment of inertia at all instrumented cross sections was expected to be approximately the same, but, because of the interface gaps, it was not expected to be much higher than that of the stringers alone.

The results of the flexural distribution at cross sections 1-1 to 8-8 are illustrated graphically in Figs. 45 through 52. In these graphs, the strain distributions in the panels were not plotted because of the lack of data. The points that are not connected to the linear fit represent some strain measurements made at the bottom surface of the precast panels. The linear fit was done at every loading. Note that the lines cross the y-axis at approximately the same point, the neutral axis.

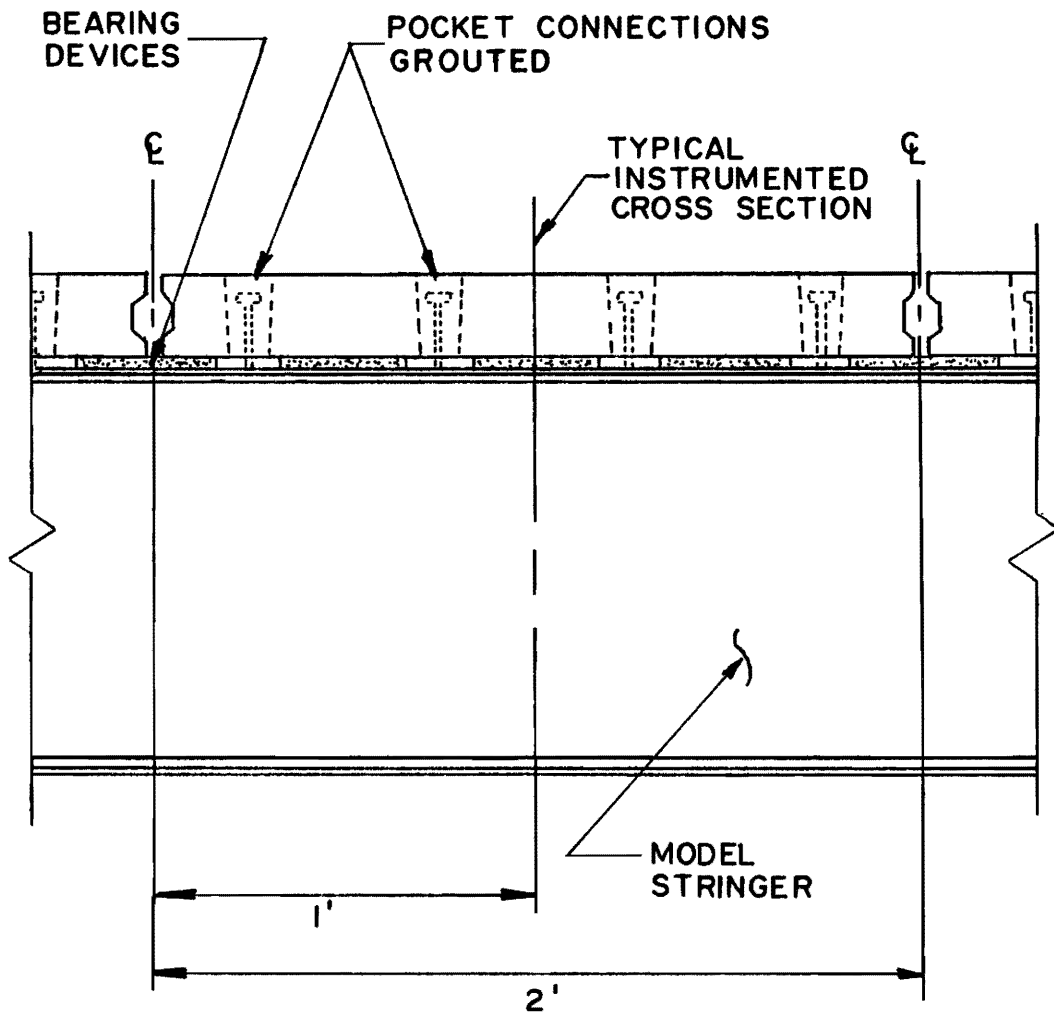
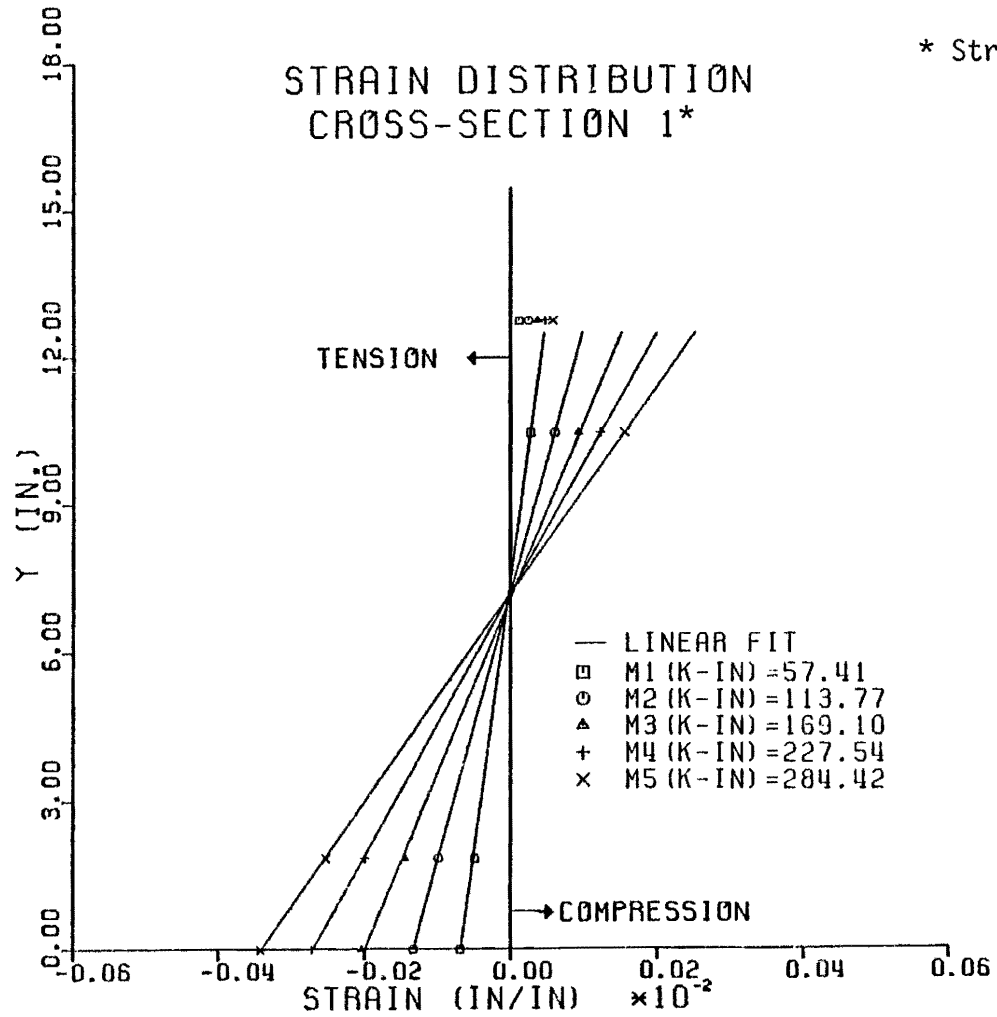


FIG. 44. Typical Location of Cross Section Instrumented for Flexure Relative to Shear Key Joints.



* Stringer 1, 15 ft from left end

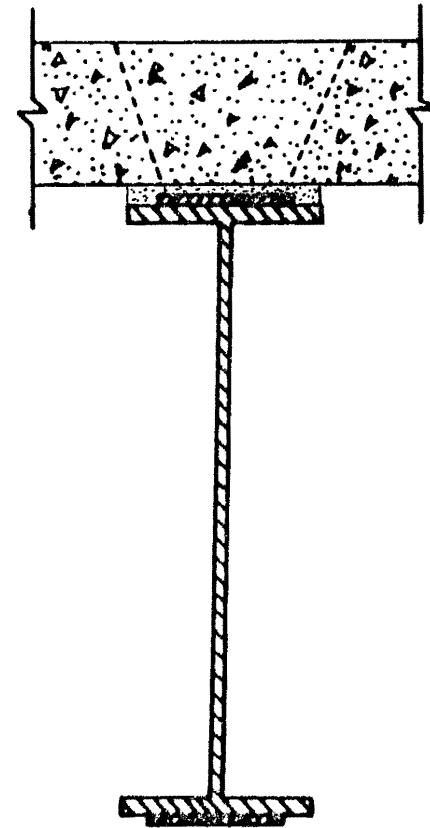
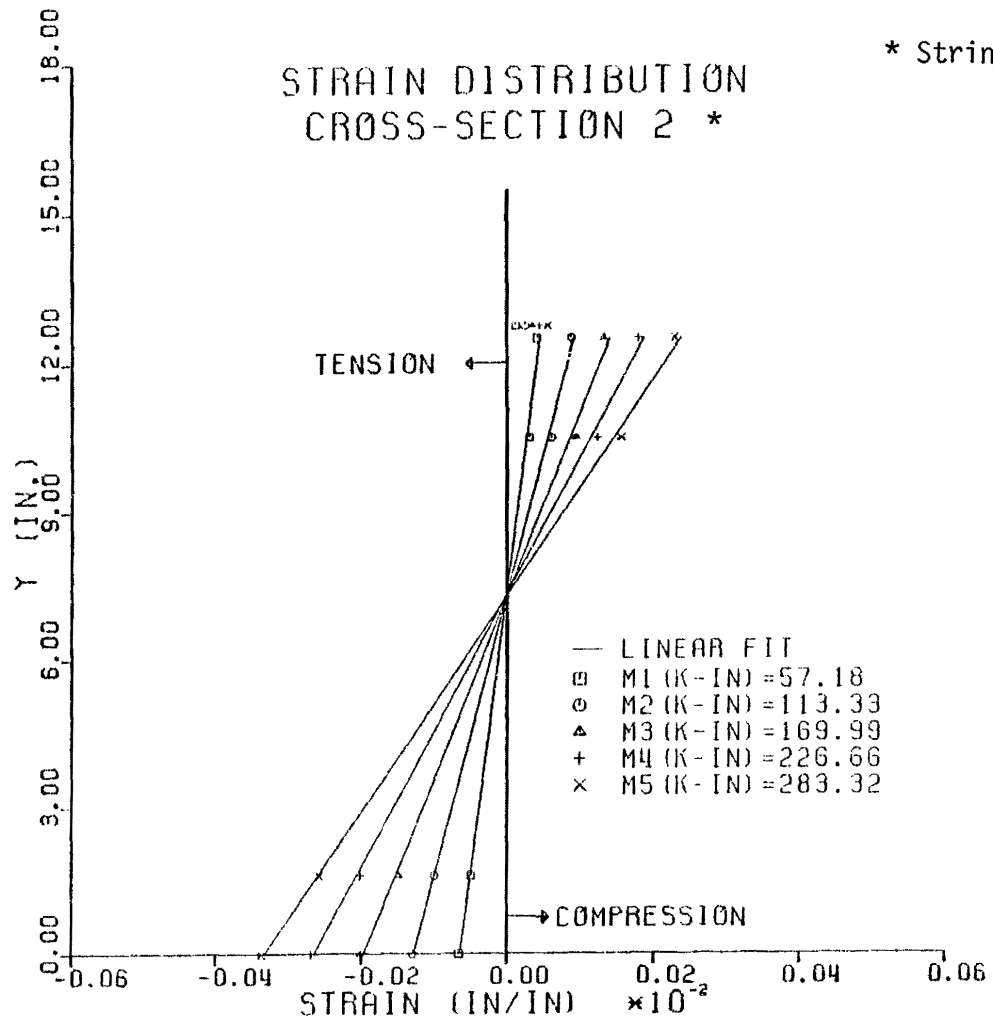


FIG. 45. Flexural Strain Distribution, Cross Section 1-1, Test No. 2.



* Stringer 2, 15 ft from left end

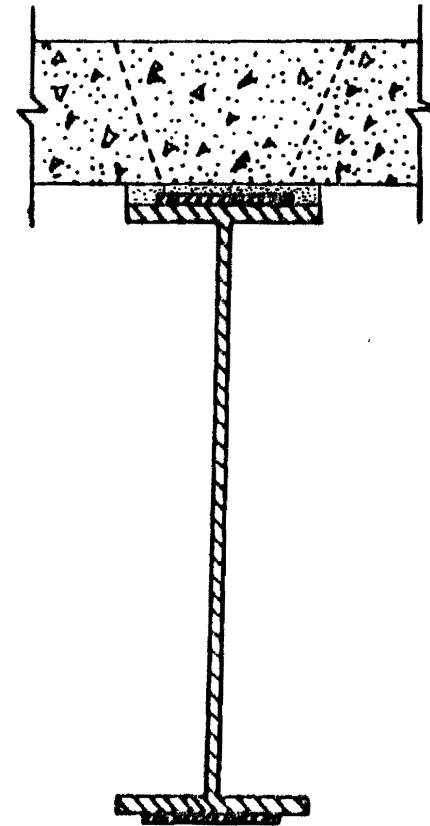


FIG. 46. Flexural Strain Distribution, Cross Section 2-2, Test No. 2.

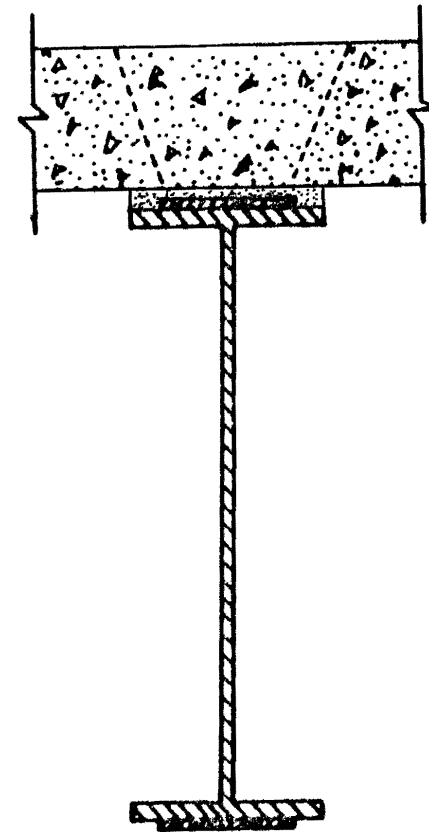
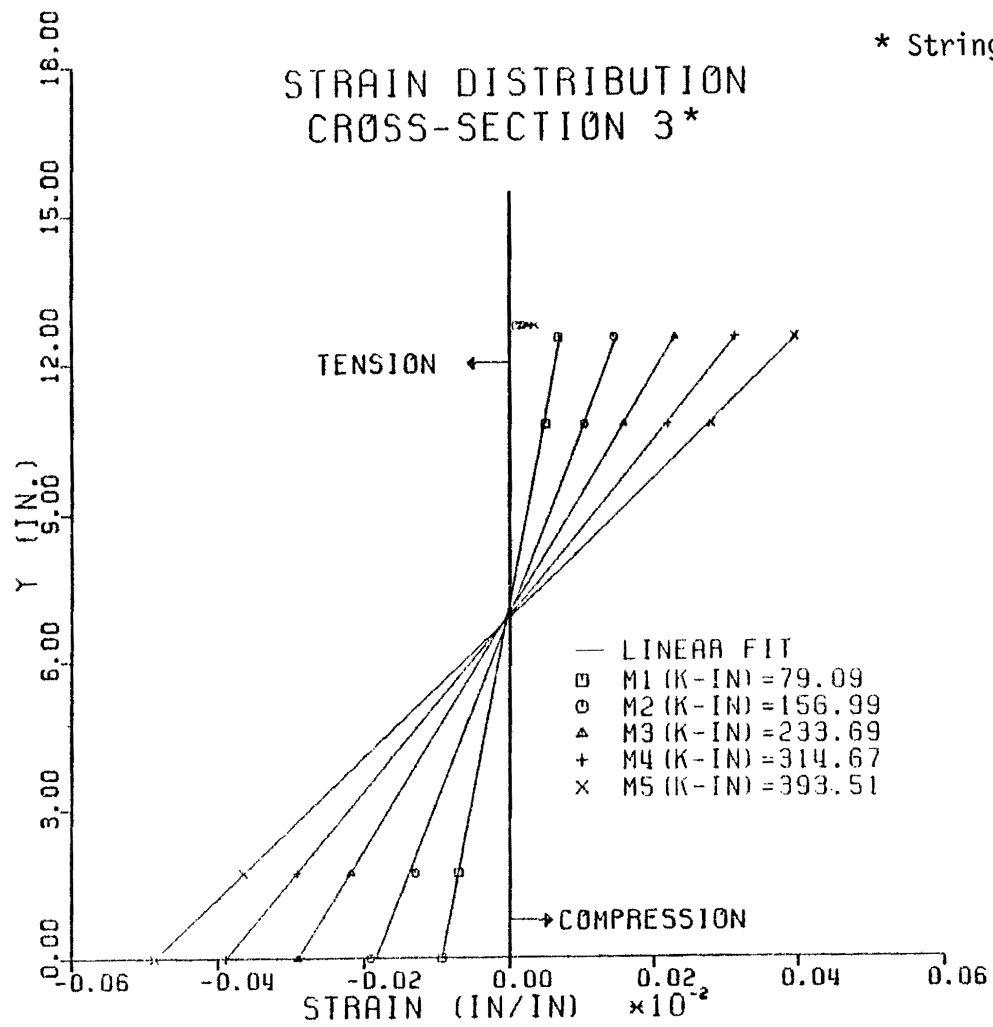
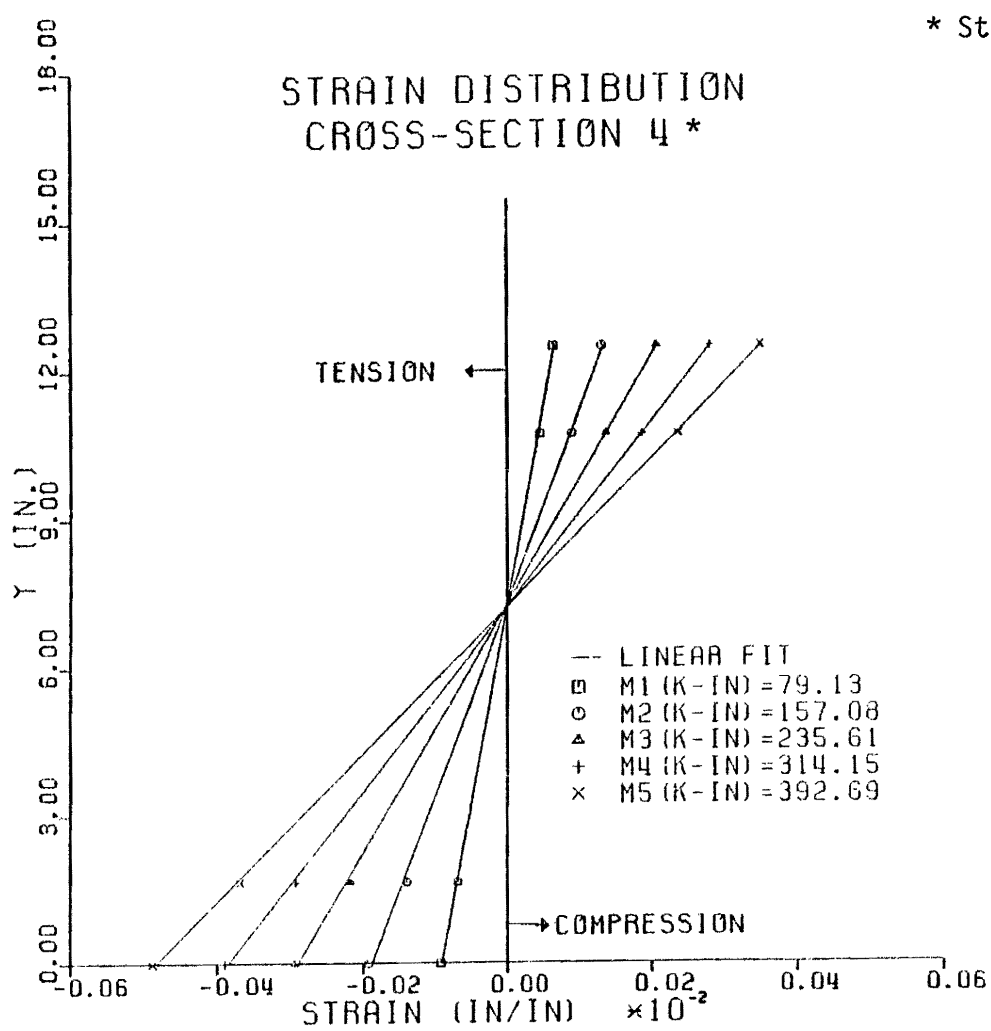


FIG. 47. Flexural Strain Distribution, Cross Section 3-3, Test No. 2.



* Stringer 2, 11 ft from left end

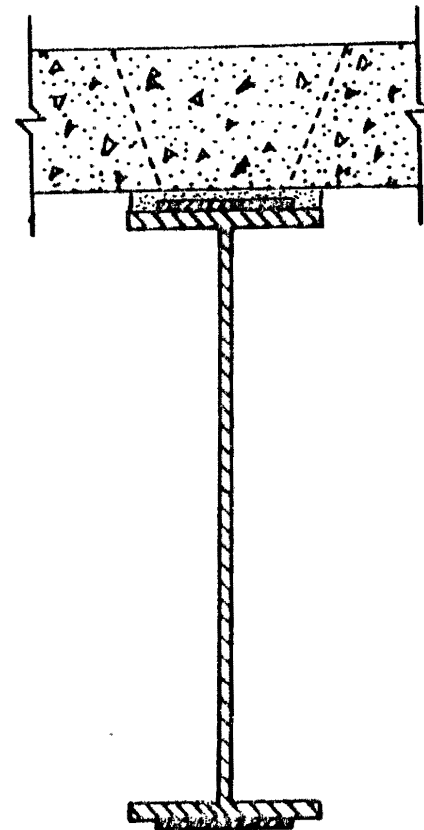


FIG. 48. Flexural Strain Distribution, Cross Section 4-4, Test No. 2.

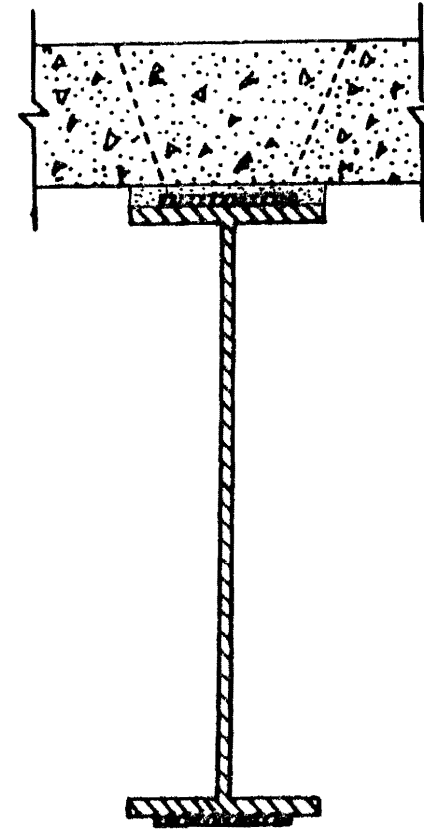
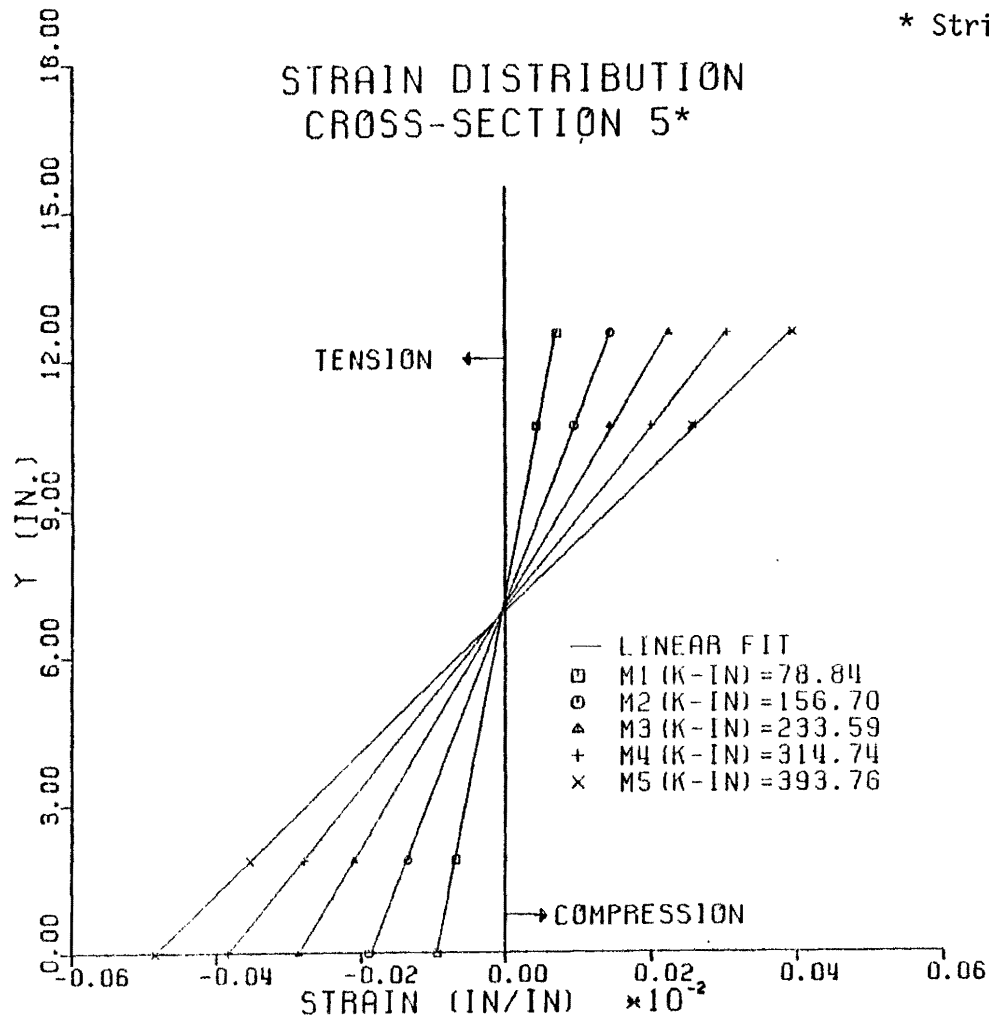
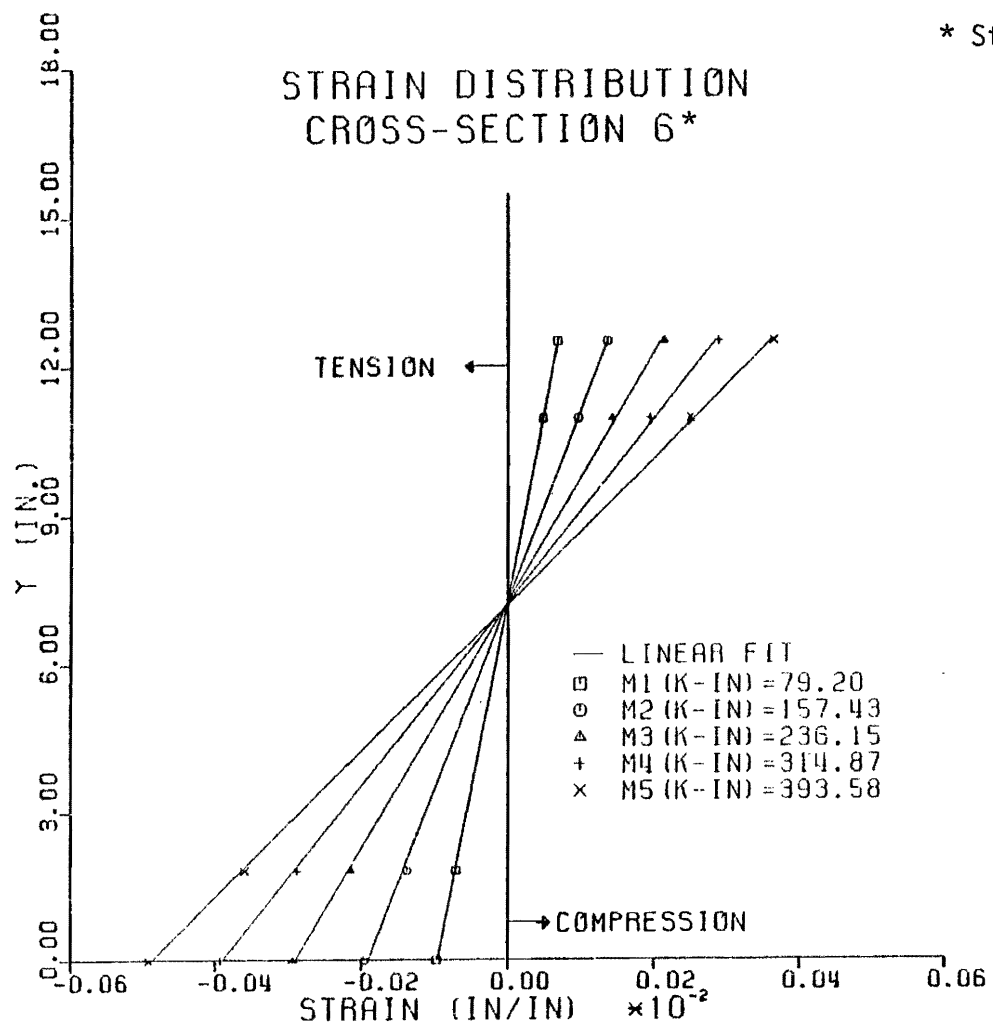


FIG. 49. Flexural Strain Distribution, Cross Section 5-5, Test No. 2.



* Stringer 2, 9 ft from left end

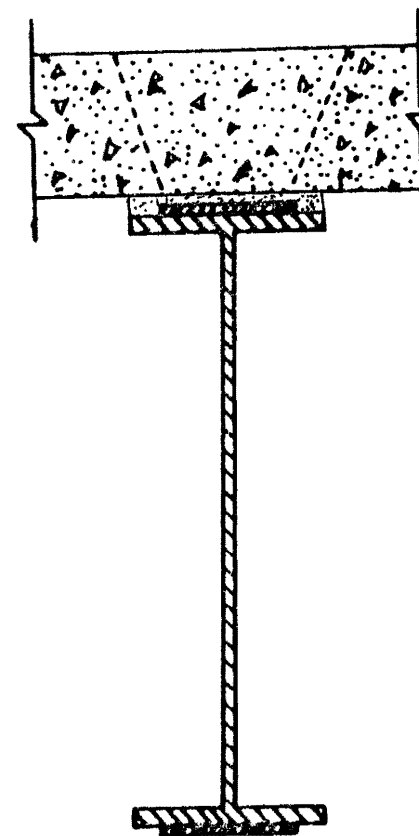
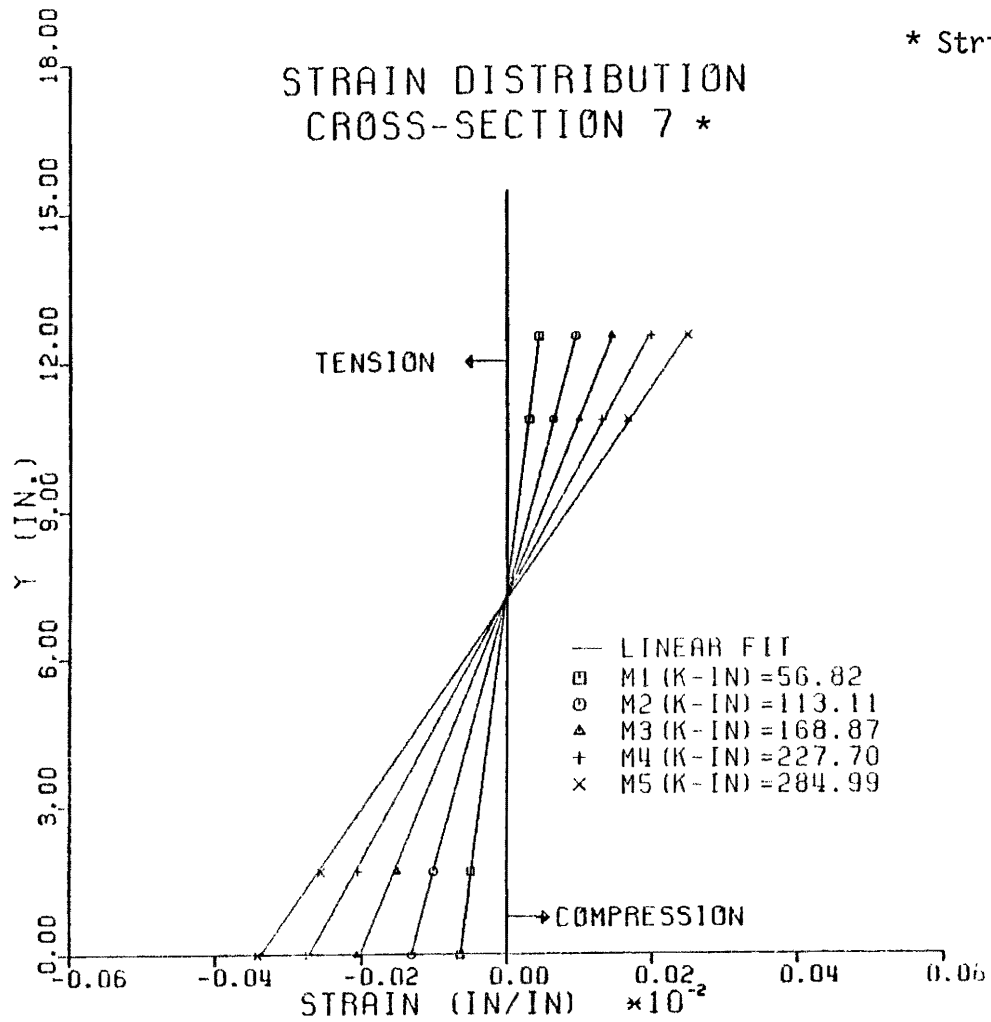


FIG. 50. Flexural Strain Distribution, Cross Section 6-6, Test No. 2.



* Stringer 1, 5 ft from left end

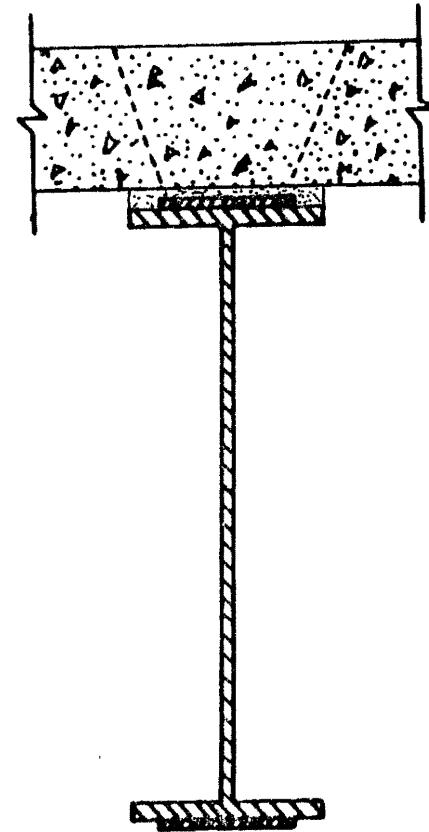
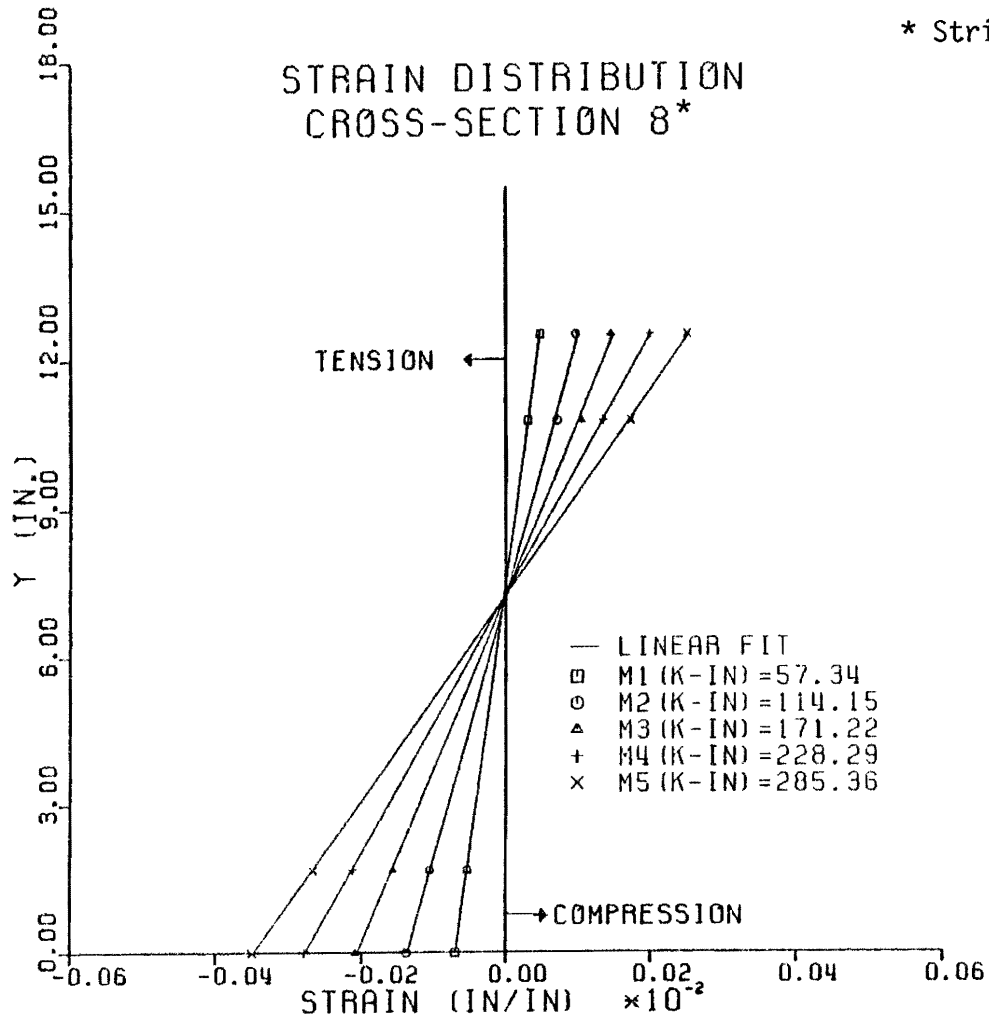


FIG. 51. Flexural Strain Distribution, Cross Section 7-7, Test No. 2.



* Stringer 2, 5 ft from left end

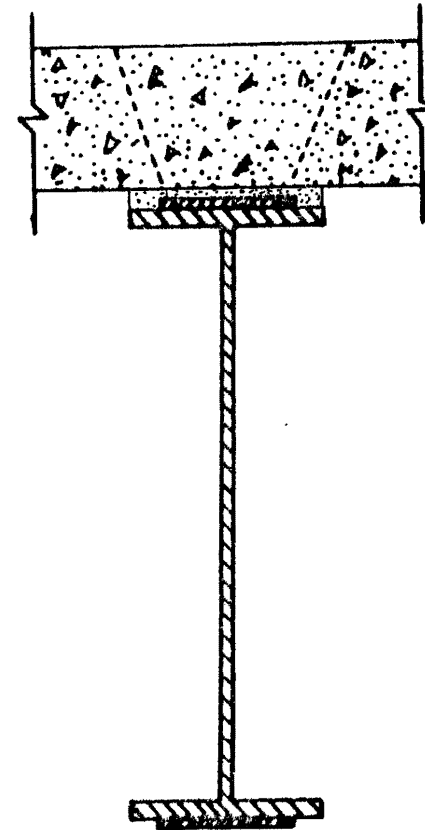


FIG. 52. Flexural Strain Distribution, Cross Section 8-8, Test No. 2.

By comparing the measured strains at cross sections 2-2 and 3-3, it can be observed that the strains at the bottom surface of the precast panels were larger in cross section 2-2 than in cross section 3-3, even though the moments applied were smaller. This can be attributed to the fact that cross section 3-3 was located in a pure moment region.

Deflections

Deflections were measured at the same locations as in Test No. 1. Deflection readings were made at every load increment. The main objective for taking this data was to evaluate the overall stiffness improvement of the model bridge due to the pocket connections alone.

The deflections were not correlated with the theory because the variability of the moment of inertia along the model stringers makes it difficult to formulate an analytical solution for deflections.

The measured deflections are tabulated in Tables 25 and 26 for model stringers 1 and 2, respectively. The load-midspan deflection curves are plotted in Fig. 53 for both model stringers. It can be observed that the stringers were deflecting with a very slight differential, probably because one of the beams developed greater moments of inertia than the other. The model stringers deflected at an average rate of 0.08 in. per 1 kip of third point load.

Test No. 3 - Full Composite Test

Static load tests were performed on the model with the pockets and shear key joints grouted. Flexural strain data was obtained at four cross sections using strain gages mounted on both the precast panels and steel stringers. Shear strain data was taken at three cross sections. Deflection data was taken at the six quarter points of both model stringers, and four displacement transducers were used to measure the relative slip displacement between the precast panels and the steel stringers at approximately 18 in. from each of the supports.

TABLE 25. Deflections of Model Stringer 1, Test No.2.

Deflection of Model Stringer 1 Test No. 2 in inches			
Average Load, in pounds	Dial Indicator #1 Quarter Point	Dial Indicator #2 Midspan	Dial Indicator #3 Quarter Point
1000	0.052	0.076	.059
2000	0.113	0.154	.112
3000	0.170	0.233	.172
4000	0.228	0.313	.230
5000	0.287	0.397	.291

TABLE 26. Deflections of Model Stringer 2, Test No. 2.

Deflection of Model Stringer 2 Test No. 2 in inches			
Average Load, in pounds	Dial Indicator #4 Quarter Point	Dial Indicator #5 Midspan	Dial Indicator #6 Quarter Point
1000	0.061	0.082	0.058
2000	0.121	0.163	0.117
3000	0.184	0.245	0.176
4000	0.244	0.327	0.235
5000	0.306	0.407	0.296

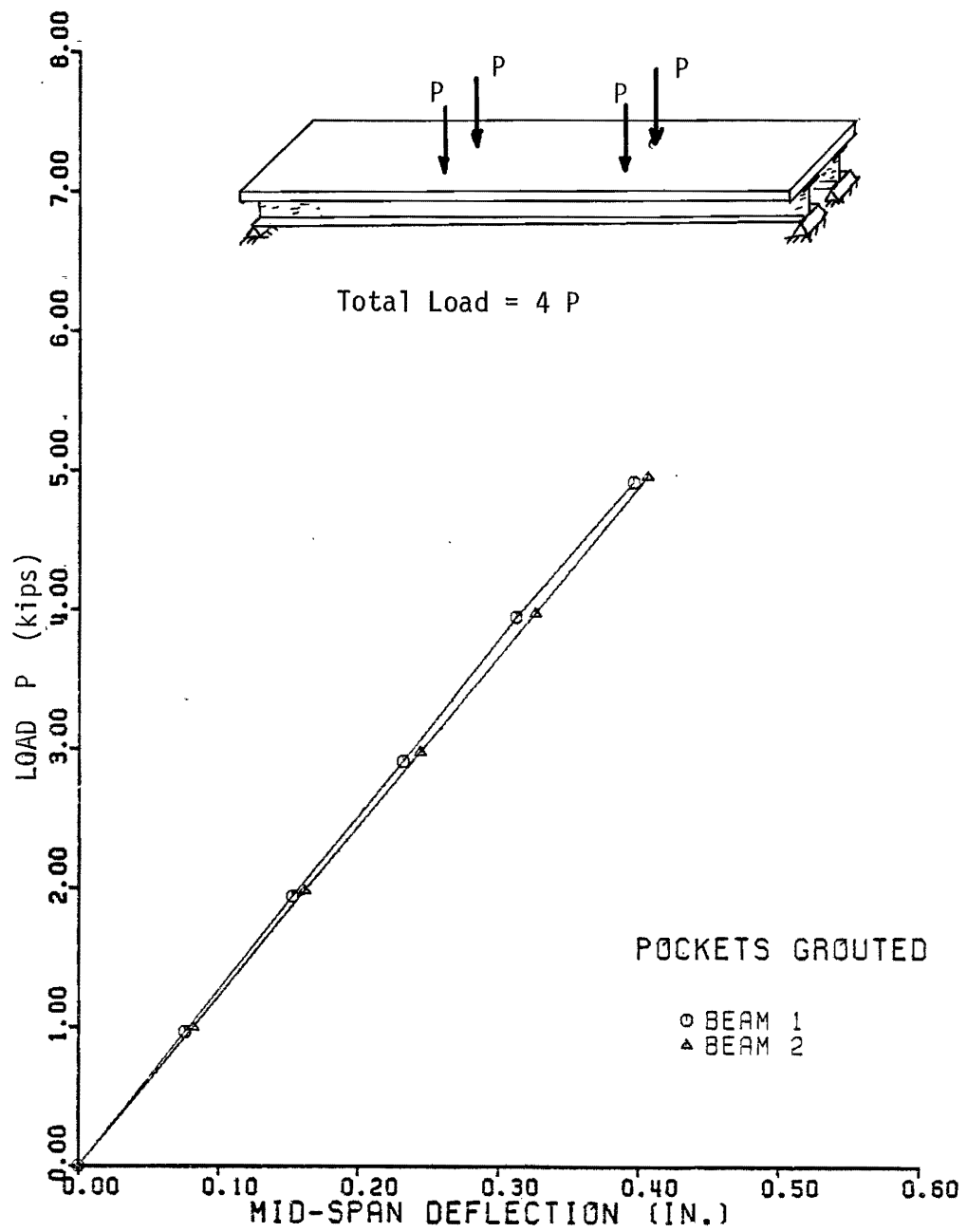


FIG. 53. Mid-Span Deflections, Test No. 2.

This test was performed 24 hours after the shear key joints were grouted and 72 hours after the pocket connections were grouted. The main objective of this test was to verify that full composite behavior was achieved. This was accomplished by obtaining flexural strain data and measuring the relative slip between the precast panels and the model stringers.

Description of Test No. 3

Static loads were applied with four hydraulic rams placed over the third points of each of the two stringers of the model. All the pockets and transverse shear key joints were grouted. The model was loaded quasi-statically up to 6 kips per ram in one-kip increments. Thus, the maximum total load on the model was 24 kips. Flexural strain data, shear strain data, deflections, and relative slip displacements were recorded.

Cross sections 1-1 to 4-4 were instrumented for flexure; and cross sections A-A, B-B, and C-C were instrumented for shear. The strain gages either embedded in or bonded to the precast panels were used.

Flexural Strain Distribution

The flexural strain data obtained in this test was reduced by multiplying the recorded strain readings of each gage by its corresponding correction factor. The data obtained was correlated to the theory. The theoretical flexural strains, ϵ_{th} , were computed using the formula:

$$\epsilon_{th} = \frac{M y}{I E_s}$$

where

M = the moment acting on the cross section under consideration,

y = the distance from the neutral axis of the transformed composite section to the particular location of each strain gage,

I = the moment of inertia of the transformed composite section, and
E = the modulus of elasticity of the steel stringers, taken to be 29,000
ksi.

The measured flexural strains at the instrumented cross sections are illustrated in Figs. 54 through 57 along with the theoretical flexural strain distributions. It can be observed that the measured strain correlated satisfactorily with the theory. The measured strains were considered as true strains because of the accuracy obtained in Test No. 1.

Shear Strain Distribution

Strain rosette data were obtained for cross sections A-A, B-B, and C-C. The shear strain data were reduced using the same procedures as in Test No. 1. The same strain rosettes were instrumented.

The measured horizontal shear strains, ϵ_{xy} , were compared to the theoretical horizontal shear strains, $\epsilon_{xy th}$, computed from the formula:

$$\epsilon_{xy th} = \frac{V Q}{I t G}$$

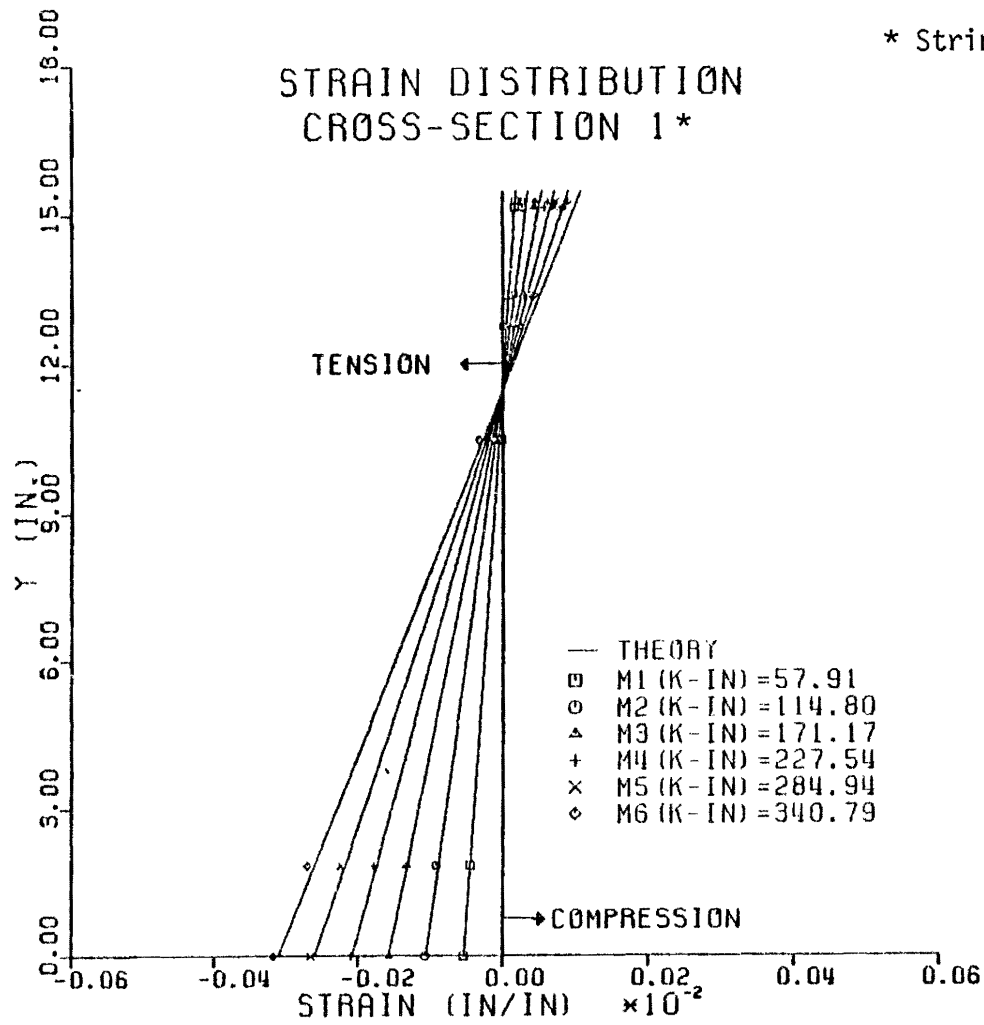
where

- V = the shear force acting on the cross section under investigation,
- Q = the first moment of area about the neutral axis of the transformed composite section of the area outside the gage,
- I = the moment of inertia of the transformed composite section,
- t = the thickness of the plane under investigation, and
- G = the modulus of rigidity of steel.

Figs. 58 to 60 show the shear strains measured along the x-y plane at cross sections A-A, B-B, and C-C, respectively, correlated with the theoretical values.

Deflections

Deflections were measured at five points of the model, three at the quarter points of model stringer No. 1 and two at midspan and one quarter



* Stringer 1, 15 ft from left end

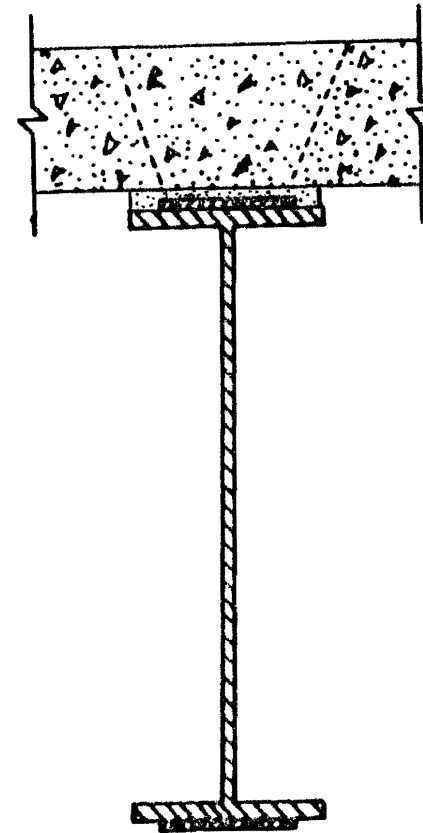
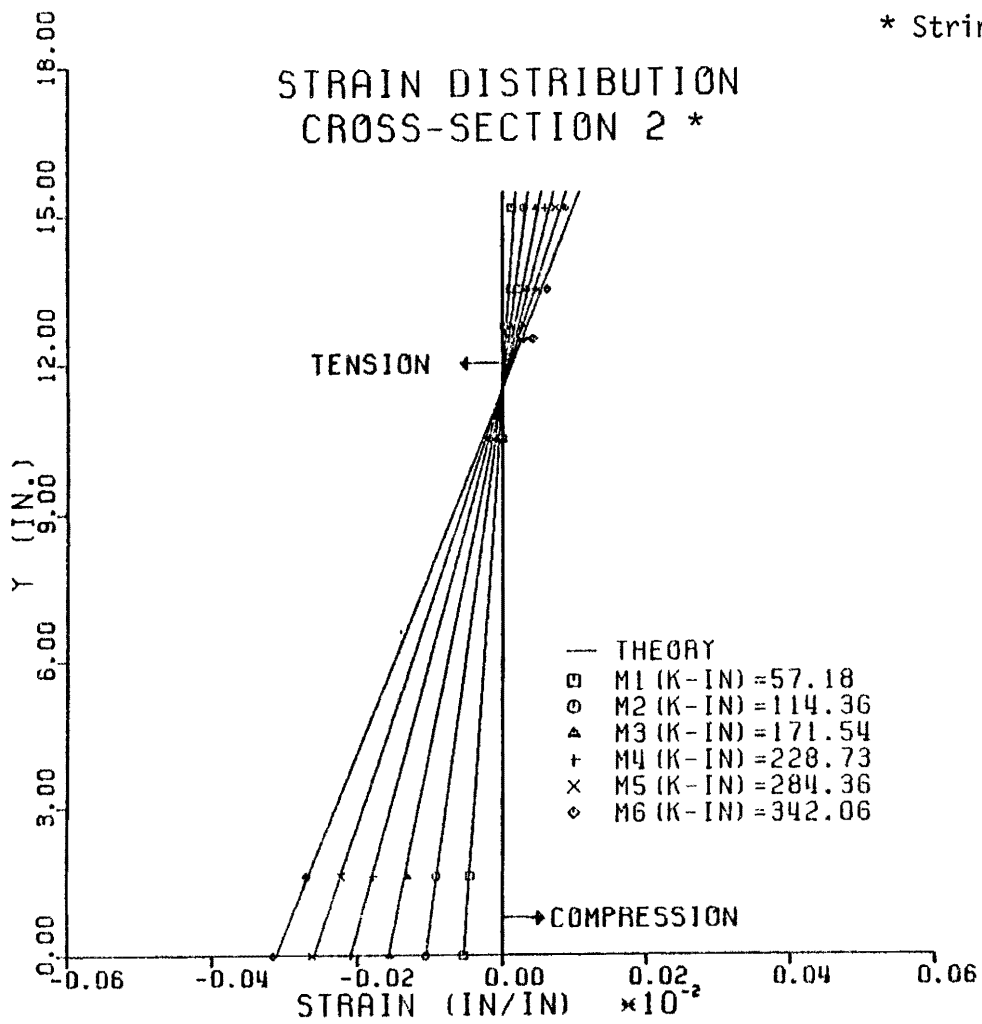


FIG. 54. Flexural Strain Distribution, Cross Section 1-1, Test No. 3.



* Stringer 2, 15 ft from left end

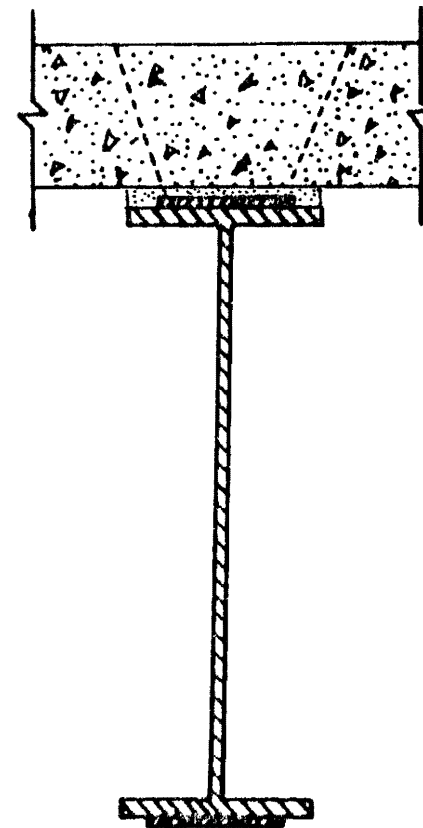
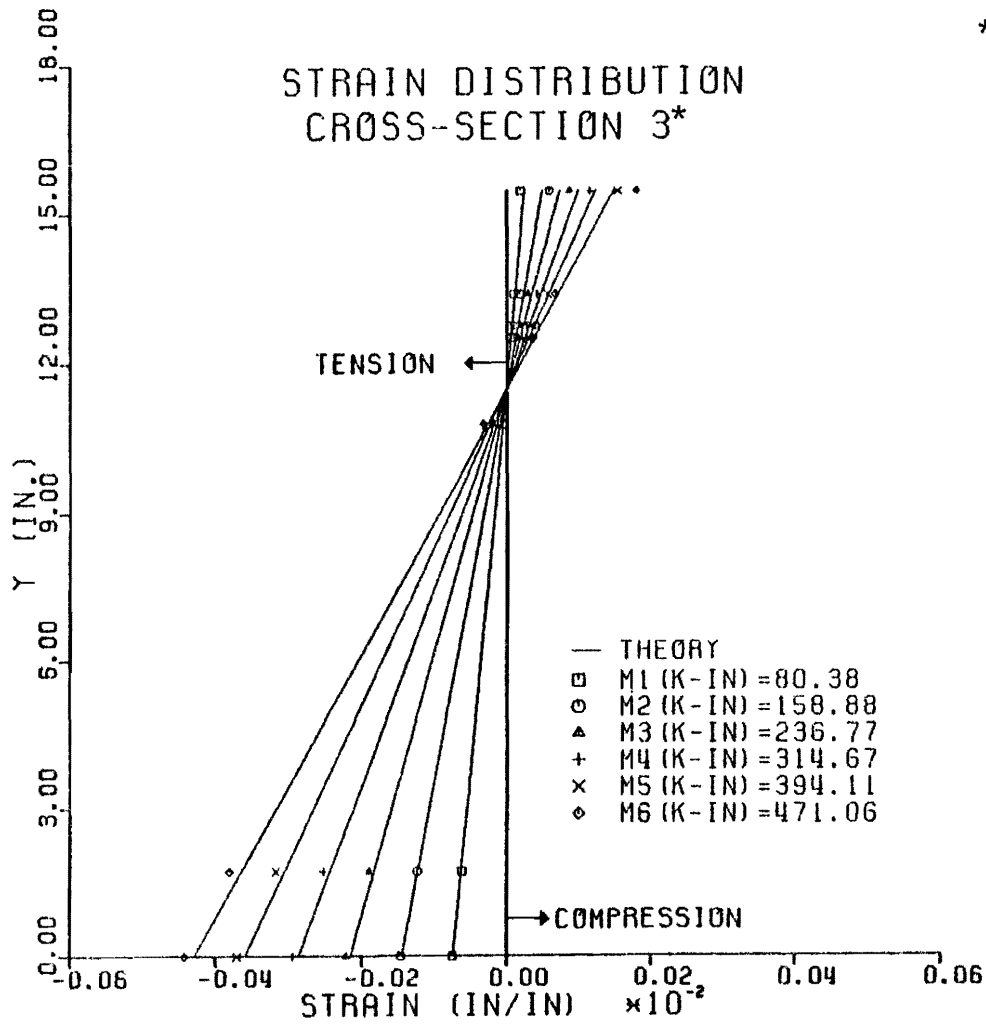


FIG. 55. Flexural Strain Distribution, Cross Section 2-2, Test No. 3.



* Stringer 1, 11 ft from left end

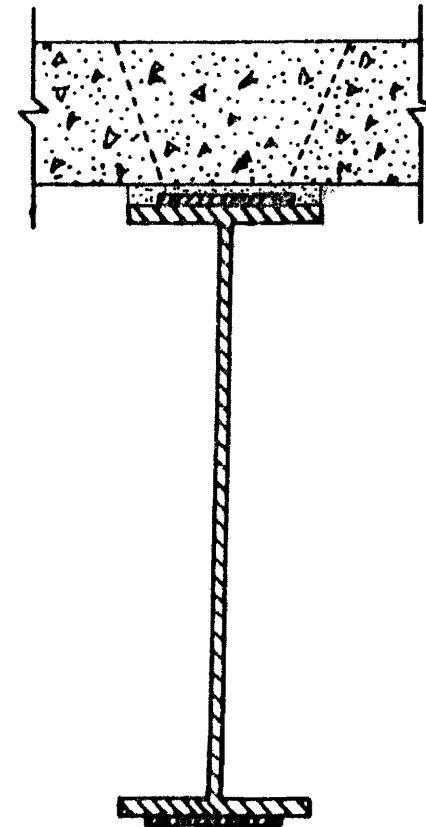
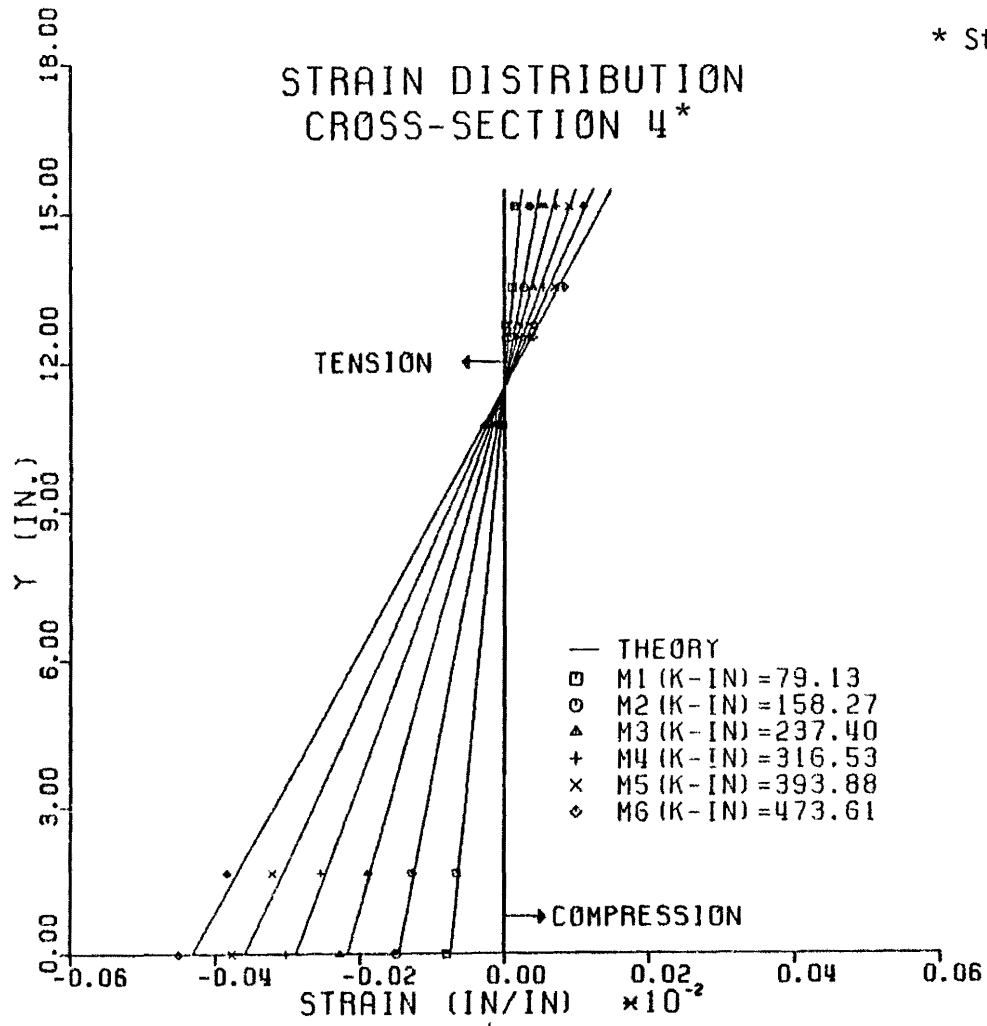


FIG. 56. Flexural Strain Distribution, Cross Section 3-3, Test No. 3.



* Stringer 2, 11 ft from left end

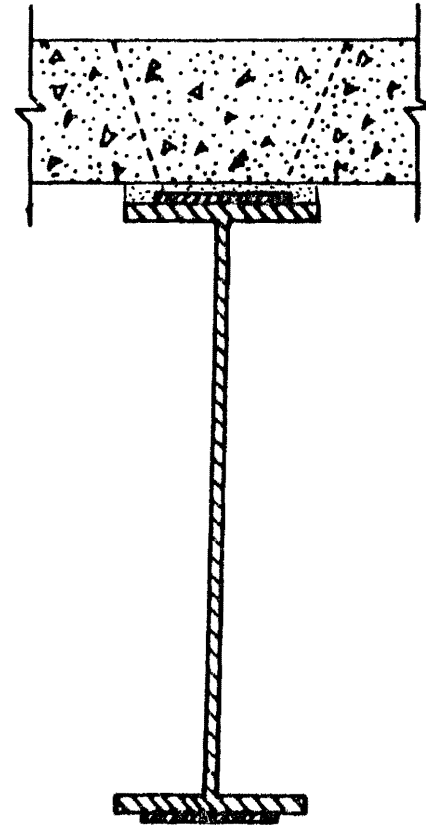
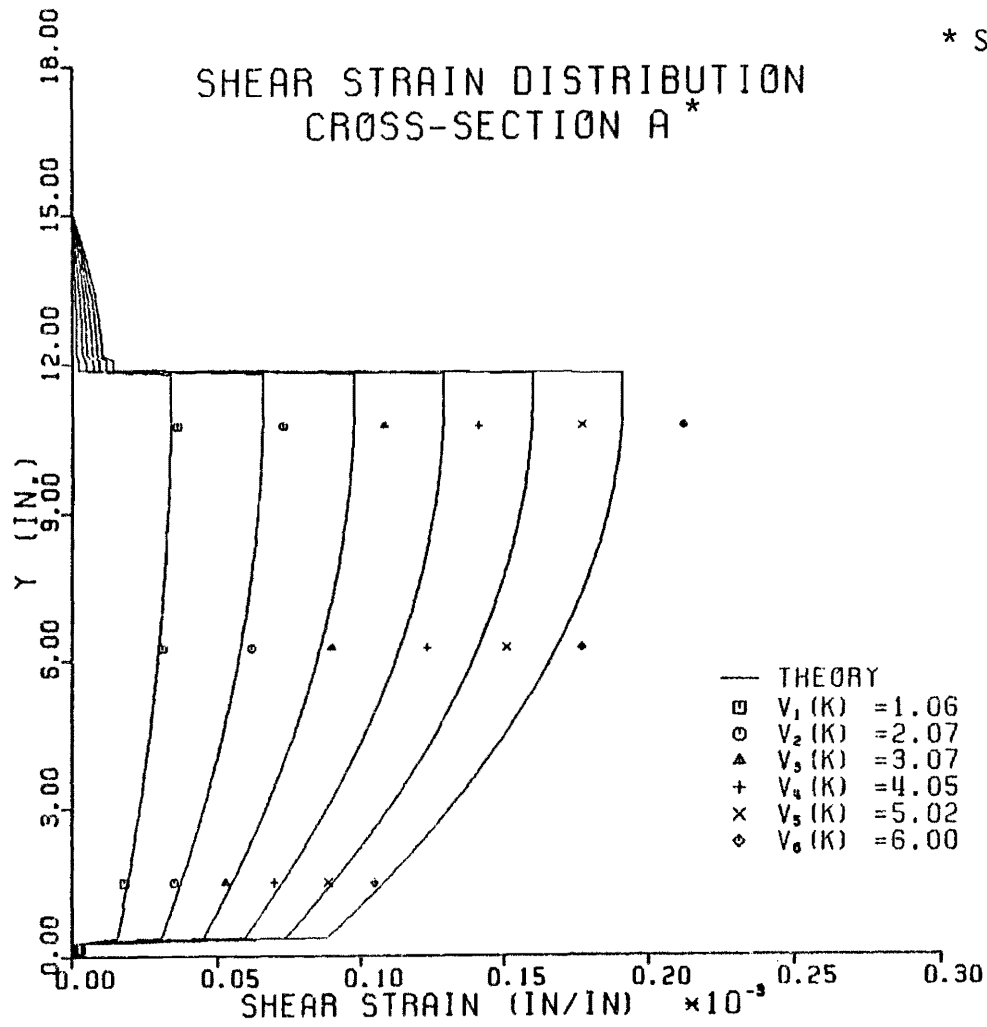


FIG. 57. Flexural Strain Distribution, Cross Section 4-4, Test No. 3.



* Stringer 1, 19 ft from left end

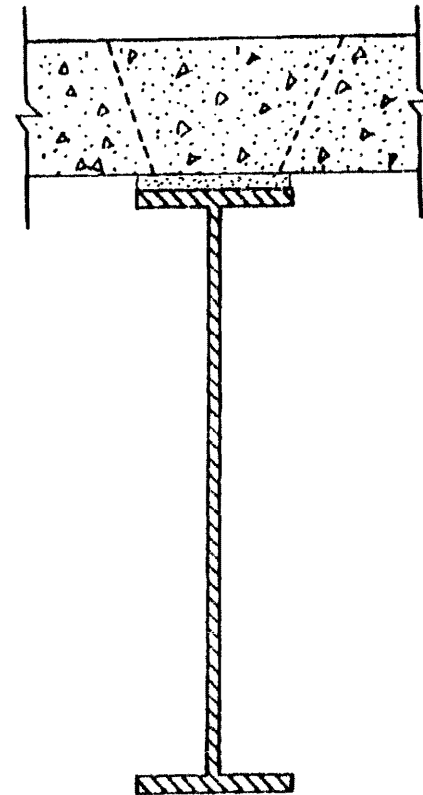
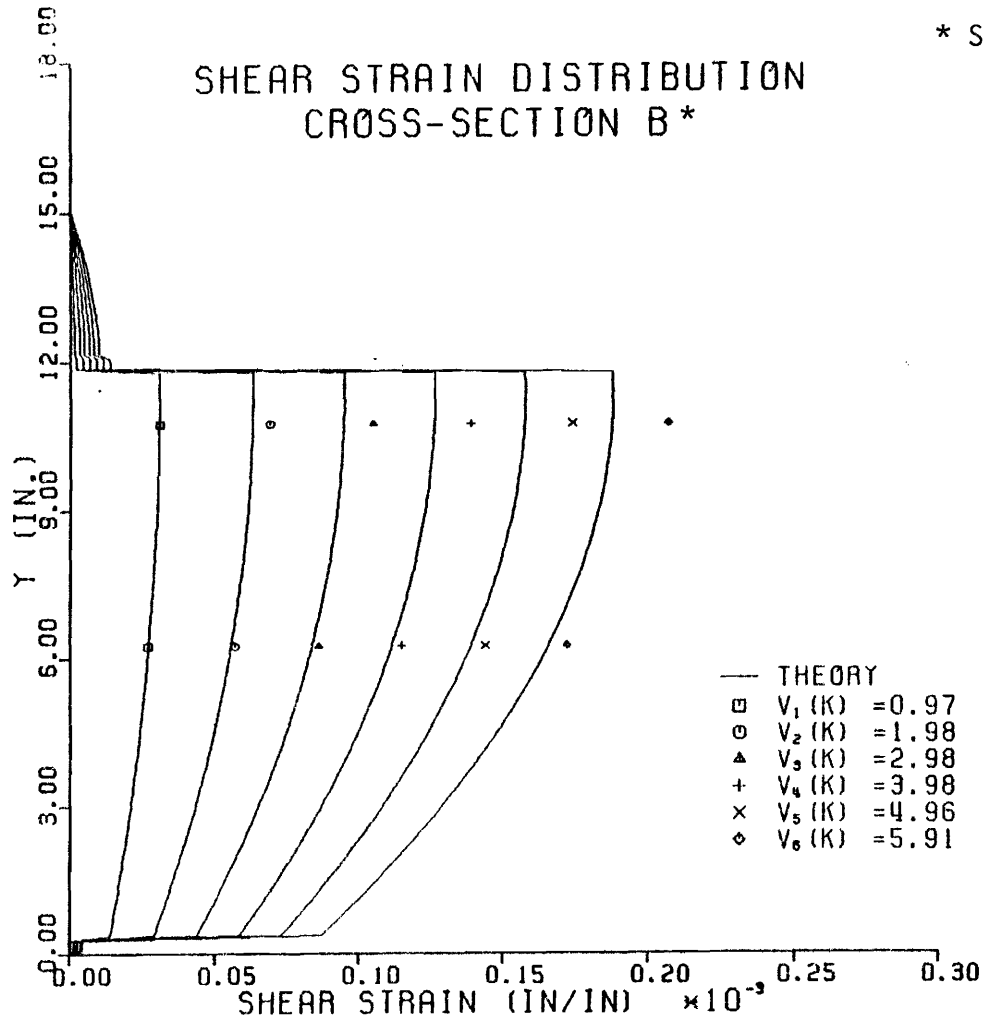


FIG. 58. Shear Strain Distribution, Cross Section A-A, Test No. 3.



* Stringer 2, 19 ft from left end

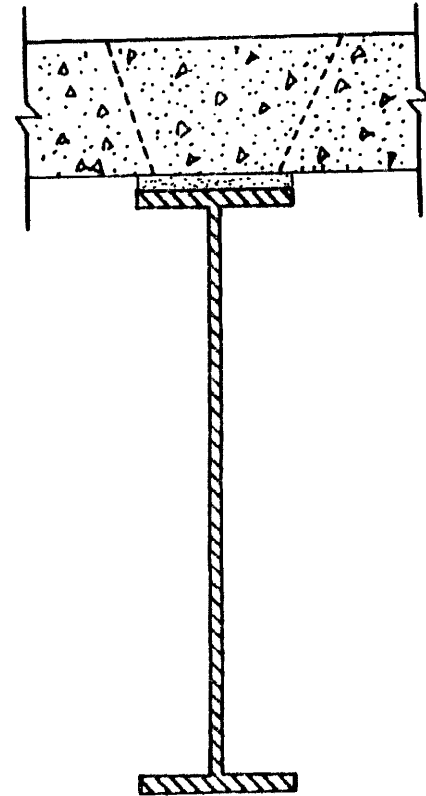
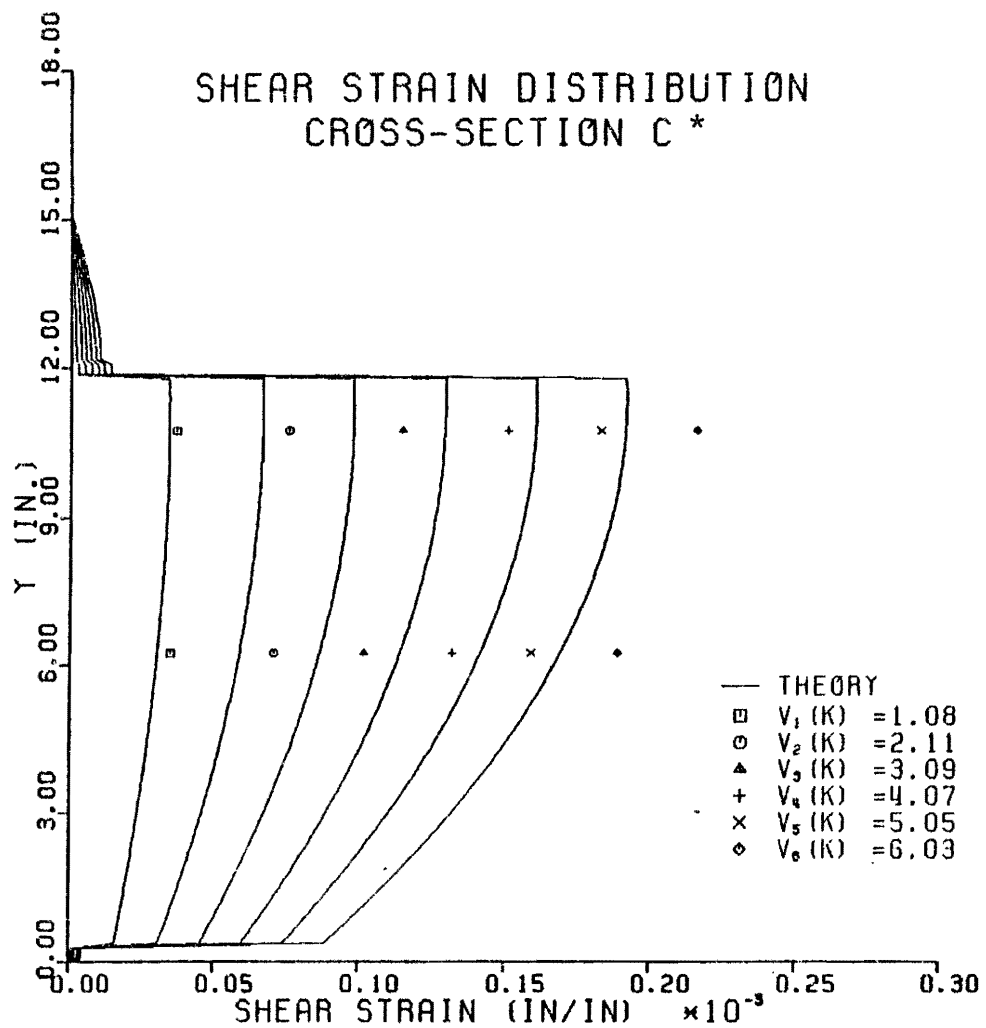


FIG. 59. Shear Strain Distribution, Cross Section B-B, Test No. 3.



* Stringer 1, i ft from left end

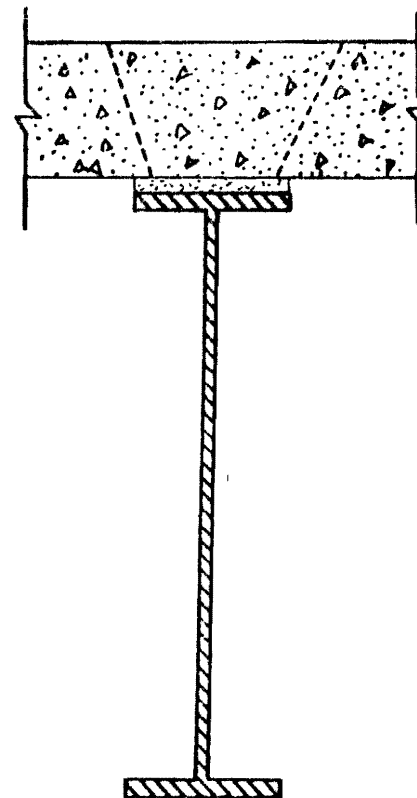


FIG. 60. Shear Strain Distribution, Cross Section C-C, Test No. 3.

point of model stringer No. 2. Dial indicator No. 4 was accidentally disturbed during the test.

The objectives of the deflections were to evaluate the overall improvement in the model bridge as full composite behavior was achieved. The measured deflections are tabulated in Tables 27 and 28 for model stringer Nos. 1 and 2, respectively. The midspan deflections of both model stringers were plotted against the average third point load applied, as illustrated in Fig. 61. The model was deflected at an average rate of 0.037 in. per 1 kip of third point load.

Relative Slip Displacement

The relative slip displacements between the precast panels and the steel stringers were measured at four different locations at the two ends of each of the two model stringers. The slips were measured with the displacement transducers that were placed about 18 in. from each of the supports.

The slips were plotted versus the horizontal shear force acting at the corresponding sections as illustrated in Fig. 62. Even though some slips were present, their magnitude was considered very small. The shear-slip curves show that the relation was linear with the average pocket connection modulus about 2.50×10^6 lbs per in. of slip.

TABLE 27. Deflections of Model Stringer 1, Test No. 3.

Deflection of Model Stringer 1, Test No. 3 in inches			
Average Load, in pounds	Dial Indicator #1 Quarter Point	Dial Indicator #2 Midspan	Dial Indicator #3 Quarter Point
1000	0.026	0.040	0.025
2000	0.054	0.077	0.050
3000	0.080	0.112	0.078
4000	0.108	0.150	0.105
5000	0.134	0.185	0.130
6000	0.160	0.219	0.157

TABLE 28. Deflections of Model Stringer 2, Test No. 3.

Deflection of Model Stringer 2, Test No. 3 in inches			
Average Load, in pounds	Dial Indicator #4 Quarter Point	Dial Indicator #5 Midspan	Dial Indicator #6 Quarter Point
1000	-	0.038	0.029
2000	-	0.078	0.057
3000	-	0.115	0.084
4000	-	0.153	0.110
5000	-	0.190	0.136
6000	-	0.226	0.160

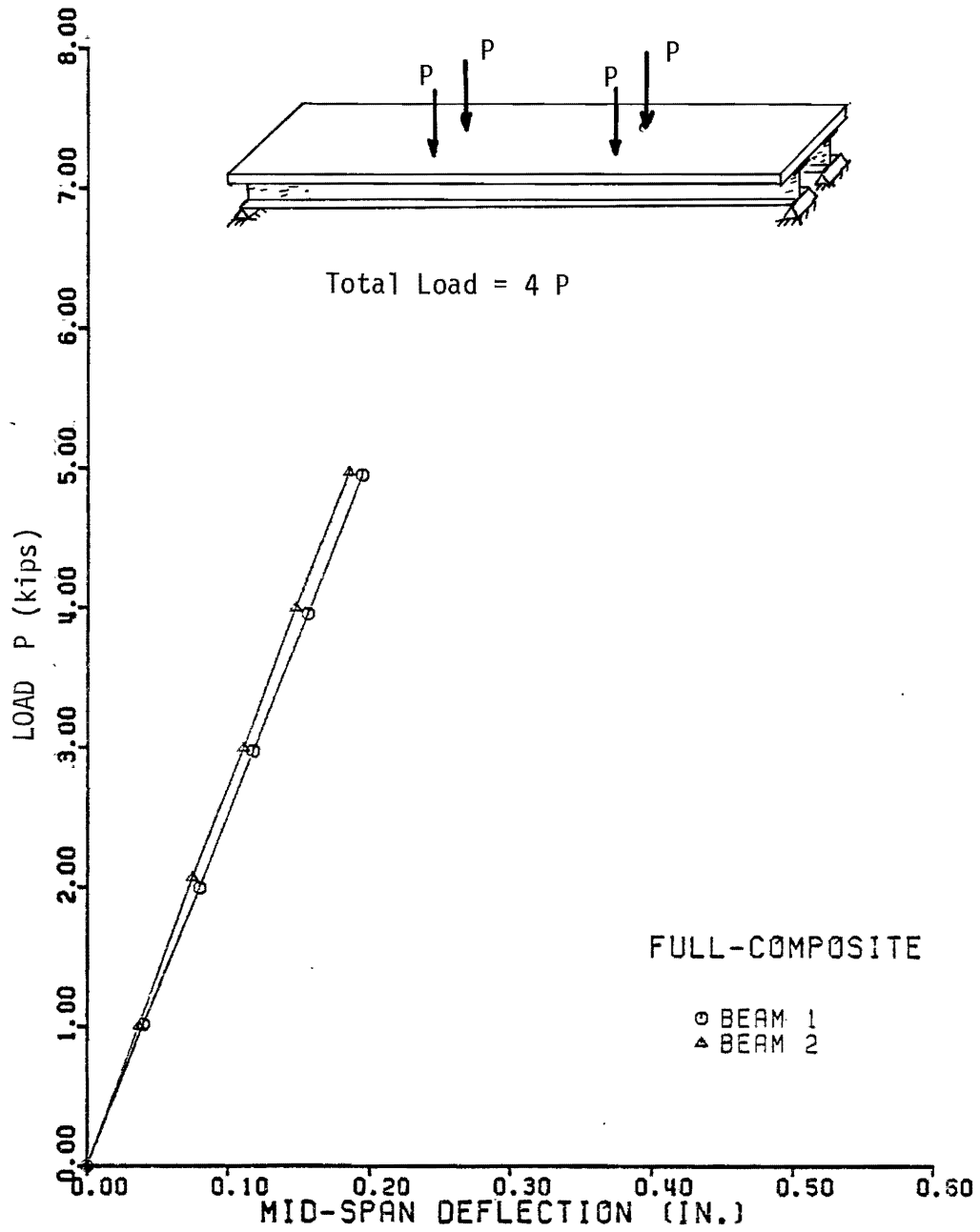


FIG. 61. Mid-Span Deflections, Test No. 3.

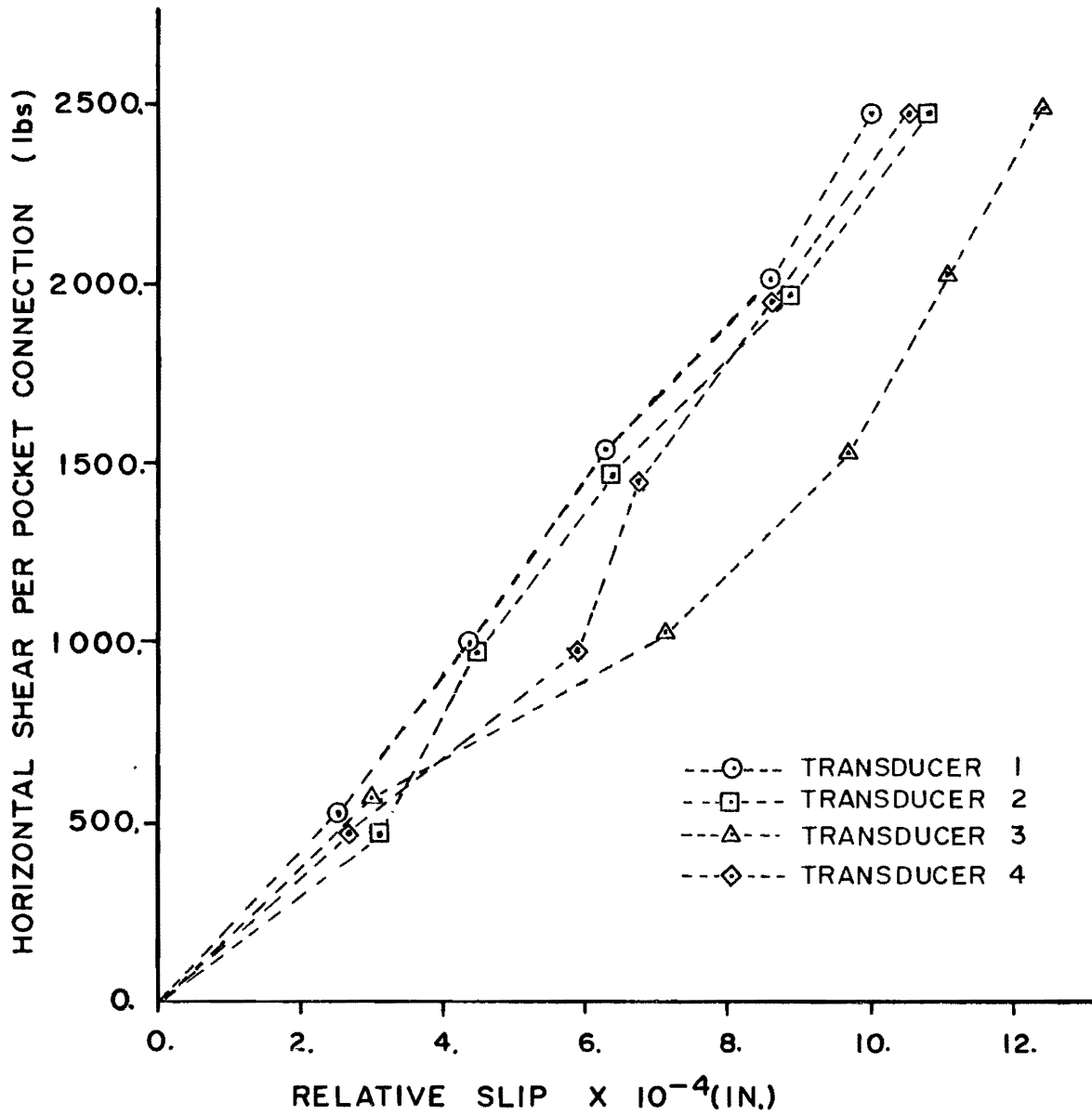


FIG. 62. Slip Displacements, Test No. 3.

C H A P T E R I V

DISCUSSION OF TEST RESULTS

General

The static load test results reported in Chapter 3 were obtained by applying static loads to the 1/3 full-scale model at three different stages during construction of the model:

- 1) prior to placing the model precast concrete panels,
- 2) after placing the model precast panels and grouting the pocket connections only, and
- 3) after grouting the shear key joints between adjacent panels.

The flexural strain and the shear strain data of Test No. 1 were normalized and compared to the theory to determine the validity of the test results. The flexural strain data of Test No. 2 was not correlated with the theory; a linear fit was done instead.

The flexural strain distributions for Tests No. 1 through No. 3 are compared as the structural behavior of the model went through a transition from noncomposite to full composite. The shear strain distributions of Tests No. 1 and No. 3 are compared. The midspan deflections obtained for all tests are also compared.

The flexural strains and deflections of the full composite test are compared to theoretical values of the prototype bridge. The flexural strains were only compared at the top fibers of the slab and at the bottom fibers of the stringers. The deflections are compared at the midspan of the structure. The theoretical section properties of the prototype were computed assuming a 3/4 in. gap between the panels and stringers, and assuming a concrete having a modulus of elasticity of 3.625×10^6 psi which yields a value for the ratio of the moduli of steel and concrete of 8.

The shear strain data was not compared to the prototype because it is highly dependent on the thickness of the web, which was not directly scaled in the model.

Noncomposite Test

The uniaxial flexural strain and the shear strain data obtained in Test No. 1 were normalized and compared to the theory to verify the measured data.

Normalized Flexural Stress Distribution

The uniaxial flexural strains obtained in Test No. 1 for cross sections 1-1 through 8-8 were normalized and plotted in one graph. The measured strains, ϵ , were multiplied by the modulus of elasticity of the steel, E_s , and were divided by the acting moment, M . Then the results were plotted at the corresponding distance from the bottom fibers of the stringer cross section.

Fig. 63 shows the theoretical stress distribution and the normalized measured data. This plot contains 160 data points and it can be observed that a good correlation was obtained with the theory. The stresses at the bottom fibers of the model steel stringer were 37.4 psi per every kip-in. of applied moment.

Normalized Shear Stress Distribution

The measured shear strain data, ϵ_{xy} , for cross sections A-A through C-C were normalized and compared to the theory. This was accomplished by multiplying the shear strains, ϵ_{xy} , by the modulus of rigidity, G , and divided by the shear force, V . Then the results were plotted at the corresponding distance from the bottom fibers. Fig. 64 shows the normalized shear stress values along with the theoretical normalized shear stress distribution. This plot contains 35 normalized data points, 15 at the top web, 15 at the neutral axis and 5 at the bottom web. The data is more scattered, but the average percent error of 5.2% is relatively small. The shear stresses at the neutral axis of the stringer cross section were 42.1 psi per every kip of applied shear.

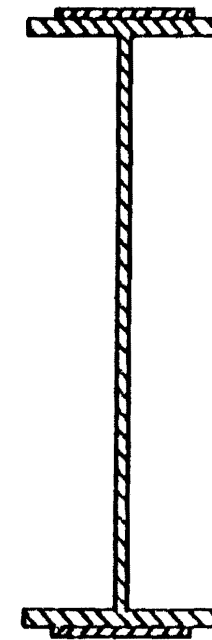
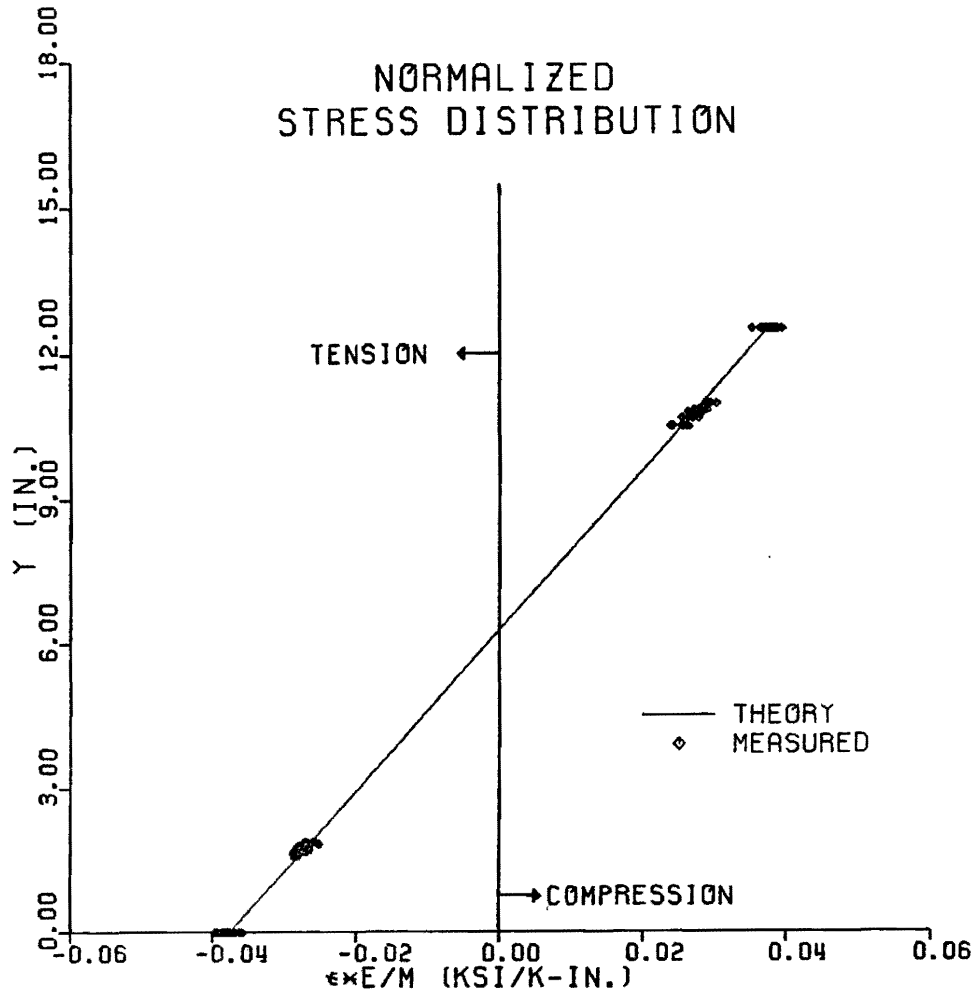


FIG. 63. Normalized Flexural Stress Distribution, Test No. 1.

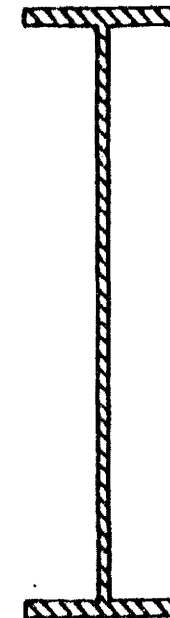
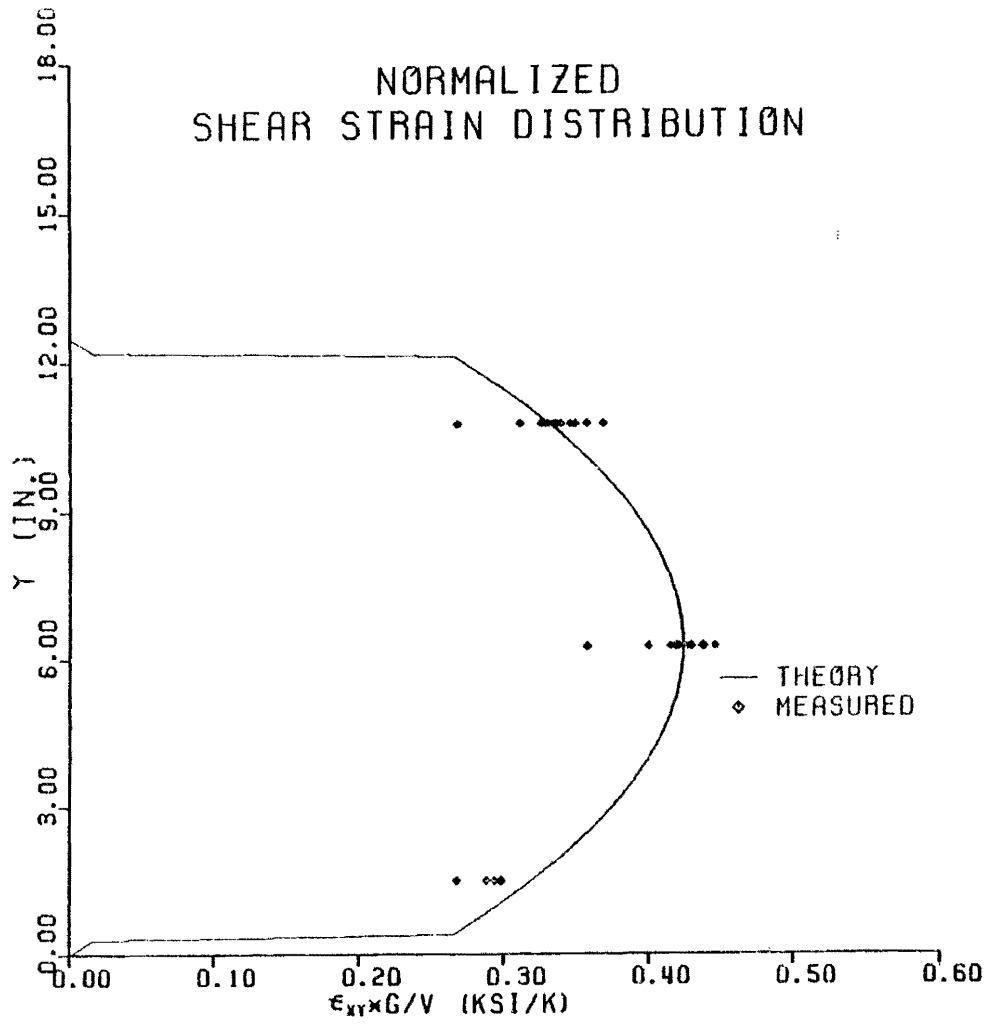


FIG. 64. Normalized Shear Stress Distribution, Test No. 1.

Partial Composite Test

The uniaxial flexural strain data obtained in Test No. 2 for cross sections 1-1 through 8-8 were normalized. This data was not correlated to the theory; a linear fit was done instead.

Normalized Flexural Stress Distribution

The normalized stress distribution was obtained by multiplying the measured uniaxial strains, ϵ , by the modulus of elasticity of steel, E_s , and dividing them by the corresponding acting moment, M . The results were plotted and a linear fit was done. Fig. 65 shows the normalized data points along with the linear fit. This plot contains 170 data points, 15 at the bottom surface of the precast panels, 35 at the top fibers of the model stringers, 40 at the top web, 40 at the bottom web and 40 at the bottom fibers of the model stringers.

The data is more scattered at the top flange and at the top web of the model stringer than at the bottom flange. This is attributed to the inconsistent degree of interaction between the panels and the model stringers achieved by the pocket connections. However, the deviations were relatively small. The stresses at the bottom fibers of the model stringers were 34.7 psi per kip-in. of applied moment.

Full Composite Test

The uniaxial flexural strain and the shear strain data obtained in Test No. 3 were normalized and compared to the theoretical stress distributions.

Normalized Flexural Stress Distribution

The flexural strain data obtained in Test No. 3 for composite cross sections 1-1 through 4-4 were normalized and compared to the normalized theoretical stress distribution. The measured strains, ϵ , were multiplied by

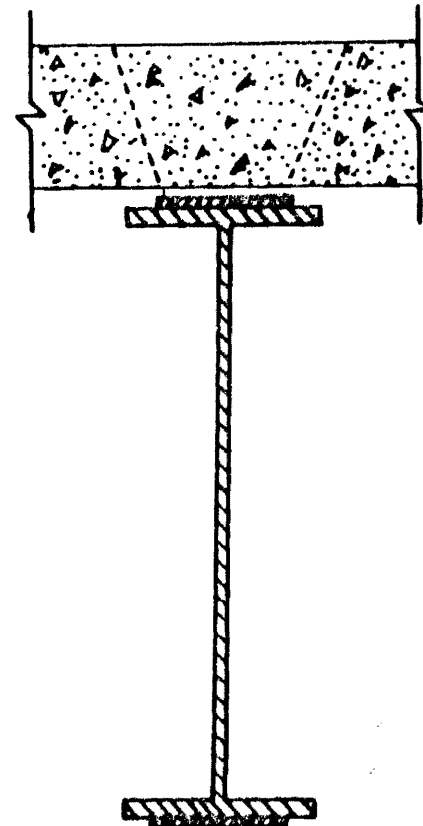
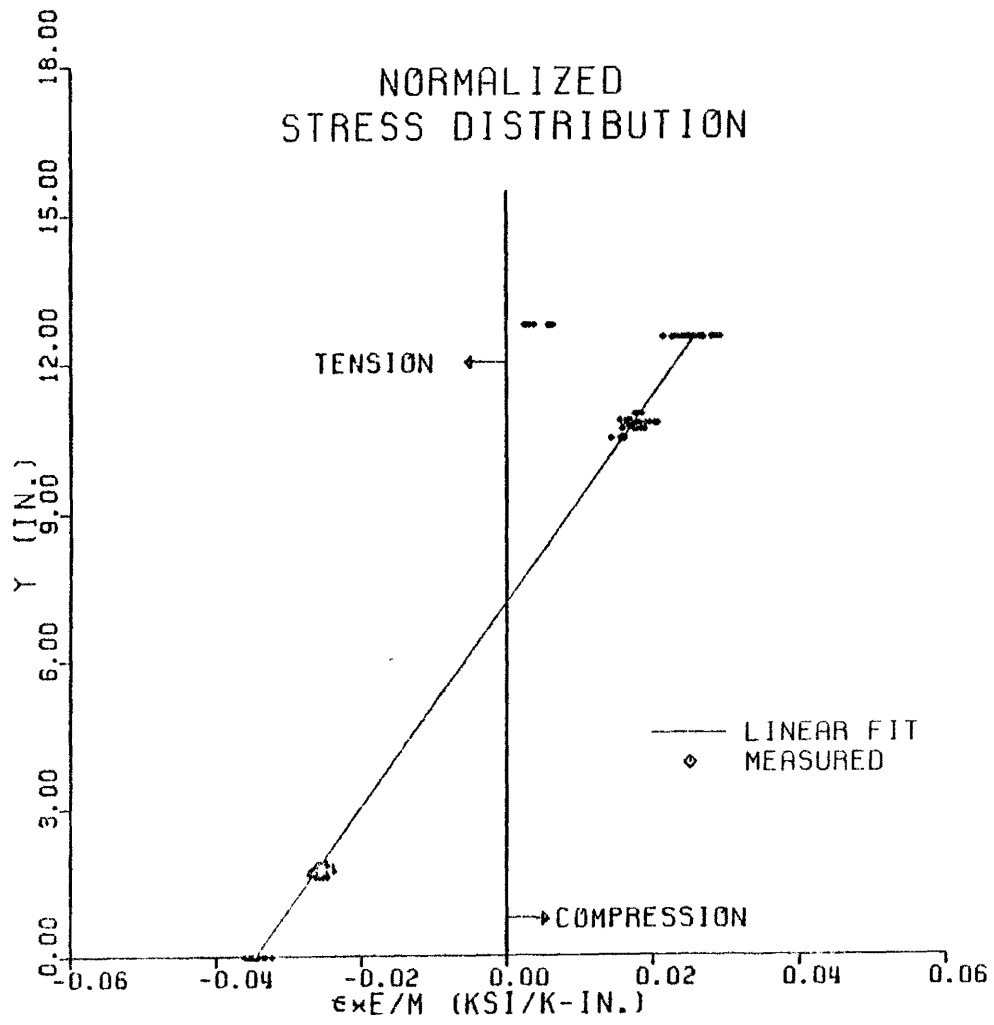


FIG. 65. Normalized Flexural Stress Distribution, Test No. 2.

either the modulus of elasticity of steel, E_s , or that of concrete E_c , depending upon the location of the strain measurements. Then they were divided by the corresponding acting moment, M . Fig. 66 shows the theoretical stress distribution along with the normalized strain data. This plot contains 176 data points, 86 of which were taken at the concrete of the precast panels. The rest of the data points were obtained from strain gages at the model stringers. The stresses at the bottom fibers were 27.2 psi per kip-in. of applied moment.

Normalized Shear Stress Distribution

The measured shear strain data obtained in Test No. 3 was normalized and compared to theoretical normalized values. The shear strains, ϵ_{xy} , were multiplied by the modulus of rigidity, G , and divided by the corresponding active shear force, V . The results were plotted and compared to the theoretical normalized shear stress distribution as illustrated in Fig. 67. It can be noticed that the composite cross section caused the maximum shear stresses to be not at the neutral axis of the model stringer but closer to the top flange of the stringer.

Comparison of Flexural Stress Distribution

The flexural stress distributions of Tests No. 1, No. 2 and No. 3 were compared to quantify the percent improvement in the flexural resistance as the model went from noncomposite to partial composite and to full composite.

Some sectional parameters were determined from the experimentally measured flexural strains of Tests No. 1, No. 2, and No. 3. The main parameters that were evaluated were the moment of inertia, I , the location of the neutral axis, y , and the section modulus at the bottom fibers of the model stringers.

The locations of the neutral axis were computed using the strain measurements at the top and bottom fibers of the model stringers, which are believed to be more reliable. The locations of the neutral axis, y_b , were solved using the formula:

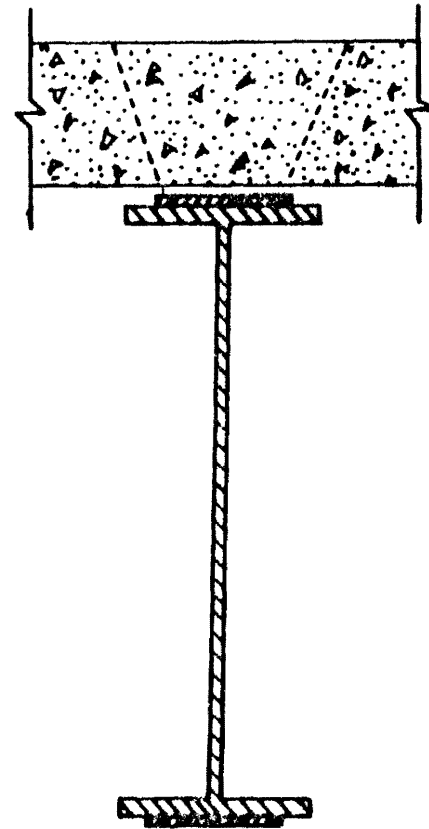
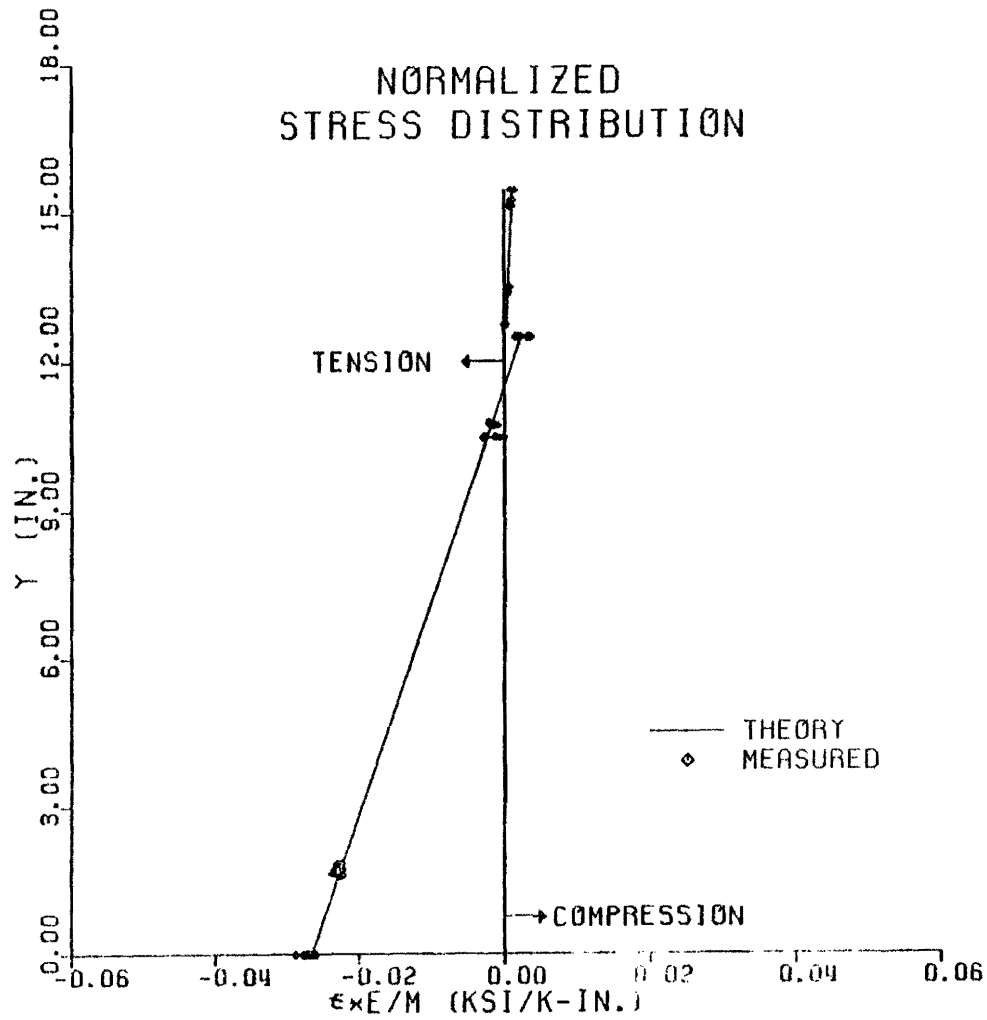


FIG. 66. Normalized Flexural Stress Distribution, Test No. 3.

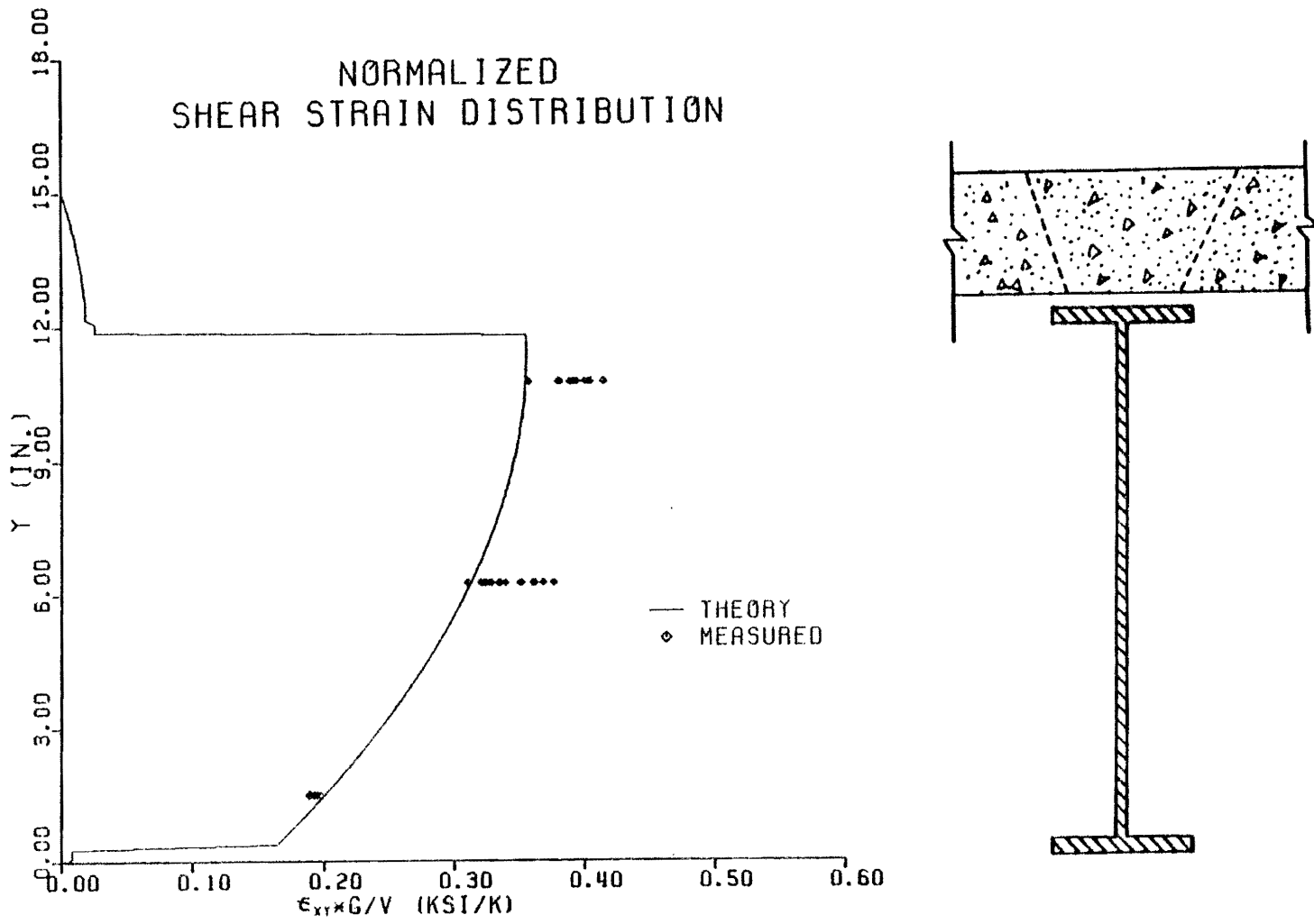


FIG. 67. Normalized Shear Stress Distribution, Test No. 3.

$$y_b = \frac{d \epsilon_{bot}}{\epsilon_{bot} + \epsilon_{top}}$$

where

d = the depth of the model stringers,

ϵ_{bot} = the measured flexural strain at the bottom fibers of the model stringer, and

ϵ_{top} = the measured flexural strain at the top fiber of the model stringers.

After the locations of the neutral axis were computed, the moments of inertia, I , were determined using the following formula:

$$I = \frac{M y_b}{\epsilon_{bot} E_s}$$

where

M = the acting internal moment,

y_b = the distance from the neutral axis to the bottom fibers of the model stringers,

ϵ_{bot} = the measured flexural strains at the bottom fibers of the model stringer, and

E_s = the modulus of elasticity of steel.

Once the locations of the neutral axis and the moments of inertia were determined for every cross section at every test, the section moduli at the bottom fibers of the stringers were also determined. The average values of the location of the neutral axis, moment of inertia, and section modulus at the bottom fibers were obtained for every test.

The percent increases of the mentioned parameters were computed for Test No. 2 and No. 3 relative to those parameters obtained in Test No. 1. Table 29 shows the experimentally determined moment of inertia, locations of the neutral axis and section moduli for Tests No. 1, No. 2 and No. 3, along with the percent increase of those parameters of Test No. 2 and No. 3 relative to those of Test No. 1.

As the pocket connections were grouted, some sectional properties along the model stringers showed some increase, indicating some composite interaction. However, those sections at the location of the shear key joints did not act compositely since the shear keys had not been grouted yet. This is why the sectional parameters and their percent increase in Test No. 2 are tabulated as ranges in Table 29.

The maximum indicated average moment of inertia computed for Test No. 2 was 202 in.⁴ and represents a 21.0% increase over the value indicated by Test No. 1. The location of the neutral axis was raised 0.9 in. and the section modulus increased 5.7%.

As the grouting of the shear key joints was completed, the moment of inertia increased 154.1% to an average of 424.1 in.⁴. The location of the neutral axis moved up 5.29 in., which was 42.3% of the depth of the model stringers, indicating very clearly that significant composite action was achieved.

The section modulus of the bottom fibers of the model stringers experienced a 37.6% increase. The design of these bridges is normally controlled by the stresses at the bottom fibers which are directly computed from the acting moment divided by the section modulus. Therefore, as full composite action was achieved, the live-load carrying capacity of the model was also increased by 37.6 %.

The above discussion is illustrated graphically in Fig. 68, which shows the normalized flexural stress distribution for Test No. 1, No. 2 and No. 3. By observing the transition of the flexural stress distribution from Test No. 2 to Test No. 3, the importance is pointed out of having the shear key joints grouted for full development of composite interaction between the precast concrete panels and the steel stringers.

Comparison of Shear Stress Distribution

The normalized shear stress distributions of Tests No. 1 and No. 3 were compared to quantify the percent improvement in the shear capacity of the 1/3 model as it went from noncomposite to full composite at the end cross

TABLE 29. Apparent Sectional Properties of Model.

Parameter	Test No.1 Noncomposite	Test No.2 Partial Composite		Test No.3 Full Composite	
			Percent Increase		Percent Increase
I in inches ⁴	167.	167.-202	0.-21.0	424.4	154.1
Y in inches	6.25	6.25-7.15	0.-14.4	11.54	84.6
S _{bot} in inches ³	26.72	26.72-28.25	0.-5.7	36.77	37.6

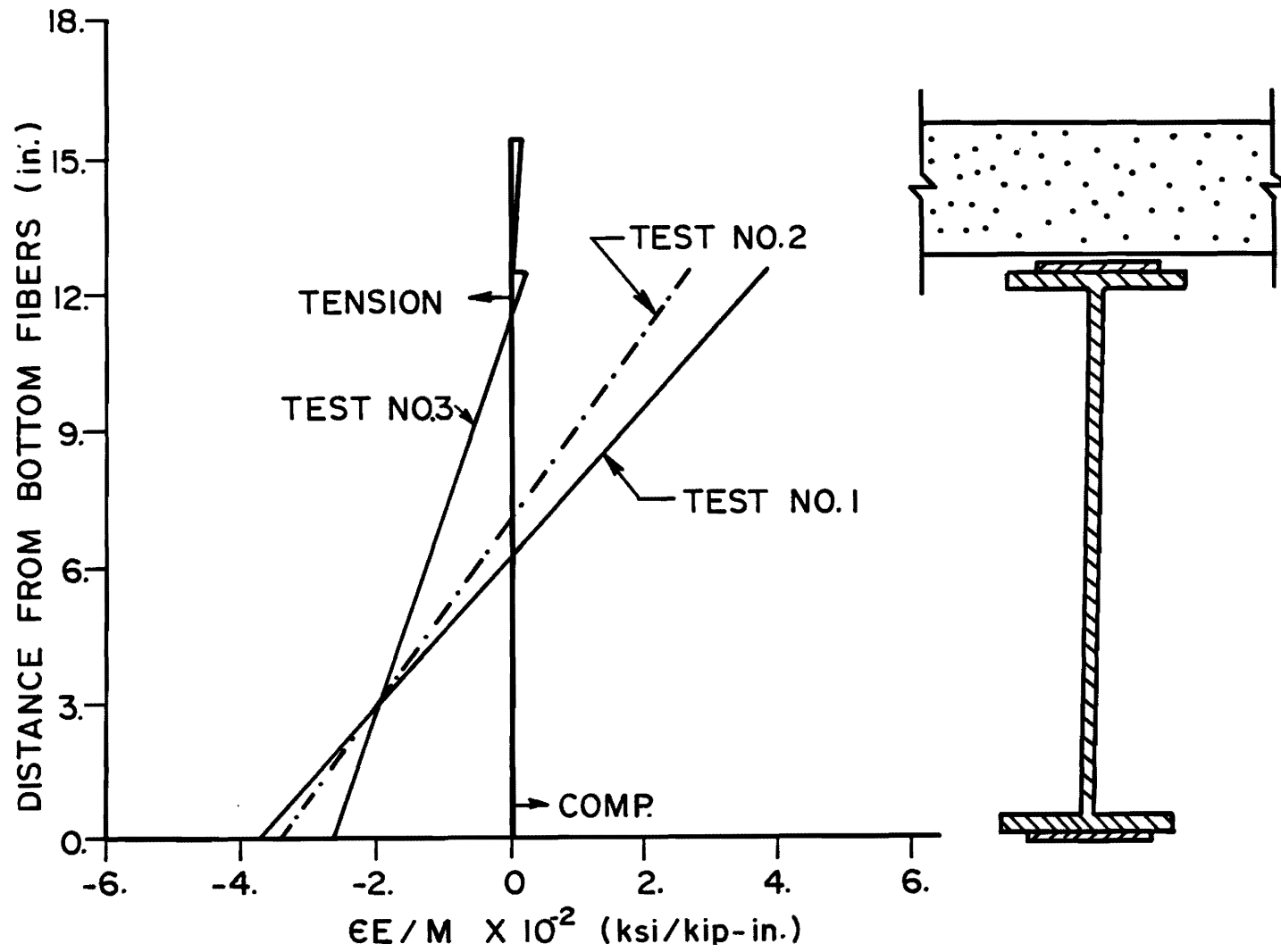


FIG. 68. Comparison of Flexural Stress Distributions of Tests No. 1, No. 2, and No. 3.

sections. The shear stresses were compared in terms of maximum shear stresses independent from the location.

For comparison purposes, the shear strains measured at the top web in the full composite test were assumed maximum. Then the ratios of the statical moment about the neutral axis, Q , over the moment of inertia, I , were solved for the instrumented cross sections using the maximum measured shear strains of Tests No. 1 and No. 3, computed by the formula:

$$\frac{Q}{I} = \frac{\epsilon_{\max} G t_w}{V}$$

where

- I = the moment of inertia,
- Q = the statical moment about the neutral axis,
- V = the acting shear force,
- t_w = the web thickness,
- ϵ_{\max} = the maximum measured shear strain, and
- G = modulus of rigidity of steel.

The computed ratios of Q over I , for the noncomposite and full composite tests are tabulated in Table 30, along with the percent decrease as the model went from noncomposite to full composite.

~~The average percent decrease of the Q over I ratio was 6.73%. This percentage also represents a decrease in the maximum shear stresses produced by the same shear force, since the Q over I ratio is directly proportional to the magnitude of shear stresses. The two shear strain distributions for Tests No. 1 and No. 3 are illustrated in Fig. 69.~~

Comparison of Midspan Deflections

The midspan deflections measured in Tests No. 1, No. 2 and No. 3 were compared as the model went from noncomposite, to partial composite and to full composite. The average midspan deflections of the two model stringers were obtained and plotted versus the average applied concentrated loads for Tests No. 1, No. 2, and No. 3, as illustrated in Fig. 70. It can be observed that the deflections were reduced drastically when full composite interaction

TABLE 30. Ratio of Statical Moment and Moment of Inertia About the Neutral Axis, Q/I, Tests No. 1 and No. 3.

Cross Section	Test No. 1 Q/I at Neutral Axis in inches ⁻¹	Test No. 3 Q/I at Neutral Axis in inches ⁻¹	Percent Decrease
A-A	0.1012	0.0948	6.34
B-B	0.1013	0.0943	6.95
C-C	0.1041	0.0969	6.92
Average	0.1022	0.0953	6.75

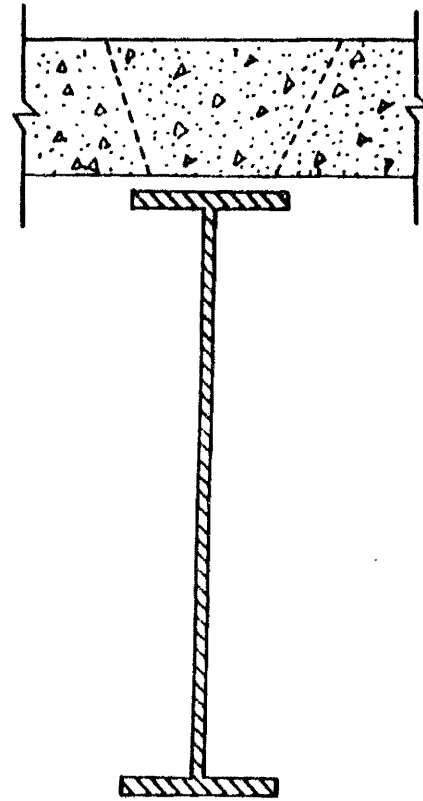
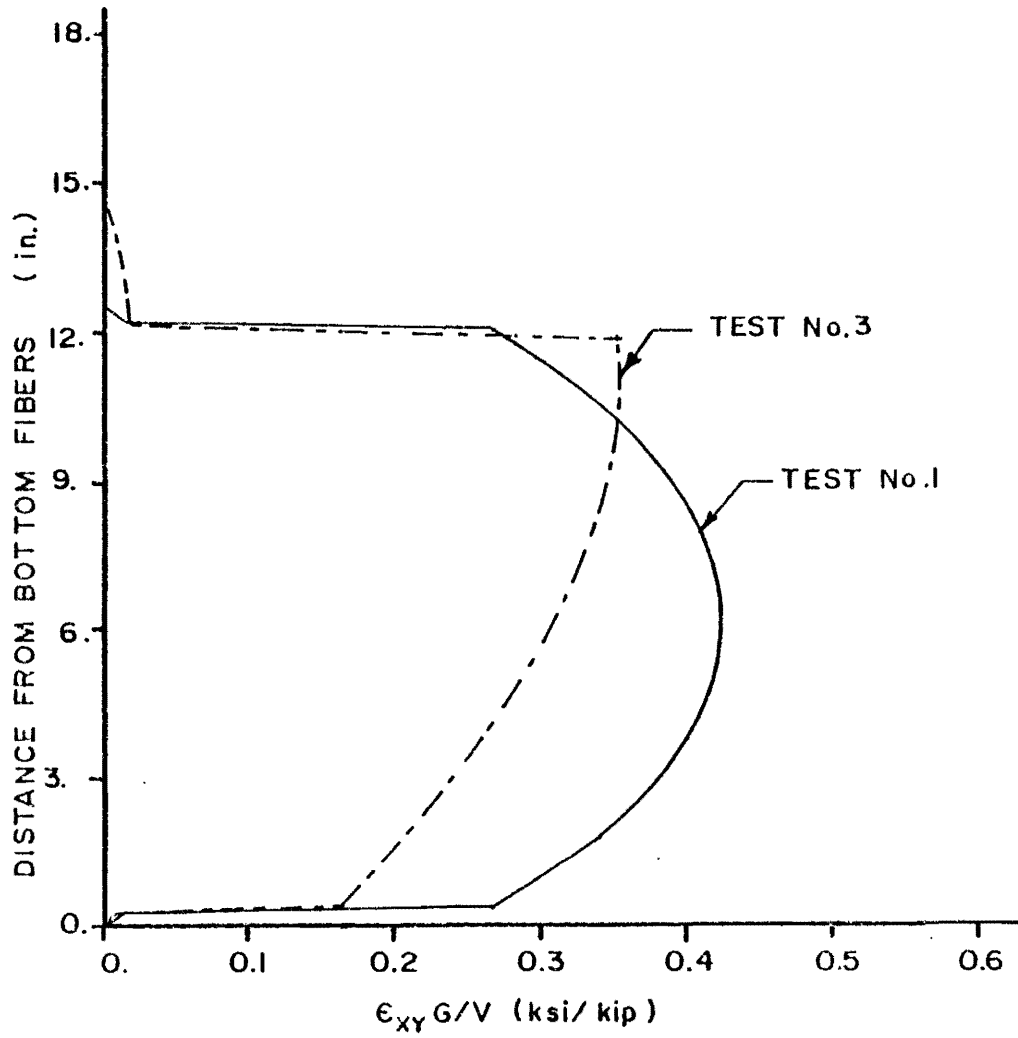


FIG. 69. Comparison of Shear Stress Distributions, Tests No. 1 and No. 3.

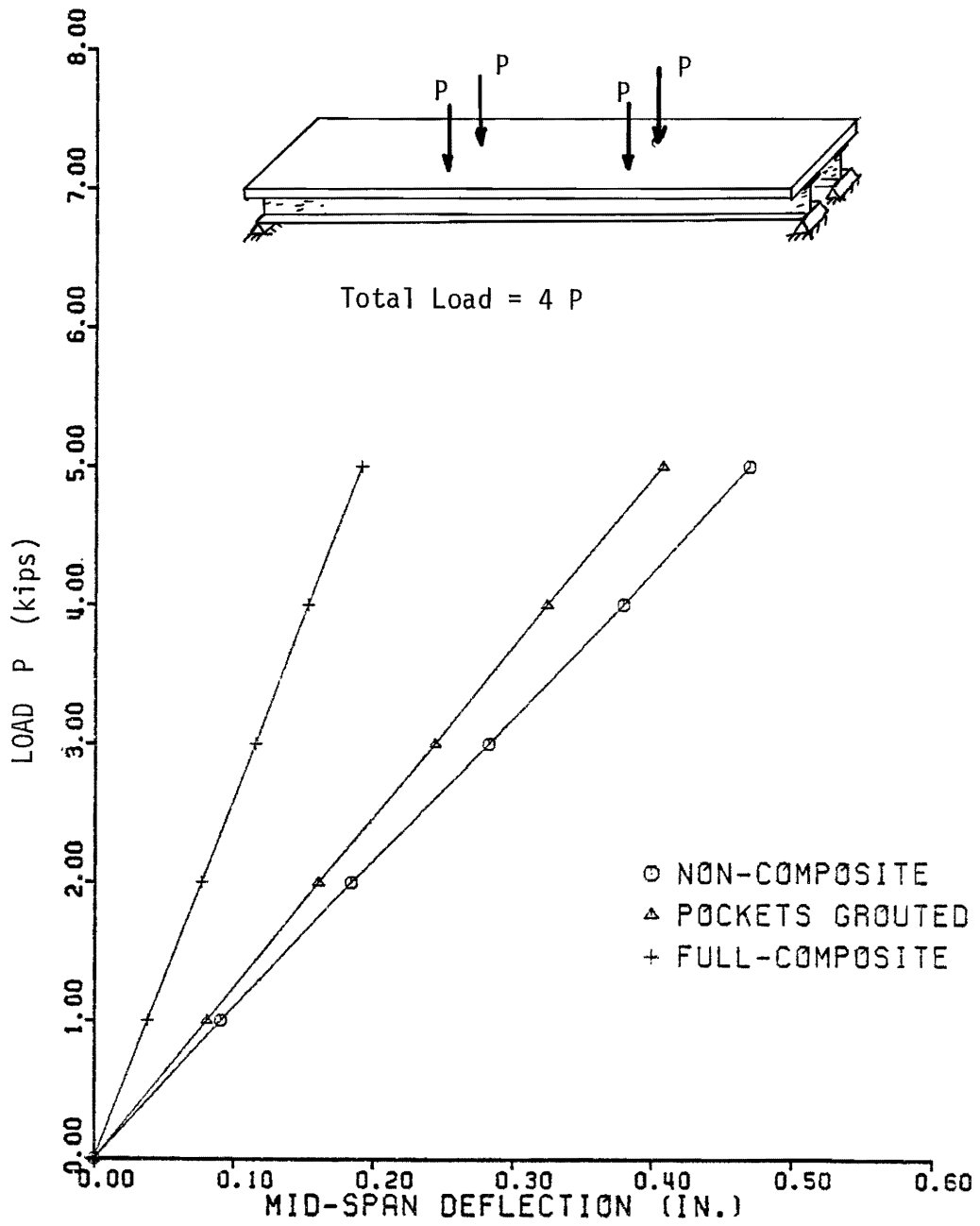


FIG. 70. Comparison of Mid-Span Deflections, Tests No. 1, No. 2 and No. 3.

was achieved. Table 31 shows the average rate of midspan deflections and their percent reduction compared to the noncomposite deflections.

As the pockets were grouted, the overall stiffness of the model increased, producing a 14.9% reduction in the deflections. After the shear key joints were grouted, the deflections and the overall flexibility of the model were decreased by 60.6%.

Comparison of Full Composite Test Results to Prototype

The flexural strain and deflection data obtained in Test No. 3 were compared to theoretical values for the full composite prototype. The theoretical strains and deflections were computed using the composite sectional properties. Appendix D shows the detailed computations of the composite cross-sectional properties of the prototype. The flexural strain data was compared for two locations: the bottom fibers of the stringers and the top fibers of the precast concrete panels.

A theoretical formulation for the deflection of a simply supported symmetrical beam having two different moments of inertia and loaded by two equal concentrated forces was used to compute the theoretical midspan deflections of the prototype and model, for comparison to the measured deflections.

Flexural Strains

The flexural strains produced by internal moments in the model during the full composite test were compared to theoretical flexural strains caused by moment 27 times larger acting in the transformed composite cross section in the prototype.

The transformed sectional properties of the prototype structure were computed assuming the ratio of moduli of elasticity of steel and concrete of 8, and a gap of 3/4 in. between the precast concrete panels and the stringers. The transformed sectional properties of the model were computed using the same moduli ratio and a 1/4 in. gap between the model panels and the model stringers.

TABLE 31. Rate of Midspan Deflection and Percent Reduction.

Test	Rate of Deflection, in inches per kip	Percent Reduction
Test No. 1 Noncomposite	0.094	-
Test No. 2 Partial Composite	0.080	14.9
Test No. 3 Full Composite	0.037	60.6

The flexural strains were compared at two locations, at the bottom fibers of the stringers and at the top fibers of the precast panels. Fig. 71 shows the comparison of the flexural strains at the bottom fibers of the stringers of the model and prototype. The measured flexural strains at the bottom fibers in the model were plotted against the acting internal moments using the left-hand scale. The theoretical strains in the model were also graphed using the same scale. Then the theoretical strains of the prototype were graphed using the scale factors given by similitude. That is, the moment of the right-hand scale represents moments 27 times those of the model and the top scale represents the prototype strains. In this case, the model and prototype strains are the same. By making this model-prototype comparison, it is concluded that an excellent similitude was obtained at the bottom fibers of the stringers validating that the live load carrying capacity of the prototype increases by 37.6 percent.

Fig. 72 shows the comparison of flexural strains at the top fibers of the precast panels of the model and prototype. The measured strains at the top layer of the reinforcement were projected to the top fibers of the precast panels using similar triangles.

The projected strains were plotted versus the moment, along with the theoretical strains for the model, using the left-hand scale. The theoretical prototype strains were graphed using a moment scale 27 times larger than that of the model. It can be noticed that the projected strains were more scattered probably because uncertainties of the height locations. But still, the projected strains fell near the theoretical values.

Deflections

The measured midspan deflections of the model were compared to theoretical midspan deflections of the prototype produced by similar loading conditions. A general expression was derived for the midspan deflections of a beam having two different moments of inertia and being loaded by two equal symmetrical concentrated loads. The derivation of this expression is shown in Appendix E. The derived expression for the midspan deflection, δ_m , is:

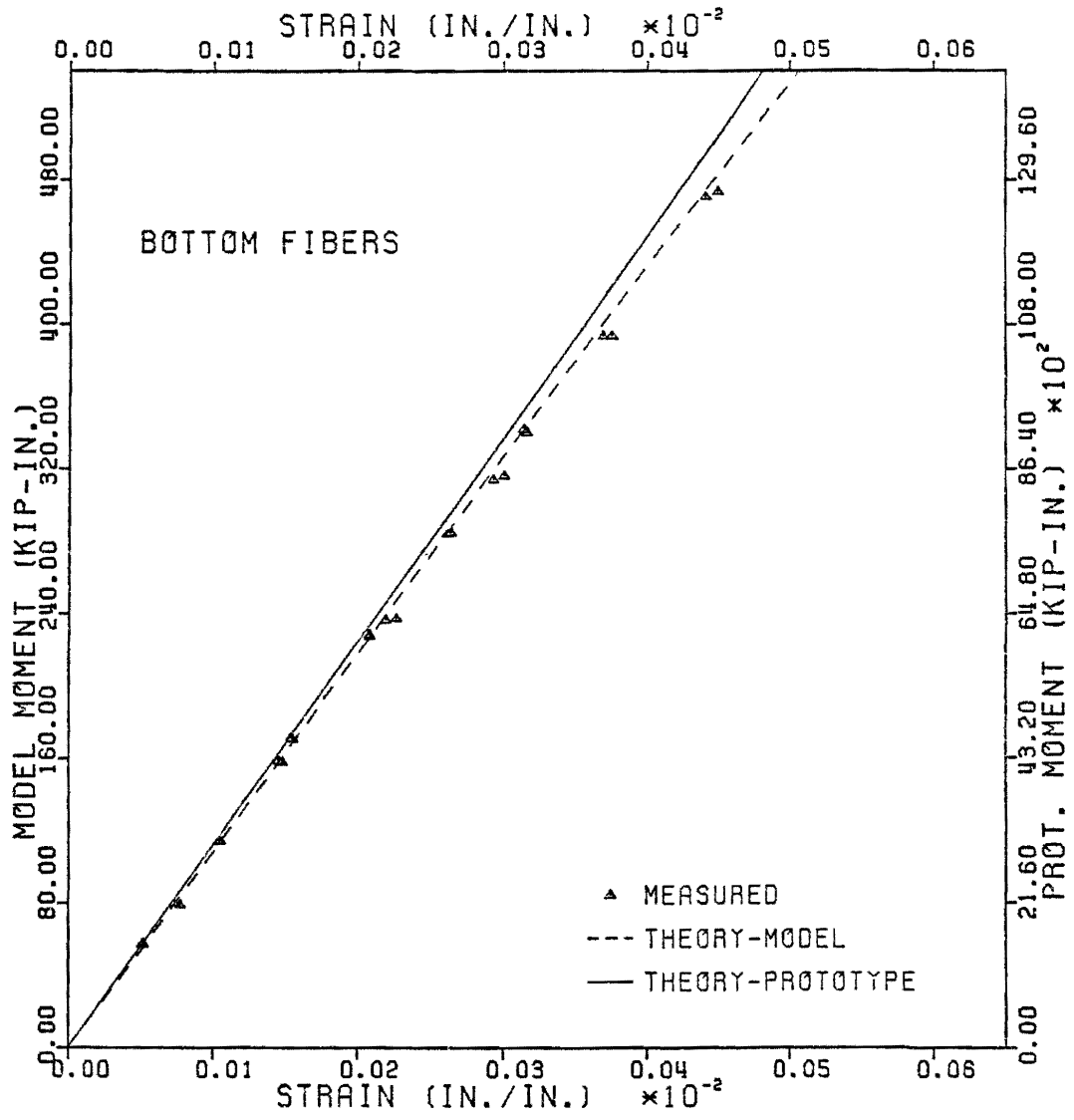


FIG. 71. Comparison of Model Composite Flexural Strains at Bottom Fibers of Stringers with Prototype.

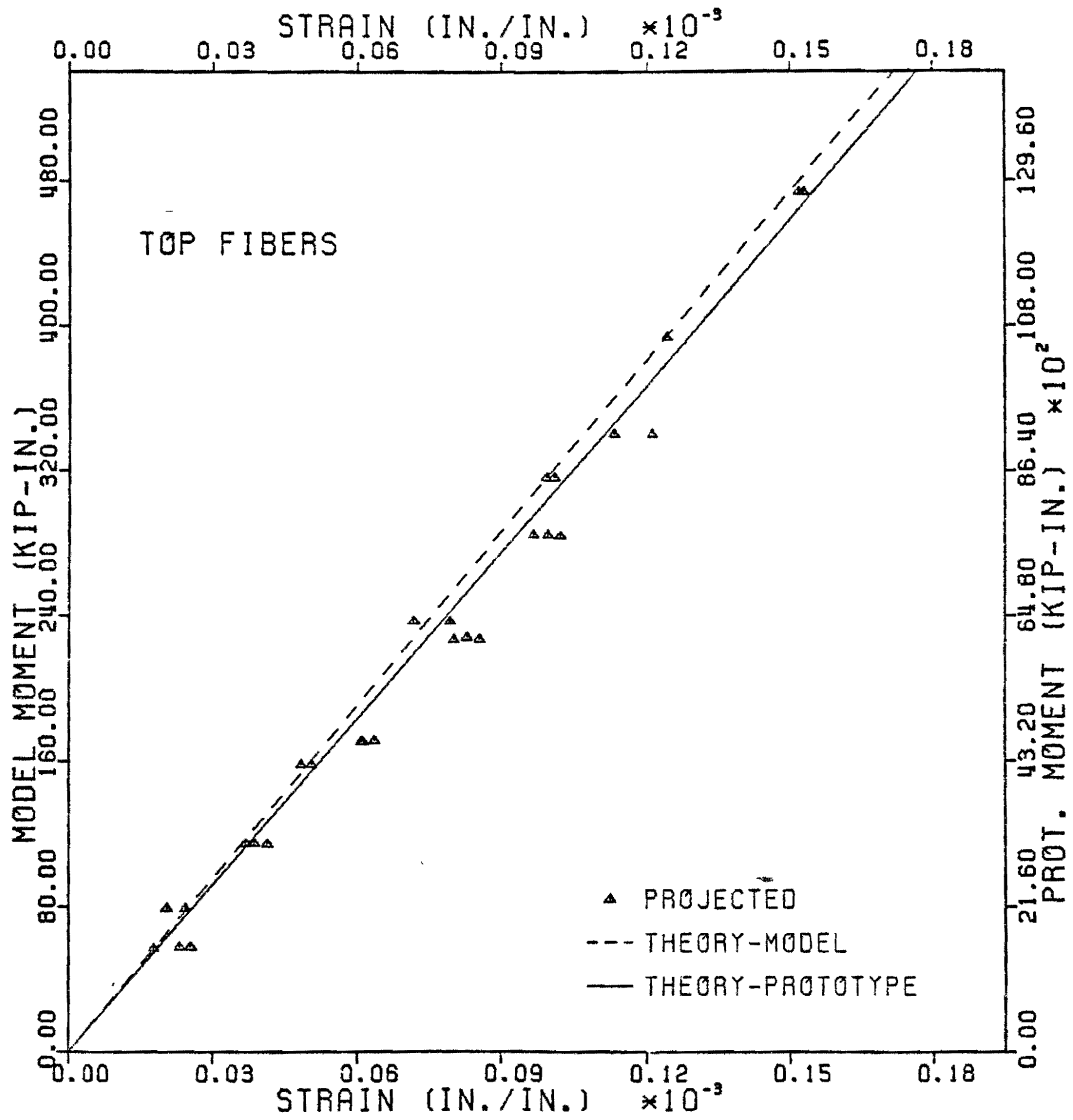


FIG. 72. Comparison of Model Composite Flexural Strains at Top Fibers of Panels with Prototype.

$$\delta_m = \frac{P}{2 E_s I_2} \left\{ \frac{L^2 b}{4} - \frac{2 a^3}{3} - \frac{b^3}{3} \right\} + \frac{P a^3}{3 E_s I_1}$$

where

- P = the symmetrical concentrated load,
 L = the span length of the beam,
 a = the distance from left support to the point at which the moment of inertia changes,
 b = the distance from the support to the point at which the concentrated load P is applied,
 I₁ = the moment of inertia of the end portion of the beam,
 I₂ = the moment of inertia of the central portion of the beam, and
 E_s = the modulus of elasticity of the steel stringers.

Fig. 73 shows the measured midspan deflection plotted versus the applied concentrated load. The theoretical model midspan deflections are also plotted. The bottom and left scales are used for the model. The theoretical midspan deflections for the prototype are also plotted using a different scale. The deflections of the prototype are three times those of the model, and the prototype loads are nine times those of the model.

Discussion of Slip Displacements

The slip displacements measured in the full composite test were compared to slip displacements expected in the two 1/4 in.-steel shear stud connectors if they had been embedded in normal-weight concrete. The slip displacements for the shear studs in concrete were computed using empirical formulations obtained from two-slab push-out tests conducted by Ollgaard (11). Ollgaard determined that the ultimate shear capacity of shear studs embedded in concrete, S_u, is given by the formula:

$$S_u = \frac{1}{2} A_s \sqrt{f'_c E_c}$$

where

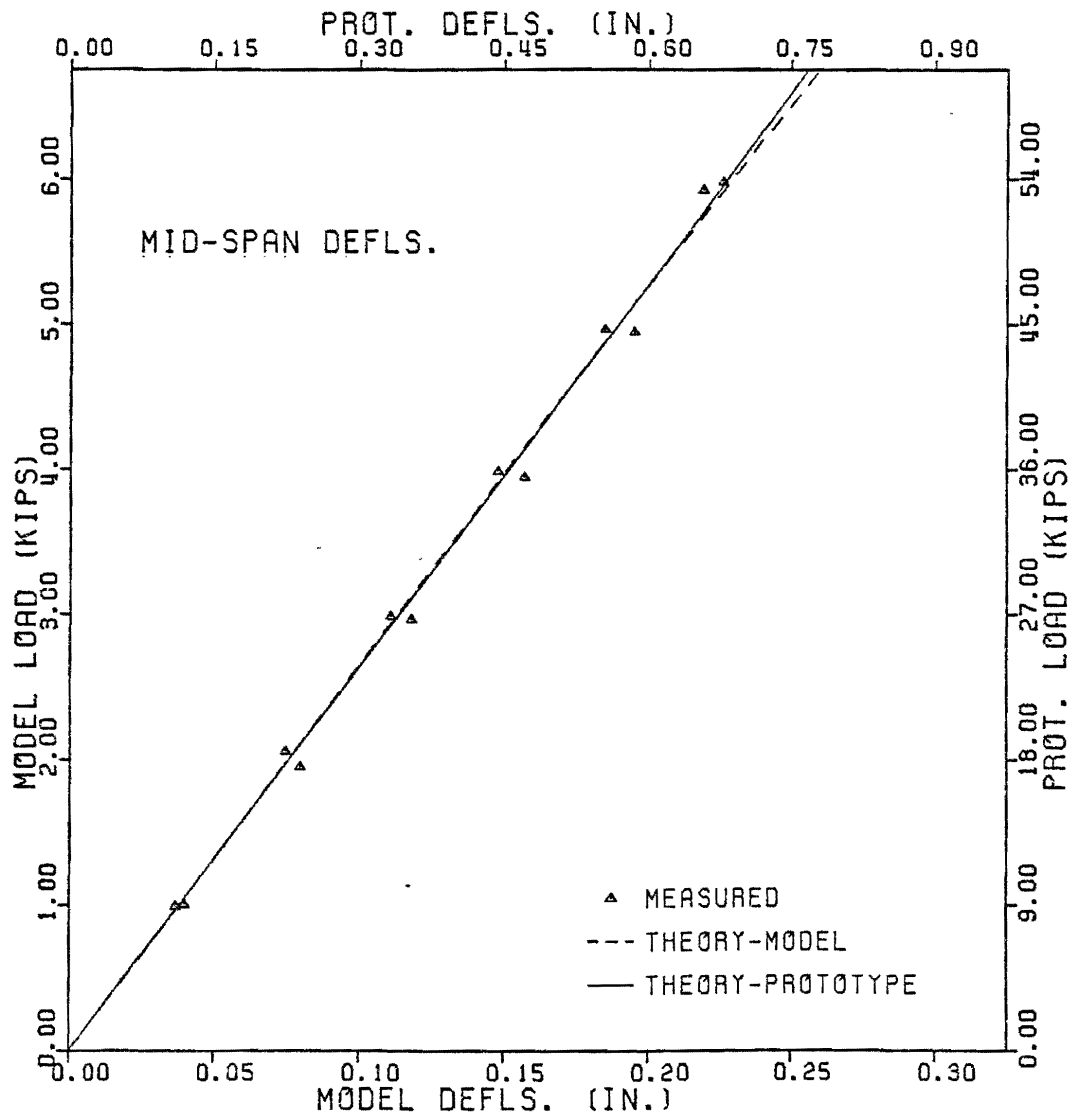


FIG. 73. Comparison of Mid-Span Deflections with Theoretical Model and Prototype Mid-Span Deflections.

A_s = the area of the shear studs,
 f'_c = the compressive strength of concrete, and
 E_c = the modulus of elasticity of concrete.

Ollgaard also concluded that the shear-slip displacement curves followed the same pattern independent of the type of concrete used, for both normal weight and lightweight concrete. The shear-slip displacement curves were determined empirically and are given by the formula:

$$S_u = S (1 - e^{-18\Delta})^{0.40}$$

where

S = the shear force applied at the shear stud connectors,
 S_u = the ultimate shear capacity of the shear stud connectors, and
 Δ = the slip displacement.

These empirical formulations were determined from push-out tests, which approximate the loading conditions encountered in the slabs. Since the slip displacement measurements in the model were performed near the supports, the empirical formulations were used to compare the measured slip displacements with those computed if the shear studs had been embedded in normal-weight concrete.

Fig. 74 shows the measured slip displacements plotted against the horizontal shear per pocket connections along with the empirical slip displacements of two 1/4 in. shear studs embedded in normal weight concrete. It is noteworthy that the pocket connections formed with two 1/4 in. shear studs embedded in epoxy mortar have greater shear resistance than the same shear studs embedded in normal weight concrete. It can also be noticed that the measured slip-displacements did not show signs of nonlinearity up to the level of stresses the model was loaded.

Comparison to Design Stresses

The magnitude of stresses induced in the full composite model were compared to the magnitude of the design stresses produced by the HS20-44 AASHTO design truck. Flexural strains and stresses were compared at the

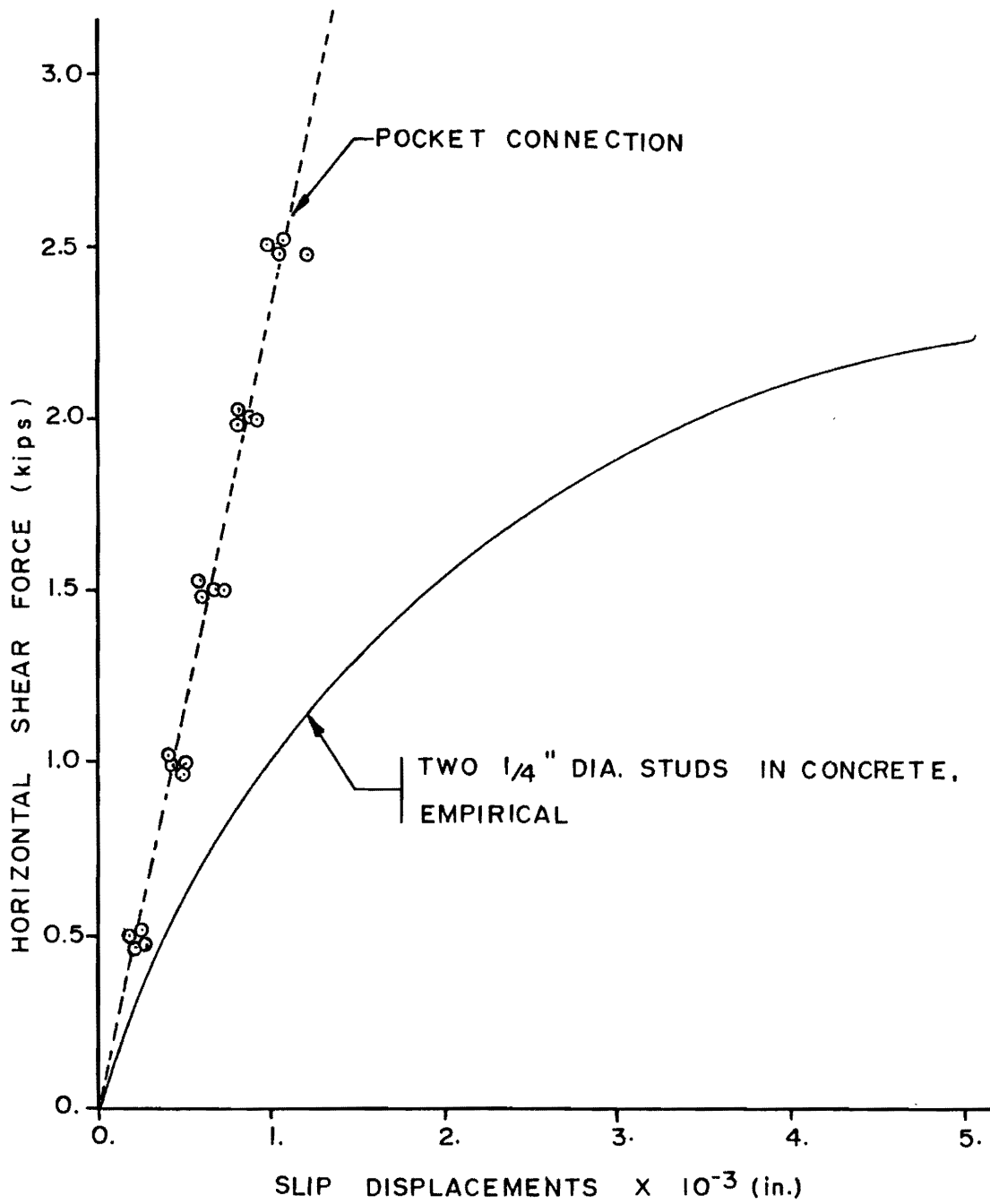


FIG. 74. Slip Displacements of Pocket Connections Compared to Empirical Slip Displacements of Two 1/4 in. Studs in Concrete.

bottom fibers of the stringers and at the top surface of the precast concrete panels. The magnitude of the horizontal shear forces at the precast panel-stringer interface were also compared to the prototype.

Flexural Strains and Stresses

The maximum flexural strains and stresses applied in the 1/3 model were compared to strains and stresses produced by the HS20-44 AASHTO design truck acting on the prototype bridge. Table 32 shows the magnitudes of moments, strains and stresses produced by the design truck on the prototype; the scaled magnitudes of moments, strains and stresses produced by the same truck; and the magnitudes of moments, strains and stresses applied to the 1/3 model.

The maximum live-load moment applied in the model exceeded the scaled design live-load moments of the prototype by 47.2 percent. The maximum actual dead-load moment acting on the model was 34.4 percent of the scaled dead-load moment acting on the prototype. However, the total maximum moment on the model exceeded the scaled total moments of the prototype by 7.3 percent.

The maximum live-load strains and stresses at the bottom fibers of the model stringers exceeded the design live-load strains and stresses at the bottom fibers of the prototype stringers by 54.8 percent. The dead-load strains and stresses in the model were 35.8 percent those of the prototype. The total strains and stresses at the bottom fibers exceeded those of the prototype by 3.3 percent.

The maximum stresses and strains at the top surface of the precast concrete panels of the model exceeded the design strains and stresses in the prototype by 35.8 percent.

Horizontal Shear Forces at Panel-Stringer Interface

The horizontal shear forces at the panel-stringer interface applied in the model were compared to the design forces of the prototype. Table 33

TABLE 32. Comparison of Maximum Flexural Strains and Stresses of Model with Design Strains and Stresses of Prototype.

		Design, Prototype	Scaled Design, Prototype	Maximum Applied, 1/3 model
Moment, in kips-feet	Live Load	724.12	26.82	39.48
	Dead Load	398.39	14.75	5.08
	Total	1122.51	41.56	44.56
Strain at Bottom Fibers, in 10^{-6} inches per inch	Live Load	287.	287.	444.
	Dead Load	219.	219.	79.
	Total	506.	506.	523.
Stress at Bottom Fibers, in kips per square inch	Live Load	8.32	8.32	12.88
	Dead Load	6.36	6.36	2.28
	Total	14.68	14.68	15.16
Strain at Top Fibers, in 10^{-6} inches per inch	Live Load	112.	112.	152.
	Dead Load	0.	0.	0.
Stress at Top Fibers, in kips per square inch	Live Load	0.41	0.41	0.55
	Dead Load	0.	0.	0.

shows the comparison of the vertical shear forces and the horizontal shear forces per pocket connection between the prototype and the 1/3 scale model.

The maximum horizontal shear force per pocket connection induced in the model did not exceed the design scaled forces of the pocket connections of the prototype. However, the linearity obtained in the measured slip displacements led to the conclusion that the pocket connections are stiffer than a shear connection made with steel studs embedded in concrete.

TABLE 33. Comparison of Maximum Applied Shear Forces of Model with Design Shear Forces of Prototype.

	Design, Prototype	Scaled Design, Prototype	Maximum Applied 1/3 Model
Live Load Shear Force, in kips	55.97	6.22	6.0
Horizontal Shear Force per Pocket Connections in kips	27.56	3.06	3.0

Relationship of Applied Loads to Yield and Ultimate Load

All experiment results reported in Chapter III are essentially linear because the applied loads were designed not to exceed the elastic range. In the full-composite test or Test No. 3, the applied loads exceeded the live load design service moments by 47.2 %, but the maximum resulting stresses were 40.7 percent of the design yield strength of the model stringers. Furthermore, the maximum applied loads were only 25 percent of the loads required to form a plastic hinge. The behavior of the model above the service load range is to be determined in a further investigation.

CHAPTER V

CONCLUSIONS AND RECOMMENDATIONS

General

The static load tests performed on the 1/3 model led to the conclusion that full composite behavior of the bridge is achieved as soon as the curing of the epoxy mortar of the pocket connections and shear key joints is completed. Therefore, the replacement bridge deck can be put into service more quickly than can a cast-in-place deck. It was found that the full composite action was accomplished by a combination of the mechanical properties of the shear studs and the adhesive strength of the epoxy mortar. However, to ensure the full composite action of the bridge, and still be able to overcome fit-up problems of the precast panels with the steel stringers and with adjacent panels, careful attention should be given to the pocket connections, the shear key joints, and the epoxy mortar.

The replacement of bridge decks using precast concrete panels is perfectly suitable for simple span bridges because the concrete panels are in compression at all times. Further research is recommended to make this type of replacement suitable for continuous bridges where negative moment regions are encountered. When negative moments are applied to the composite cross section, tension failures can be expected at or near shear key joints.

Further research is also recommended to determine the ultimate shear capacity of the steel shear studs of the pocket connections, as well as to investigate the fatigue and aging characteristics of the connections involved. The slip measurements of the model led to the conclusion that the pocket connections are very stiff and are expected to be stiffer than shear studs embedded in normal-weight concrete.

Conclusions

Static load tests were performed on a 1/3 model bridge simulating a deck replacement with precast concrete panels. The model bridge consisted of 10 precast panels on two stringers. Each panel consisted of eight pocket holes

to allow room for steel shear studs and a groove at both transverse sides so two adjacent panels form a shear key joint. The pocket holes and the shear key joints were filled with epoxy mortar.

The static load tests were performed at three different stages during construction: 1) prior to placing the precast panels, 2) after the pocket connections of the panels were grouted, and 3) after the shear key joints were grouted. These tests led to the following conclusions:

1) The new precast bridge deck is fully operational and can be opened to traffic after the curing of the epoxy mortar of the connections is completed. Curing time will normally be 6 hours.

2) The new structure can be at least as strong as the original structure. If original structure was non-composite a significant increase is achieved with the composite panels.

3) Fit-up problems between the precast panels and the steel systems are conveniently overcome using the epoxy mortar as a pad or filler.

4) The pocket connections for the shear transfer between the panels and steel stringers are expected to be stiffer than shear connectors embedded in normal-weight concrete.

5) The transfer of normal forces between adjacent panels is fundamental for the proper development of full composite behavior.

As the new precast bridge deck is installed, the bridge composite behavior depends entirely on the connection of the precast panels with the steel stringers and with adjacent panels. For this reason, traffic may be allowed only after the connections are capable of transferring the basic loads required for composite interaction: transfer of shear forces between the precast panels and the steel stringers, and transfer of normal forces and vertical shear forces between adjacent panels. Therefore, the epoxy mortar must be cured before allowing any live loads on the bridges.

The static load tests on the 1/3 model revealed the following improvements as the bridge went from noncomposite to full composite:

1) The moment of inertia was increased by 154.1 percent.

2) The live load carrying capacity increased by 37.6 percent.

3) The live load deflections were reduced by 60.1 percent.

If the original bridge is noncomposite, the new structure may be expected to exhibit improvements of about the same magnitude as these. Hence the new structure would be stronger than the original. If the original structure is composite, the new structure would exhibit some improvement if the gap between the precast panels and the steel stringer increases the composite sectional properties of the bridge.

The fit-up problems of the precast panels can be overcome. To overcome fitting problems in the longitudinal direction between adjacent panels, the nominal longitudinal dimension must be reduced between one and two inches. To overcome the fitting of the shear studs into the pocket holes, the pockets should be oversized enough to allow room to weld the shear studs from the top. The problem of placing flat precast panels on the top of the existing stringers that have different elevations is corrected by placing epoxy mortar beds of different thicknesses.

The measurement of the relative slip displacements between the precast concrete panels and the steel stringers led to the observation that the overall pocket connections are expected to be stiffer than shear studs embedded in normal-weight concrete, even though the concrete is twice as stiff as the epoxy mortar. The epoxy around the pocket connections remained adhered to the top surface of the steel stringers during testing, contributing to the effective area for horizontal shear transfer. Therefore, the full composite interaction was accomplished by a combination of the mechanical properties of the shear studs and the adhesive strength of the epoxy mortar. However, the amount of horizontal shear transmitted by the epoxy mortar was minimized because the epoxy was intentionally cast only around the pockets and not between pockets.

Grouted shear key joints are necessary and fundamental for the development of full composite interaction. This is concluded by comparing the flexural strain distributions obtained from the static load test performed with the pockets grouted only, with the flexural strain distributions obtained from the static load test with the pockets and the shear key joints grouted. The maximum moment of inertia developed with only the pocket connections grouted was $202. \text{ in.}^4$; and that developed by grouting

the pockets and shear key joints was 424.2 in.⁴. This means that the pocket connections only developed a maximum of 7.4 percent of the extra moment of inertia available with all connections grouted. The obvious conclusion that the transfer of normal forces between adjacent panels is necessary for full composite behavior was confirmed.

Recommendations

It is recommended that further investigations be conducted to make precast bridge deck replacement applicable to continuous bridges, and still be able to develop composite interaction. In these bridges, if composite interaction is achieved in regions of negative moments, the precast panel deck will be subjected to tensile stresses which, in combination with extreme temperature changes, will likely cause the concrete to crack transversely. If the cracks occur in the reinforced portion of the panels, the cross section would exhibit composite sectional properties given by the area of the stringers and area of the longitudinal reinforcement of the panels. It is very likely that the flexural shear distribution along this cross section would be similar to that obtained in Test No. 2, with tension at the top fibers and compression at the bottom fibers. However, if the transverse cracks occur in the shear key joints, no composite interaction would be achieved because there is no continuity of reinforcement between two adjacent panels. Further static testing is recommended to investigate crack patterns in regions of negative moment. Knowledge of the crack patterns would facilitate the design of the location of expansion joints, control cracks, and the composite sectional properties can be optimized where they are most needed.

It is also recommended to investigate in detail the behavior of pocket connections resisting horizontal shear forces. Knowledge of the load-slip behavior and the ultimate shear capacity of these connections would determine design formulas. In this study it was found that the horizontal shear forces at the pocket connection were carried not only by the shear studs but also by the epoxy mortar around the pocket connections. The epoxy mortar around the pocket connections remained bonded to the top surface of the steel stringers,

causing the effective area resisting shear to increase and making the connection stiffer than shear studs embedded in normal-weight concrete. This was accomplished in the laboratory where quality control on the bonding of epoxy mortar was easily accomplished, and good bonding was ensured. In field conditions it is very questionable whether a good epoxy mortar bonding to steel surfaces could be obtained. It is suggested that the laboratory investigation of the behavior of the pocket connections be done simulating field conditions by eliminating any possible bonding of the epoxy mortar to the top surface of the steel stringers and letting the mechanical shear studs embedded in epoxy mortar carry all the horizontal shear forces.

Another suggested research objective is to determine the fatigue characteristics of the connections involved in precast bridge deck replacement. Such an investigation would provide fatigue data of epoxy mortar which is not presently available. Fatigue is expected to occur in the epoxy mortar bearing against the shear connectors, thus causing greater slip displacement as the number of cycles is increased. The composite sectional properties of a bridge are directly related to slip displacements. Therefore, if the slip displacements increase, the composite sectional properties of the bridge decrease. It is suggested to investigate 1) the overall fatigue life of the pocket connections themselves, and 2) the effects of repetitive loading on the composite cross sectional properties of the bridge.

REFERENCES

1. ACI Committee 318, Building Code Requirements for Reinforced Concrete, American Concrete Institute, Detroit, Michigan, 1977, pp. 26.
2. Biswas, M., et al., "Bridge Replacements with Precast Concrete Panels," Special Report 148, Transportation Research Board, Washington, D. C., 1974, pp. 136-148.
3. Donnaruma, R. C., "A Review of the Development of Systems of Composite I-Beam Bridges," Report to the Research Committee, International Bridge, Tunnel and Turnpike Association, Chicago, Illinois, Aug., 1974.
4. Drawing and Details for I-Beam Bridges, Texas Highway Department, Austin, Texas, Nov., 1960, Revised 1962.
5. Greiner Engineering Group, Inc., "Widening and Replacement of Concrete Deck of Woodrow Wilson Memorial Bridge," presented at the January, 1983, Modular Bridge Decks Session of the Transportation Research Board's 62nd Annual Meeting, held at Washington, D. C.
6. Gutzwiller, M. J., Lee, R. H., and Scholer, C. F., "Precast, Prestressed Concrete for Bridge Decks," Special Report 116, Highway Research Board, Washington, D. C., 1970, pp. 30-41.
7. "Instructions for the Use of Texas Highway Department Epoxy Binder B-102," Report of the Materials and Test Division, Texas Highway Department, Austin, Texas.
8. Knudsen, C. V., "Re-decking of a Bridge with Precast Concrete," ASCE Civil Engineering, American Society of Civil Engineers, Vol. 50, Apr., 1980, pp. 75-77.
9. Manual of Steel Construction, 8th ed., American Institute of Steel Construction, New York, 1980.
10. Manual of Steel Construction, 6th ed., American Institute of Steel Construction, New York, 1963.

11. Ollgaard, J. G., Slutter, R. G., and Fisher, J. W., "Shear Strength of Stud Connectors in Lightweight and Normal-weight Concrete," Engineering Journal, American Institute of Steel Construction, Vol. 8, No. 2, Apr., 1971, pp. 55-64.
12. Ontario Bridge Design Code, "Section 7", Ontario Ministry of Transportation and Communication, Ontario, Canada, 1973.
13. Scholer, C. F., "Eleven-Year Performance of Two Precast, Prestressed Concrete Bridge Decks," Transportation Research Record 871, Transportation Research Board, Washington, D. C., 1982, pp. 34-37.
14. Slavis, C., "Precast Concrete Deck Modules for Bridge Deck Reconstruction," Transportation Research Record 871, Transportation Research Board, Washington, D. C., 1982, pp. 30-33.
15. Standard Specifications for Transportation Materials, 12th ed., Part I, American Association of State Highway and Transportation Officials (AASHTO), Washington, D. C., 1978.
16. Standard Specifications for Highway Bridges, 12th ed., American Association of State Highway and Transportation Officials (AASHTO), Washington, D. C., 1977.
17. The Consulting Engineers Group, Inc., "Connections for Modular Precast Concrete Bridge Decks," Interim Report submitted to the United States Department of Transportation, Federal Highway Administration, Glenview, Illinois, Dec., 1982.

APPENDIX A

NOTATION

- a = distance from one support of stringer to point at which moment of inertia changes
- A_s = sectional area of steel shear stud connector
- A_{st} = sectional area of steel reinforcement
- b = distance from one support of stringer to the closest symmetric concentrated load
- b_f = flange width of stringer section
- d = depth of stringer section
- D = diameter of epoxy mortar sample
- E = modulus of elasticity
- E_c = modulus of elasticity of concrete
- E_s = modulus of elasticity of steel
- f'_c = compressive strength of concrete
- F_y = yield strength of steel
- G = modulus of rigidity of steel
- I = moment of inertia of any section
- I_1 = moment of inertia of end portion of stringer, without cover plates
- I_2 = moment of inertia of middle portion of stringer, with cover plates
- l = length of epoxy mortar sample
- L = span length
- L_0 = original length of epoxy mortar sample
- M = internal moment at any section
- P = applied symmetrical concentrated load
- Q = statical moment about the neutral axis of an area outside a particular point
- S = horizontal shear force per inch at panel-stringer interface

S_{bot} = section modulus at a particular section, calculated using the distance from the neutral axis to the bottom fibers
 S_{top} = section modulus at particular section, calculated using the distance from the neutral axis to the top fibers
 S_u = ultimate horizontal shear capacity of shear stud connectors
 t = thickness
 t_f = flange thickness of stringer section
 t_w = web thickness of stringer section
 V = vertical shear force at any section
 w = unit weight of concrete
 y = distance from neutral axis of a section to a point under investigation
 y_b = distance from neutral axis of a section to the bottom fibers
 y_t = distance from neutral axis of a section to top fibers
 δ_m = deformation of epoxy mortar sample under axial loading
 δ_m = midspan deflection of model
 ϵ = uniaxial normal strain
 ϵ_a = measured strain in direction A
 ϵ_b = measured strain in direction B
 ϵ_c = measured strain in direction C
 ϵ_{mea} = measured flexural strain
 ϵ_{th} = theoretical flexural strain
 ϵ_{xx} = horizontal normal strain
 ϵ_{xy} = horizontal shear strain
 $\epsilon_{xy th}$ = theoretical horizontal shear strain
 ϵ_{yy} = strain in vertical axis
 θ_a = angle of gage A from horizontal
 θ_b = angle of gage B from horizontal
 θ_c = angle of gage C from horizontal
 σ_a = axial stress
 σ_t = tensile strength of epoxy mortar

APPENDIX B

DIMENSIONAL ANALYSIS

A dimensional analysis is performed to obtain scale factors to design a 1/3 model of the prototype bridge described in Chapter 2. The scale factors are determined so that the strains, stresses and deflections are scaled at any section of both the prototype and the model. Dead load effects were not considered in the dimensional analysis.

The principal variables are stresses, σ , strains, ϵ , and deflections, δ , which are functions of the sectional and material properties, and the loading conditions shown, all shown in Table B-1.

The strain term is not included in the dimensional analysis, since strains are directly related to stresses. Therefore, the stresses can be represented by:

$$\sigma = F(\delta, \ell, I, S, Q, V, M, E_S, E_C, F_y, G) \quad (1)$$

The above equation can be written as follows:

$$C \sigma^a \delta^b \ell^c I^d S^e Q^f V^g M^h E_S^i E_C^j F_y^k G^m = 1 \quad (2)$$

Where C is a constant and the corresponding dimensional equation is:

$$(FL^{-2})^a L^b L^c L^{4d} L^{3e} L^{3f} F^g (FL)^h (FL^{-2})^i (FL^{-2})^j (FL^{-2})^k (FL^{-2})^m = 0 \quad (3)$$

From Eq. (3) two auxiliary equations may be written:

$$L: -2a + b + c + 4d + 3f + h - 2i - 2j - 2k - 2m = 0 \quad (3a)$$

$$F: a + g + h + i + j + k + m = 0 \quad (3b)$$

TABLE B-1. Parameters Involved in the Dimensional Analysis.

	Parameter	Dimension
Principal Variables	σ Stress	FL ⁻²
	ϵ Strain	-
	δ Deflection	L
Geometric Properties	I Moment of Inertia	L ⁴
	S Section Modulus	L ³
	Q First Moment of Area	L ³
	ℓ Span Length	L
Material Properties	E_s Modulus of Elasticity of Steel	FL ⁻²
	E_c Modulus of Elasticity of Concrete	FL ⁻²
	F_y Yield Stress of Steel	FL ⁻²
	G Modulus of Rigidity of Steel	FL ⁻²
Loading Conditions	V Shear Force	F
	M Moment	FL

Since only two equations are available to solve the 12 unknowns, arbitrary values are assigned for the coefficients a, b, d, e, f, g, h, j, k and m. The determinant of the remaining coefficients c and i is:

$$\begin{vmatrix} 1 & -2 \\ 0 & 1 \end{vmatrix} = 1$$

Since this determinant is not equal to zero, the resulting equations are independent and the selection is valid. Values are assigned as follows:

$$\begin{array}{llll} a = 1 & b = 0 & d = 0 & e = 0 \\ f = 0 & g = 0 & h = 0 & j = 0 \\ k = 0 & m = 0 & & \end{array}$$

These values are substituted in the auxiliary equations, Eqs. (3a) and (3b), giving:

$$-2 + c - 2i = 0$$

$$1 + i = 0$$

So, a = 1, c = 0, i = -1, and substituting these values into Eq. (2), and dropping the constant C, the first π term is obtained:

$$\pi_1 = \frac{\sigma}{E_s}$$

Similarly, the other nine π terms are obtained. Table B-2 shows a summary of the computations and the results.

The values for the coefficients c and i of Table B-2 were obtained by solving the system of equations given by Eqs. (3a) and (3b). The values for the coefficients c and i were then substituted into Eq. (2) to solve for the dimensionless or π terms. One possible form of the general equation is:

$$\frac{\delta}{\ell}, \frac{\sigma}{E_s} = F\left(\frac{I}{\ell^4}, \frac{S}{\ell^3}, \frac{Q}{\ell^3}, \frac{V}{E_s \ell^2}, \frac{M}{E_s \ell^3}, \frac{E_c}{E_s}, \frac{F_y}{E_s}, \frac{G}{E_s} \right) \quad (4)$$

TABLE B-2. Dimensionless Terms and Summary of Computations.

Independent Coefficients (Arbitrary)										c	i	Term
a	b	d	e	f	g	h	j	k	m			
1	0	0	0	0	0	0	0	0	0	0	-1	$\pi_1 = \frac{\sigma}{E_s}$
0	1	0	0	0	0	0	0	0	0	-1	0	$\pi_2 = \frac{\delta}{\ell}$
0	0	1	0	0	0	0	0	0	0	-4	0	$\pi_3 = \frac{I}{\ell^4}$
0	0	0	1	0	0	0	0	0	0	-3	0	$\pi_4 = \frac{S}{\ell^3}$
0	0	0	0	1	0	0	0	0	0	-3	0	$\pi_5 = \frac{Q}{\ell^3}$
0	0	0	0	0	1	0	0	0	0	-2	-1	$\pi_6 = \frac{V}{E_s \ell^2}$
0	0	0	0	0	0	1	0	0	0	-3	-1	$\pi_7 = \frac{M}{E_s \ell^3}$
0	0	0	0	0	0	0	1	0	0	0	-1	$\pi_8 = \frac{E_c}{E_s}$
0	0	0	0	0	0	0	0	1	0	0	-1	$\pi_9 = \frac{F_y}{E_s}$
0	0	0	0	0	0	0	0	0	1	0	-1	$\pi_{10} = \frac{G}{E_s}$

Since the deflections, δ , and stresses, σ , are the principal variables, there are eight design equations involving sectional and material properties, and loading conditions.

Initially, the scale factor was arbitrarily selected and equal to three, thus,

$$\frac{l_p}{l_m} = 3 \quad (5)$$

The materials of the prototype and the model are basically the same, thus, the prototype and the model have the same material properties.

Considering the design equations given by π_8 , π_9 and π_{10} , give:

$$\frac{E_c}{E_s} = \frac{E_{cm}}{E_{sm}} \quad ; \quad \frac{E_c}{E_{cm}} = \frac{E_s}{E_{sm}} = 1 \quad (6)$$

$$\frac{F_y}{E_s} = \frac{F_{ym}}{E_{sm}} \quad ; \quad \frac{F_y}{F_{ym}} = 1 \quad (7)$$

$$\frac{G}{E_s} = \frac{G_m}{E_{sm}} \quad ; \quad \frac{G}{G_m} = 1 \quad (8)$$

Eq. (6) indicates similarity in stiffness, Eq. (7) indicates that the model and prototype must operate in the proportional range of stresses throughout their entire length, and Eq. (8) indicates that the relative stiffness in shear in the model be equal to the corresponding relative stiffness in the prototype. By using the same materials, all the above material requirements are generally met.

The sectional property requirements are given by the design equations obtained from the dimensionless terms π_3 , π_4 and π_5 . The design equation resulting from π_3 gives:

$$\frac{I}{l^4} = \frac{I_m}{l_m^4} \quad ; \quad \frac{I}{I_m} = 81 \quad (9)$$

which establishes the requirement that the moment of inertia at any section must be 81 times less than the moment of inertia of the corresponding cross section in the prototype. The design equation given by π_4 gives:

$$\frac{S}{\ell^3} = \frac{S_m}{\ell_m^3} \quad ; \quad \frac{S}{S_m} = 27 \quad (10)$$

which establishes the requirement that the section modulus at any location of consideration must be 27 times less than the section modulus at the corresponding location in the prototype. The design equation given by π_5 yields:

$$\frac{Q}{\ell^3} = \frac{Q_m}{\ell_m^3} \quad ; \quad \frac{Q}{Q_m} = 27 \quad (11)$$

thus, it is required that the first moment of area at a location of interest in the model must be 27 times less than the first moment of area at the corresponding location in the prototype.

The similitude in the loading conditions is given by π_6 and π_7 . The design equation obtained from π_6 gives:

$$\frac{V}{E_s \ell^2} = \frac{V_m}{E_{sm} \ell_m^2} \quad ; \quad \frac{V}{V_m} = 9 \quad (12)$$

which establishes that any shear force applied in the model is nine times less than the corresponding shear force in the prototype. The design equation given by π_7 gives:

$$\frac{M}{E_s \ell^3} = \frac{M_m}{E_{sm} \ell_m^3} \quad ; \quad \frac{M}{M_m} = 27 \quad (13)$$

which establishes that any live load moment internally acting in the model is 27 times less than the live load acting on the prototype.

If all design equations are completely satisfied, two prediction equations are obtained from π_1 and π_2 . The equation given by π_1 is:

$$\frac{\sigma}{E_s} = \frac{\sigma_m}{E_{sm}} \quad ; \quad \frac{\sigma}{\sigma_m} = 1 \quad (14)$$

which produces a prediction factor of one for stresses. If Eq. (14) is extended and σ is replaced by ϵE , it gives:

$$\frac{\epsilon E_s}{\epsilon_m E_{sm}} = 1 \quad ; \quad \frac{\epsilon}{\epsilon_m} = 1 \quad (15)$$

which says that the strains also have a prediction factor of one. And the prediction equation given by π_2 yields:

$$\frac{\delta}{\ell} = \frac{\delta_m}{\ell_m} \quad ; \quad \frac{\delta}{\delta_m} = 3 \quad (16)$$

and indicates that any deflection measured in the model is three times smaller than the corresponding deflection in the prototype under the same loading conditions.

APPENDIX C

DESIGN COMPOSITE INERTIA CALCULATIONS OF PROTOTYPE AND MODEL

The inertia properties of the design prototype bridge and the design model were computed using the AASHTO code. The middle and end sections of the prototype were considered. A concrete strength of 5,000 psi and a 3/4 in. gap between the steel section and the precast panels were assumed. The effective width of the precast panel is given by the distance between stringers.

Prototype Middle Section

The middle section of the prototype consists of a 36 WF 150 wide flange section with 3/4 in. thick, 10 in. wide cover plates welded to the top and bottom flanges. The prototype middle section is illustrated in Fig. C-1.

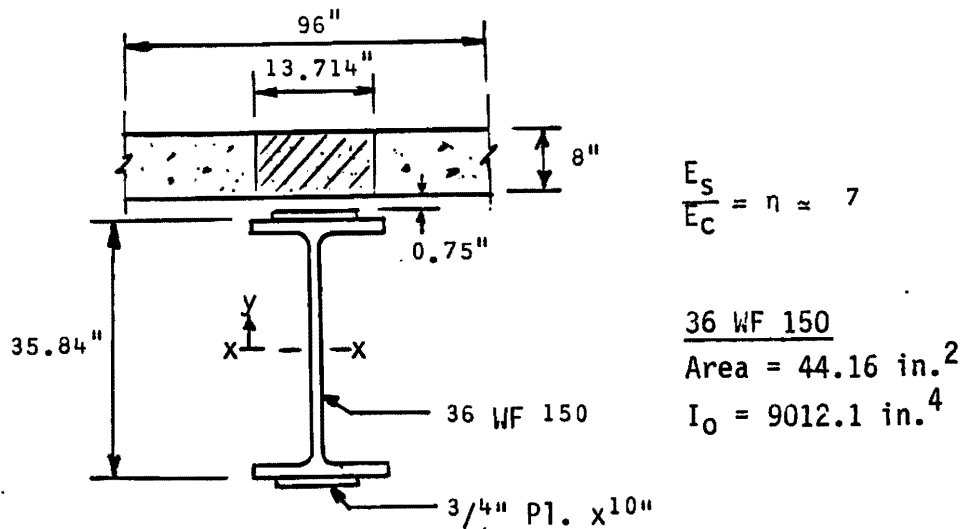


FIG. C-1. Prototype Composite Middle Section.

The calculations of the inertia properties of the middle section of the prototype are tabulated in Table C-1.

TABLE C-1. Prototype Middle Section Inertia Calculations.

Section	A (in ²)	y (in)	A y (in. ³)	A y ² (in. ⁴)	I _o (in. ⁴)
Slab	109.71	23.42	2569.41	60175.5	585.13
36 WF 150	44.16	0.	0.	0.	9012.1
Top Plate	7.5	18.295	137.21	2510.3	0.35
Bot. Plate	7.5	-18.295	-137.21	2510.3	0.35
Total Σ	168.9		2569.41	65196.1	9597.9

Compute location of neutral axis from stringer centroid

$$\bar{y} = \frac{\Sigma A y}{\Sigma A} = \frac{2569.41 \text{ in}^3}{168.9 \text{ in}^2} = 15.21 \text{ in.}$$

Distance from neutral axis to bottom and top fibers

$$y_b = 33.88 \text{ in.} \quad y_t = 12.21 \text{ in.}$$

Compute moment of inertia

$$I = \Sigma I_o + \Sigma A y^2 - (\bar{y}^2)(\Sigma A).$$

$$I = 9597.9 \text{ in.}^4 + 65196.1 \text{ in.}^4 - (15.21 \text{ in.})^2(168.9 \text{ in.}^2)$$

$$I = 35720.0 \text{ in.}^4$$

Compute section modulus at bottom and top fibers

$$S_{bot} = I / y_b = (35720.0 \text{ in.}^4) / (33.88 \text{ in.}) = 1054. \text{ in.}^3$$

$$S_{top} = I / y_t = (35720.0 \text{ in.}^4) / (12.21 \text{ in.}) = 2925. \text{ in.}^3$$

Compute Q at panel-stringer interface

$$Q = A y = (109.71 \text{ in.}^2)(8.2 \text{ in.}) = 899.6 \text{ in.}^3$$

Compute I/Q ratio

$$I/Q = (35720.0 \text{ in.}^4) / (899.6 \text{ in.}^3) = 39.71 \text{ in.}$$

Prototype End Sections

The end section of the prototype bridge consists of 36 WF 150 wide flange stringers with no cover plates. The prototype end section is illustrated in Fig. C-2.

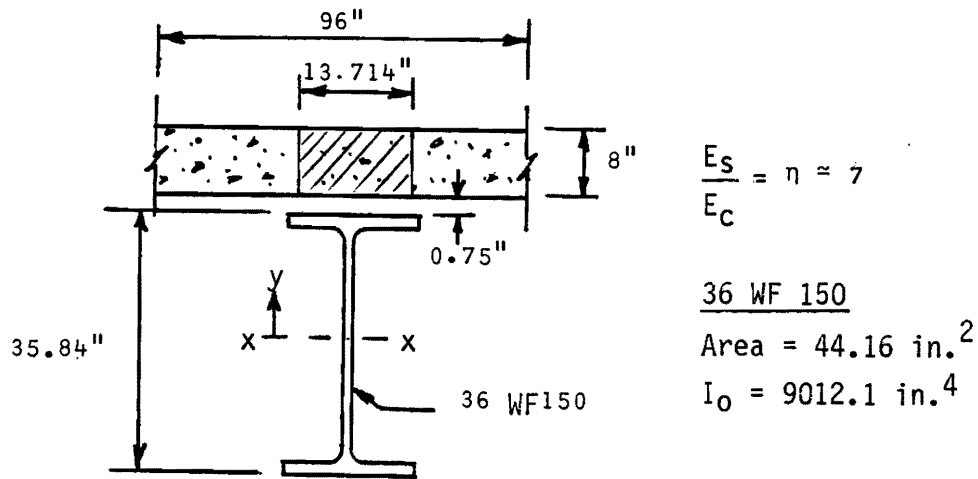


FIG. C-2. Prototype Composite End Section.

The calculations of the composite inertia properties of the end section of the prototype bridge are tabulated in Table C-2

TABLE C-2. Prototype End Section Inertia Calculations.

Section	A (in ²)	y (in)	A y (in. ³)	A y ² (in. ⁴)	I _o (in. ⁴)
Slab	109.71	22.67	2487.13	56383.1	585.83
36 WF 150	44.16	0.	0.	0.	9012.1
Total Σ	153.87		2487.13	56383.1	9597.9

Compute location of neutral axis from stringer centroid

$$\bar{y} = \frac{\Sigma A y}{\Sigma A} = \frac{2487.13 \text{ in}^3}{153.87 \text{ in}^2} = 16.16 \text{ in.}$$

Distance from neutral axis to bottom and top fibers

$$y_b = 34.08 \text{ in.} \quad y_t = 10.51 \text{ in.}$$

Compute moment of inertia

$$I = \Sigma I_o + \Sigma A y^2 - (\bar{y}^2)(\Sigma A)$$

$$I = 9597.9 \text{ in}^4 + 56383.1 \text{ in}^4 - (16.16 \text{ in.})^2(153.87 \text{ in}^2)$$

$$I = 25778.8 \text{ in}^4$$

Compute section modulus at bottom and top fibers

$$S_{bot} = I / y_b = (25778.8 \text{ in}^4) / (34.08 \text{ in.}) = 756.4 \text{ in}^3$$

$$S_{top} = I / y_t = (25778.7 \text{ in}^4) / (10.51 \text{ in.}) = 2452.8 \text{ in}^3$$

Compute Q at panel-stringer interface

$$Q = A y = (109.71 \text{ in}^2)(6.51 \text{ in.}) = 714.2 \text{ in}^3$$

Compute I/Q ratio

$$I/Q = (25778.8 \text{ in}^4) / (714.2 \text{ in}^3) = 36.12 \text{ in.}$$

Design 1/3 Model Middle Section

The design of the 1/3 model was achieved using a W 12 X 19 wide flange section with 3/16 in. thick, 2-3/4 in. wide cover plates welded to the top and bottom flanges. The design 1/3 model middle section is illustrated in Fig. C-3.

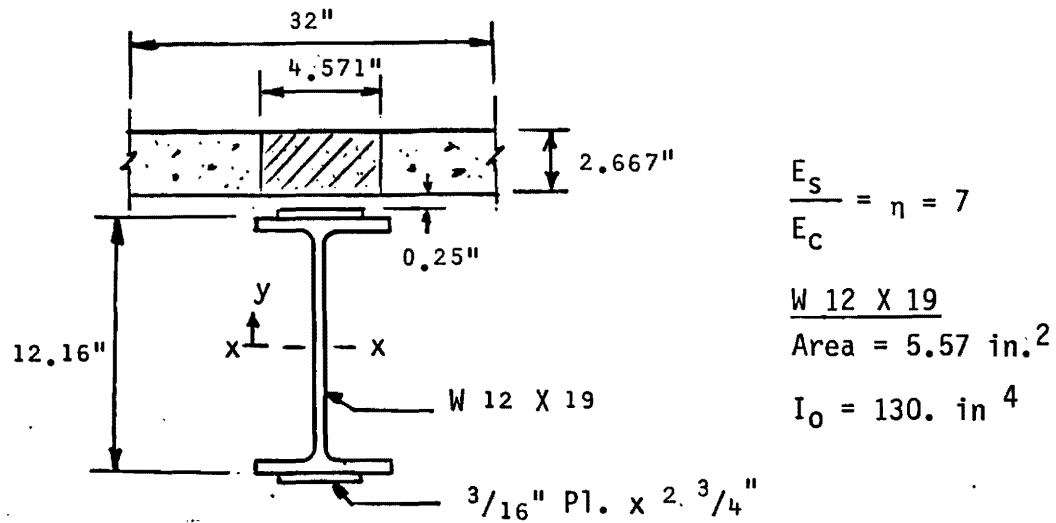


FIG. C-3. Design 1/3 Model Middle Section.

The calculations of the composite inertia properties of the middle section of the design 1/3 model bridge are tabulated in Table C-3.

TABLE C-3. Design 1/3 Model Middle Section Inertia Calculations.

Section	A (in ²)	y (in)	A y (in. ³)	A y ² (in. ⁴)	I ₀ (in. ⁴)
Slab	12.192	7.851	95.718	751.464	7.23
W 12 X 19	5.57	0.	0.	0.	130.
Top Plate	0.52	6.174	3.183	19.653	-
Bot. Plate	0.52	-6.174	-3.183	19.653	-
Total Σ	18.80		95.718	790.77	137.

Compute location of neutral axis from stringer centroid

$$\bar{y} = \frac{\sum A y}{\sum A} = \frac{95.718 \text{ in}^3}{18.80 \text{ in}^2} = 5.09 \text{ in.}$$

Distance from neutral axis to bottom and top fibers

$$y_b = 11.36 \text{ in.} \quad y_t = 4.09 \text{ in.}$$

Compute moment of inertia

$$I = \Sigma I_o + \Sigma A y^2 - (\bar{y}^2)(\Sigma A)$$

$$I = 137.23 \text{ in.}^4 + 790.77 \text{ in.}^4 - (5.09 \text{ in.})^2(18.90 \text{ in.}^2)$$

$$I = 438.33 \text{ in.}^4$$

Compute section modulus at bottom and top fibers

$$S_{bot} = I / y_b = (438.33 \text{ in.}^4) / (11.36 \text{ in.}) = 38.59 \text{ in.}^3$$

$$S_{top} = I / y_t = (438.33 \text{ in.}^4) / (4.09 \text{ in.}) = 107.17 \text{ in.}^3$$

Compute Q at panel-stringer interface

$$Q = A y = (12.19 \text{ in.}^2)(2.759 \text{ in.}) = 33.63 \text{ in.}^3$$

Compute I/Q ratio

$$I/Q = (438.33 \text{ in.}^4) / (33.63 \text{ in.}^3) = 13.03 \text{ in.}$$

Design 1/3 Model End Section

The design of the end section of the 1/3 model bridge was achieved using a W12 X 19 wide flange section with the four edges of the flanges cut 3/8 in. The design 1/3 model end section is illustrated in Fig. C-4.

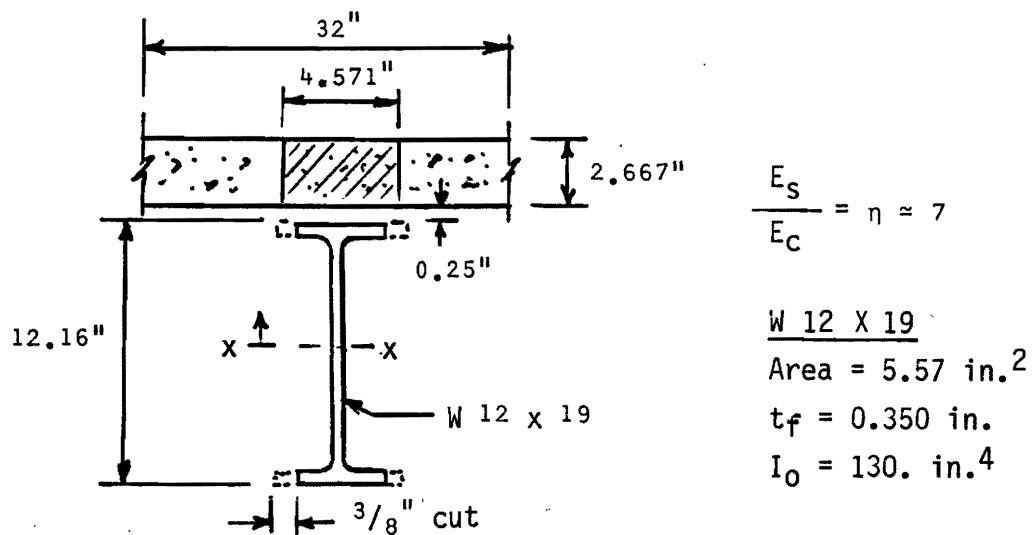


FIG. C-4. Design 1/3 Model End Section.

The calculations of the composite end section of the design 1/3 model bridge are tabulated in Table C-4.

TABLE C-4. Design 1/3 Model End Section Inertia Calculations.

Section	A (in ²)	y (in)	A y (in. ³)	A y ² (in. ⁴)	I _o (in. ⁴)
Slab	12.192	7.6635	93.433	716.027	7.23
W 12 X 19	5.57	0.	0.	0.	130.
Top Cut	-0.263	5.905	-1.550	-9.153	-
Bot. Cut	-0.263	-5.905	1.550	-9.153	-
Total Σ	17.24		93.433	697.721	137.

Compute location of neutral axis from stringer centroid

$$\bar{y} = \frac{\sum A y}{\sum A} = \frac{93.433 \text{ in}^3}{17.24 \text{ in}^2} = 5.420 \text{ in.}$$

Distance from neutral axis to bottom and top fibers

$$y_b = 11.500 \text{ in.} \quad y_t = 3.577 \text{ in.}$$

Compute moment of inertia

$$I = \sum I_o + \sum A y^2 - (\bar{y}^2)(\sum A)$$

$$I = 137. \text{ in.}^4 + 697.721 \text{ in.}^4 - (5.420 \text{ in.})^2(17.237 \text{ in.}^2)$$

$$I = 328.36 \text{ in.}^4$$

Compute section modulus at bottom and top fibers

$$S_{bot} = I / y_b = (328.36 \text{ in.}^4) / (11.500 \text{ in.}) = 28.55 \text{ in.}^3$$

$$S_{top} = I / y_t = (328.36 \text{ in.}^4) / (3.577 \text{ in.}) = 91.80 \text{ in.}^3$$

Compute Q at panel-stringer interface

$$Q = A y = (12.192 \text{ in.}^2)(2.244 \text{ in.}) = 27.35 \text{ in.}^3$$

Compute I/Q ratio

$$I/Q = (328.36 \text{ in.}^4) / (27.35 \text{ in.}^3) = 12.01 \text{ in.}$$

APPENDIX D

INERTIA CALCULATIONS OF ACTUAL MODEL AND PROTOTYPE

The actual composite inertia properties of the 1/3 model are computed using actual measurements of the model stringers and the model precast panels. The actual composite inertia properties of the prototype are computed using the same geometry as the design prototype but the ratio of the moduli of elasticity of steel to concrete is taken to be 8 instead of 7 as in Appendix C.

Actual 1/3 Model Middle Section

The actual composite inertia properties of the middle section of the 1/3 model are computed using actual measurements. The middle section of the actual model is illustrated in Fig. D-1 along with the measurements obtained.

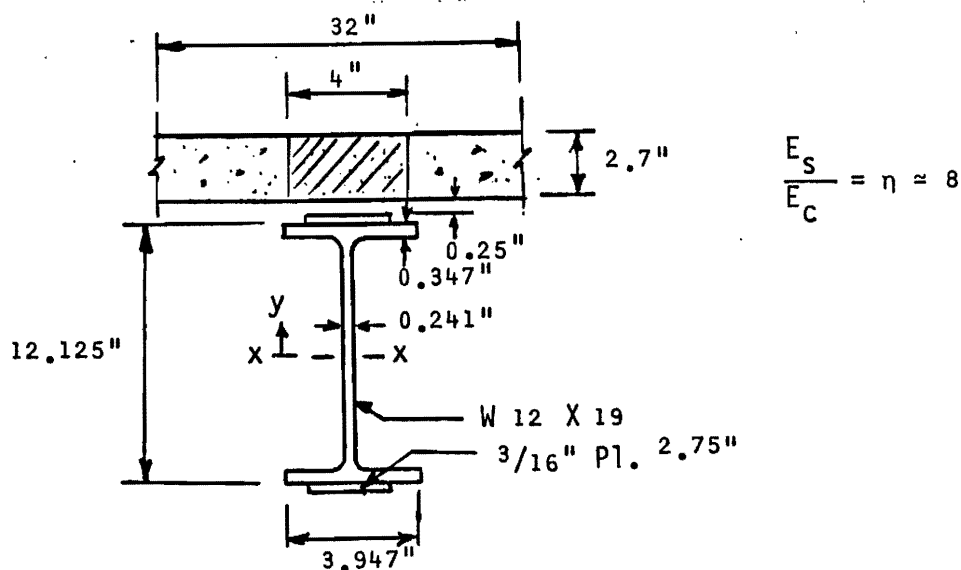


FIG. D-1. Actual Model Middle Section.

The calculations of the inertia properties of the middle section of the actual model are tabulated in Table D-1.

TABLE D-1. Actual Model Middle Section Inertia Calculations.

Section	A (in ²)	y (in)	A y (in. ³)	A y ² (in. ⁴)	I ₀ (in. ⁴)
Slab	10.80	7.85	84.78	665.5	6.561
Web	2.755	0.	0.	0.	30.00
Top Flange	1.370	5.889	8.068	47.51	0.014
Bot. Flange	1.370	-5.889	-8.068	47.51	0.014
Top Plate	0.516	6.156	3.176	19.55	-
Bot. Plate	0.516	-6.156	-3.176	19.55	-
Total Σ	17.33		84.78	799.62	36.59

Compute location of neutral axis from stringer centroid

$$\bar{y} = \frac{\Sigma A y}{\Sigma A} = \frac{84.78 \text{ in}^3}{17.33 \text{ in}^2} = 4.892 \text{ in.}$$

Distance from neutral axis to bottom and top fibers

$$y_b = 11.142 \text{ in.} \quad y_t = 4.308 \text{ in.}$$

Compute moment of inertia

$$\begin{aligned} I &= \Sigma I_0 + \Sigma A y^2 - (\bar{y}^2)(\Sigma A) \\ I &= 36.59 \text{ in.}^4 + 799.62 \text{ in.}^4 - (4.892 \text{ in.})^2(17.33 \text{ in.}^2) \\ I &= 421.47 \text{ in.}^4 \end{aligned}$$

Compute section modulus at bottom and top fibers

$$\begin{aligned} S_{bot} &= I / y_b = (421.47 \text{ in.}^4) / (11.142 \text{ in.}) = 37.83 \text{ in.}^3 \\ S_{top} &= I / y_t = (421.47 \text{ in.}^4) / (4.307 \text{ in.}) = 97.86 \text{ in.}^3 \end{aligned}$$

Compute Q at panel-stringer interface

$$Q = A y = (10.80 \text{ in.}^2)(2.974 \text{ in.}) = 31.94 \text{ in.}^3$$

Compute I/Q ratio

$$I/Q = (421.47 \text{ in.}^4) / (31.94 \text{ in.}^3) = 13.20 \text{ in.}$$

Actual 1/3 Model End Section

The end section of the actual 1/3 model is computed using the average measurement of the flanges. The end section of the actual 1/3 model is illustrated in Fig D-2 along with the measurements.

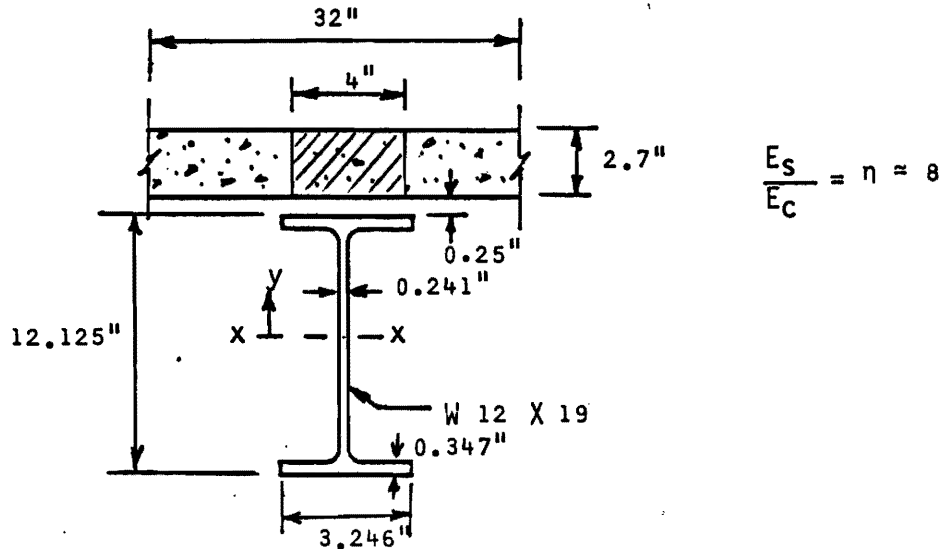


FIG. D-2. Actual Model End Section.

The calculations of the composite inertia properties of the end section of actual model bridge are tabulated in Table D-2

TABLE D-2. Actual Model End Section Inertia Calculations.

Section	A (in ²)	y (in)	A y (in. ³)	A y ² (in. ⁴)	I ₀ (in. ⁴)
Slab	10.80	7.663	82.755	634.110	6.561
Web	2.755	0.	0.	0.	30.00
Top Flange	1.126	5.889	6.633	39.063	0.11
Bot. Flange	1.126	-5.889	-6.633	39.063	0.11
Total Σ	15.81		82.755	712.236	36.78

Compute location of neutral axis from stringer centroid

$$\bar{y} = \frac{\Sigma A y}{\Sigma A} = \frac{82.755 \text{ in}^3}{15.81 \text{ in}^2} = 5.234 \text{ in.}$$

Distance from neutral axis to bottom and top fibers

$$y_b = 11.297 \text{ in.} \quad y_t = 3.778 \text{ in.}$$

Compute moment of inertia

$$I = I_{x-x} - \bar{y}^2(\Sigma A) = \Sigma I_o + \Sigma A y^2 - \bar{y}^2(\Sigma A)$$

$$I = 36.78 \text{ in.}^4 + 712.36 \text{ in.}^4 - (5.234 \text{ in.})^2(15.81 \text{ in.}^2)$$

$$I = 316.03 \text{ in.}^4$$

Compute section modulus at bottom and top fibers

$$S_{bot} = I / y_b = (316.03 \text{ in.}^4) / (11.297 \text{ in.}) = 27.97 \text{ in.}^3$$

$$S_{top} = I / y_t = (316.03 \text{ in.}^4) / (3.778 \text{ in.}) = 83.65 \text{ in.}^3$$

Compute Q at panel-stringer interface

$$Q = A y = (10.80 \text{ in.}^2)(2.427 \text{ in.}) = 26.21 \text{ in.}^3$$

Compute I/Q ratio

$$I/Q = (316.03 \text{ in.}^4) / (26.21 \text{ in.}^3) = 12.06 \text{ in.}$$

Actual Prototype Middle Section

The composite inertia properties of the actual prototype are computed using a value of 8 for the ratio of the modulus of elasticity of steel to the modulus of elasticity of concrete. The actual prototype is illustrated in Fig. D-3.

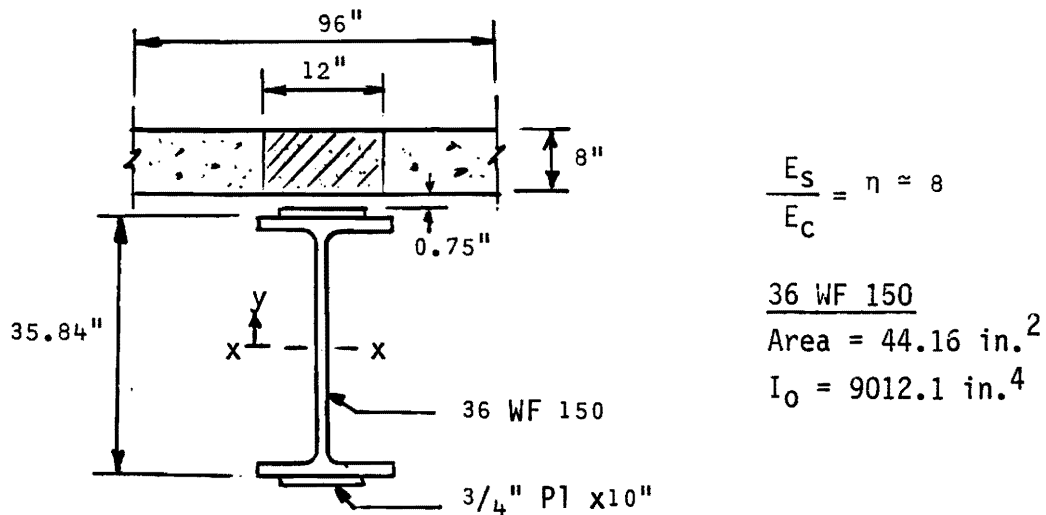


FIG. D-3. Actual Prototype Middle Section.

The calculations of the composite inertia properties of the middle section of the actual prototype bridge are tabulated in Table D-3.

TABLE D-3. Actual Prototype Middle Section Inertia Calculations.

Section	A (in ²)	y (in)	A y (in. ³)	A y ² (in. ⁴)	I _o (in. ⁴)
Slab	96.00	23.42	2248.3	52655.7	341.3
36 WF 150	44.16	0.	0.	0.	9012.1
Top Plate	7.50	18.295	137.21	2510.3	0.35
Bot. Plate	7.50	-18.295	-137.21	2510.3	0.35
Total Σ	155.16		2248.3	57676.3	9354.1

Compute location of neutral axis from stringer centroid

$$\bar{y} = \frac{\Sigma A y}{\Sigma A} = \frac{2248.3 \text{ in}^3}{155.16 \text{ in}^2} = 14.49 \text{ in.}$$

Distance from neutral axis to bottom and top fibers

$$y_b = 33.16 \text{ in.} \quad y_t = 12.93 \text{ in.}$$

Compute moment of inertia

$$I = \Sigma I_o + \Sigma A y^2 - (\bar{y}^2)(\Sigma A)$$

$$I = 9354.1 \text{ in.}^4 + 57676.3 \text{ in.}^4 - (14.49 \text{ in.})^2(155.16 \text{ in.}^2)$$

$$I = 34452.1 \text{ in.}^4$$

Compute section modulus at bottom and top fibers

$$S_{bot} = I / y_b = (34452.1 \text{ in.}^4) / (33.16 \text{ in.}) = 2664.5 \text{ in.}^3$$

$$S_{top} = I / y_t = (34452.1 \text{ in.}^4) / (12.93 \text{ in.}) = 1039.0 \text{ in.}^3$$

Compute Q at panel-stringer interface

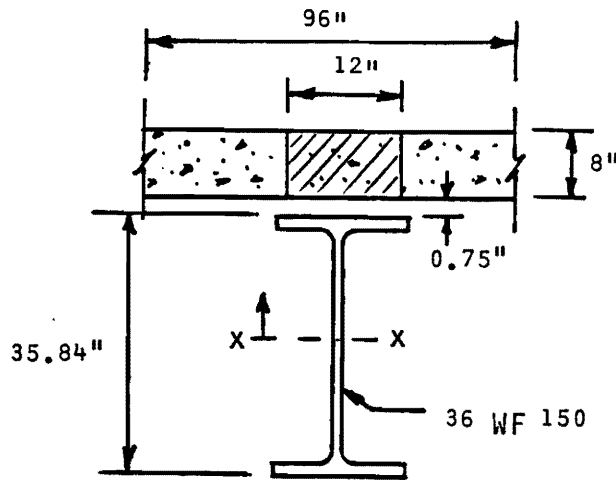
$$Q = A y = (96.00 \text{ in.}^2)(8.93 \text{ in.}) = 857.28 \text{ in.}^3$$

Compute I/Q ratio

$$I/Q = (34452.1 \text{ in.}^4) / (857.28 \text{ in.}^3) = 40.19 \text{ in.}$$

Actual Prototype End Section

The end section of the actual prototype is illustrated in Fig. D-4 along with the measurements.



$$\frac{E_s}{E_c} = \eta \approx 8$$

$$\begin{aligned} & \underline{36 \text{ WF } 150} \\ & \text{Area} = 44.16 \text{ in.}^2 \\ & I_0 = 9012.1 \text{ in.}^4 \end{aligned}$$

FIG. D-4. Actual Prototype End Section.

The calculations of the composite end section of the actual prototype bridge are tabulated in Table D-4.

TABLE D-4. Actual Prototype End Section Inertia Calculations.

Section	A (in ²)	y (in)	A y (in. ³)	A y ² (in. ⁴)	I ₀ (in. ⁴)
Slab	96.00	22.67	2176.32	49337.2	341.3
36 WF 150	44.16	0.	0.	0.	9012.1
Total Σ	140.16		2176.32	49337.1	9353.4

Compute location of neutral axis from stringer centroid

$$\bar{y} = \frac{\Sigma A y}{\Sigma A} = \frac{2176.32 \text{ in}^3}{140.16 \text{ in}^2} = 15.53 \text{ in.}$$

Distance from neutral axis to bottom and top fibers

$$y_b = 33.45 \text{ in.} \quad y_t = 11.14 \text{ in.}$$

Compute moment of inertia

$$I = \Sigma I_o + \Sigma A y^2 - (\bar{y}^2)(\Sigma A)$$

$$I = 9353.4 \text{ in.}^4 + 49337.2 \text{ in.}^4 - (15.53 \text{ in.})^2(140.16 \text{ in.}^2)$$

$$I = 24892.0 \text{ in.}^4$$

Compute section modulus at bottom and top fibers

$$S_{bot} = I / y_b = (24892.0 \text{ in.}^4) / (33.45 \text{ in.}) = 744.2 \text{ in.}^3$$

$$S_{top} = I / y_t = (24892.0 \text{ in.}^4) / (11.14 \text{ in.}) = 2233.9 \text{ in.}^3$$

Compute Q at panel stringer-interface

$$Q = A y = (96.00 \text{ in.}^2)(7.14 \text{ in.}) = 685.73 \text{ in.}^3$$

Compute I/Q ratio

$$I/Q = (24892.0 \text{ in.}^4) / (685.73 \text{ in.}^3) = 36.30 \text{ in.}$$

APPENDIX E

DERIVATION OF MIDSPAN DEFLECTION EQUATION

A general expression is derived to compute the midspan deflections of a symmetric stringer having two different moments of inertia and being loaded by two identical symmetric concentrated forces .

Thus, considering the structural system of Fig. E-1,

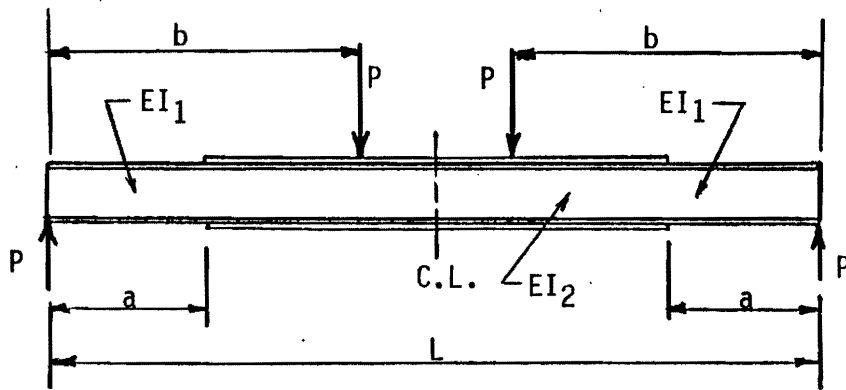


FIG. E-1. Stringer System.

which has the moment diagram shown in Fig E-2.

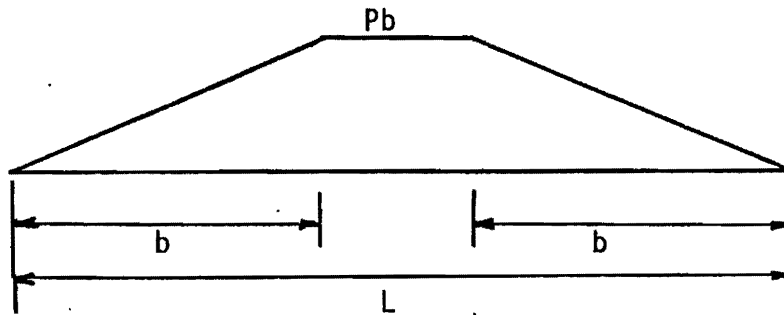


FIG. E-2. Moment Diagram

Dividing the moment diagram by the respective EI term, yields the area moment diagram of Fig. E-3.

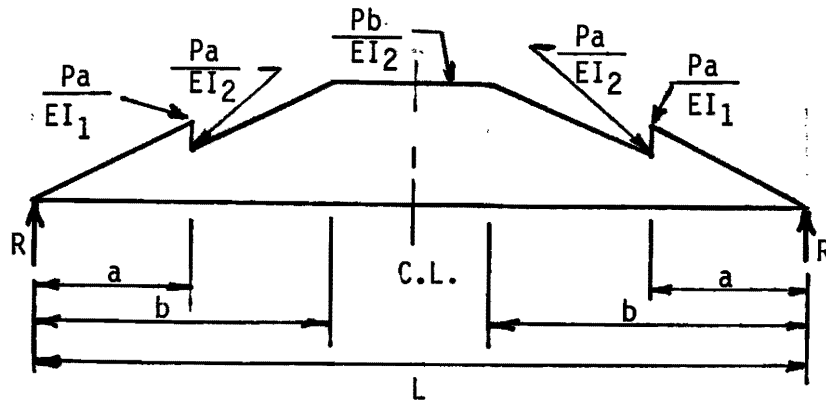


FIG. E-3. Area Moment Diagram.

where

$$R = \frac{P}{2E} \left(\frac{Lb - b^2 - a^2}{I_2} + \frac{a^3}{I_1} \right)$$

By the conjugate beam method the midspan deflection δ_m , is shown to be:

$$\delta_m = \frac{P}{2EI_2} \left(\frac{L^2b}{4} - \frac{2}{3}a^3 - \frac{b^3}{3} \right) + \frac{Pa^3}{3EI_1}$$

where

P = the applied symmetric concentrated forces,

L = the span length,

I_1 = the moment of inertia of the end portions of the stringer,

I_2 = the moment of inertia of the middle portion of the stringer,

a = the distance from support to point at which moment of inertia changes, the distance from support to the point of symmetric loading, and

E = the modulus of elasticity.